

ABSTRACT

DAMERIS, LOGAN ANDREW. The Effect of Cadmium Exposure during Critical Windows of Susceptibility on Liver Health and the Role of the Imprinted Gene Network. (Under the direction of Dr. Michael Cowley).

The heavy metal cadmium (Cd) has been designated a top ten chemical of major public health concern by the World Health Organization (WHO) due to its pervasiveness in the environment, its long biological half-life in tissues, and its association with adverse health effects in nearly all organ systems. Cd can be released into the air, water, and soil by both natural events and human activities. The primary route of exposure to Cd is through the ingestion of contaminated food products; however, individuals who live in Cd-polluted areas or who frequently inhale tobacco smoke are at even greater risk of being exposed to dangerous levels of Cd. Since Cd is not well-excreted after absorption, it can persist in the body for years or even decades. The kidneys, liver, and bones serve as major sinks for Cd accumulation, making them primary targets for toxicity.

Exposure to Cd has been shown to facilitate metabolic dysfunction-associated steatotic liver disease (MASLD) which is characterized by the accumulation of fat in hepatocytes. This buildup of fat, over time, can cause inflammation and cell damage, leading to metabolic dysfunction-associated steatohepatitis (MASH). If MASH is allowed to persist over a long period, it can promote fibrotic scarring and progress to cirrhosis and potentially even hepatocellular carcinoma (HCC). MASLD is the most common chronic liver disease in the world and is prevalent among adults and adolescents. We have demonstrated that exposure to Cd during perinatal development, a critical window of susceptibility, can program hallmarks of MASLD in the livers of juvenile mice including steatosis and fibrosis.

Critical windows of susceptibility refer to specific periods of development where individuals are especially sensitive to the effects of physiological and environmental stressors. While the perinatal period is often considered the most influential, adolescence is another important developmental window that elicits heightened sensitivity to stressors; however, it has received much less attention. Notably, imprinted genes, defined by their expression from only one parental allele, have been found to be particularly responsive to environmental factors during critical windows, making them potential catalysts for the adverse outcomes observed later in life.

In our mouse model of perinatal Cd exposure, we, concomitantly with MASLD phenotypes, detected the activation of a network of coordinately-expressed imprinted and biallelically-expressed genes in the livers of Cd exposed mice. Artificial activation of the imprinted gene network (IGN) via the upregulation of its master regulator, ZAC1, enhanced hepatic steatosis and increased pro-fibrotic gene expression, indicating a role for the IGN in facilitating MASLD during critical windows of susceptibility. The expression of another IGN member, the imprinted long non-coding RNA *H19*, was markedly increased after perinatal Cd exposure and, coincidentally, has already been implicated in the pathogenesis of MASLD.

This dissertation investigates the role H19 and ZAC1, two prominent members of the IGN, play in perturbing hepatic homeostasis to drive MASLD, especially in the context of Cd exposure during critical windows of susceptibility. In **Chapter 2**, we created a novel mouse model of adolescent and young adulthood Cd exposure to determine if Cd could facilitate MASLD phenotypes along with activating the IGN in the liver during this critical window. We show that Cd exposure is unable to induce overt MASLD phenotypes;

however, it can perturb lipid homeostasis and induce molecular signatures of MASLD in young adult mice. We also observed the activation of IGN members including *Zac1*. In **Chapter 3**, we modified our mouse model of perinatal Cd-induced MASLD to determine if the ablation of *H19* could mitigate or even prevent its pathogenesis. We found that perinatal exposure to Cd was unable to facilitate overt MASLD phenotypes in juvenile mice but could perturb the expression of steatosis, inflammation, and fibrosis genes; the deletion of *H19*, however, could not alter their expression. Members of the IGN were activated, with Cd-exposed *H19* knockout (KO) mice displaying a dramatic increase in *Igf2* expression. In **Chapter 4**, we leveraged *Zac1* overexpressing hepatoma cells and performed chromatin immunoprecipitation-sequencing (ChIP-seq) to explore ZAC1 binding at the promoters of genes involved in MASLD. Our results showed ZAC1 could enrich pathways associated with MASLD including insulin resistance, MAPK signaling, and epithelial-mesenchymal transition (EMT).

Taken together, this body of work better our understanding of adolescence and perinatal development as critical windows of susceptibility to Cd exposure-induced MASLD. It also provides new information on how H19 and ZAC1 can regulate the expression of IGN and MASLD-related genes to influence disease progression.

© Copyright 2025 by Logan Andrew Dameris

All Rights Reserved

The Effect of Cadmium Exposure during Critical Windows of Susceptibility on Liver Health and the Role of the Imprinted Gene Network

by
Logan Andrew Dameris

A dissertation submitted to the Graduate Faculty of
North Carolina State University
in partial fulfillment of the
requirements for the degree of
Doctor of Philosophy

Toxicology

Raleigh, North Carolina
2025

APPROVED BY:

Dr. Michael Cowley
Committee Chair

Dr. Jun Ninomiya-Tsuji

Dr. Albert Keung

Dr. Mauro Calabrese

DEDICATION

To my late friend Allyson Grabowski, whose relentless pursuit for excellence made anything seem possible.

BIOGRAPHY

Logan Andrew Dameris was born in Springfield, IL and raised in the small town of Pana, IL. His affection for science started at a young age, as biology and chemistry were always his favorite subjects in school. An opportunity to shadow his cousin Dr. Jennifer Walker, a then postdoctoral fellow at the Washington University School of Medicine in St. Louis, MO, during his junior year of high school sparked an interest in research science. Logan graduated as co-Valedictorian from Pana Senior High School in 2016. In the fall of 2016, he started college at Greenville University in Greenville, IL and double majored in biology and chemistry while also participating on the men's volleyball team. During his undergraduate studies, he worked on an analytical chemistry research project led by Dr. H. Darrell Iler that examined the quality of well water in a five-county region of Southern Illinois. This experience further fueled his passion for wet lab research and largely influenced his decision to pursue toxicology and environmental health sciences in graduate school. Logan graduated from Greenville University (*magna cum laude*) in 2020 with a Bachelor of Arts in Biology and Chemistry. In the fall of 2020, he joined the Toxicology Program at North Carolina State University in Raleigh, NC to pursue a doctorate in toxicology and a graduate minor in genetics. Logan joined the lab of Dr. Michael Cowley in 2021, where he would synthesize his previous research knowledge with his newfound interests in liver health, epigenetics and imprinted genes, and critical windows of susceptibility.

ACKNOWLEDGMENTS

My success in graduate school would not have been possible without the support and encouragement of so many people; I could write a whole chapter of my dissertation on this topic but will do my best to be brief. I would first like to thank my PhD advisor, Dr. Michael Cowley, for the countless hours of mentorship and support. You have helped shape me into the scientist I am today, and I will be forever grateful. To my undergraduate advisor, Dr. H. Darrell Iler, for instilling in me a passion for scientific exploration and discovery (and for helping me like the subject of Chemistry). If it was not for you, I probably would not have learned about the field of Toxicology and never would have taken this path. To all my other mentors and teachers, throughout middle school, high school, undergrad, graduate school, and in life, for helping me become a well-rounded and well-informed individual capable of accomplishing such an amazing feat. To the Snyder Bunch for your love and friendship during undergrad and beyond. Keep being great. To my best friend, Jessie Chappel, for moving out to North Carolina with me during a global pandemic to start our graduate school journey. Your love and support has meant the world to me; I cannot wait to see what you accomplish. To Joe Dahl, Jess Connelly, George Skenteris, Amanda Gough, Meredith Devlin, Joe Hildebrand, Kenzie Cox, Grant Sayre, Kiley Shepard, Nick Shirley, Rachel Polak and so many others in the North Carolina volleyball community for helping me find a home away from home. You all never failed to put a smile on face and helped me decompress during tough weeks in lab. For your love and friendship, I will be forever grateful. To all the friends I made at NC State, especially those in the Toxicology Program, for making graduate school so much more enjoyable. I want to specifically shoutout my “lab bestie”, Vicmarie Marrero-Colon, for walking by my side

on this journey. I am so incredibly proud of your resilience and of the scientist and person you have become. For that reason, I have decided to remove the “burn book” chapter from this dissertation. To all my friends and family back home, your unwavering love and support during this adventure (and during the many others before and to be had) has meant the world to me. To my parents and sister, I don’t think I can even put my feelings into words to describe what you all have meant and done for me. I know it wasn’t easy letting me move 12 hours away to start my graduate school journey, but it is you all who helped me believe anything was possible. I hope I have made you proud. To my life partner, Sarah Schmitz, for following me along on this crazy journey. I cannot express how grateful I am for you for sticking by my side and giving me endless amounts of love and support. You helped make this possible. Finally, to me, for believing in myself and for accomplishing something truly amazing.

I have no special talents, I am only passionately curious.

- Albert Einstein

TABLE OF CONTENTS

LIST OF TABLES.....	vii
LIST OF FIGURES.....	viii
CHAPTER 1: Introduction	1
CHAPTER 2: Cadmium Exposure during Adolescence and Young Adulthood Perturbs Lipid Homeostasis and Induces Signature of Metabolic Dysfunction-Associated Disease (MASLD)	13
Abstract.....	14
Introduction	15
Materials and Methods.....	17
Results	27
Discussion	41
Conclusions	47
Acknowledgements.....	47
CHAPTER 3: Systemic Deletion of the Imprinted Long Non-Coding RNA <i>H19</i> does not Mitigate the Developmental Cadmium Exposure-Induced Transcriptional Signatures of MASLD in Juvenile Mice	48
Abstract.....	49
Introduction	50
Materials and Methods.....	52
Results	61
Discussion	78
Conclusions	83
Acknowledgements	84
CHAPTER 4: The Imprinted Transcription Factor ZAC1 Binds Directly to the Promoters of Gene Enriched in Pathways Implicated in MASLD.....	85
Abstract.....	86
Introduction	87
Materials and Methods.....	88
Results	92
Discussion	98
CHAPTER 5: Conclusions and Future Directions	101
REFERENCES.....	106
APPENDICES	132
Appendix A: Chapter 2 Supplementary Tables	133
Appendix B: Chapter 3 Supplementary Tables	134

LIST OF TABLES

Supplementary Table 2.1: Sample Numbers and Statistics	133
Supplementary Table 2.2: qRT-PCR Primer Sequences	133
Supplementary Table 2.3: Lipidomics Data and Statistics.....	133
Supplementary Table 2.4: Lipid Class Key.....	133
Supplementary Table 3.1: Dam Water Consumption, Dam Food Consumption, Dam Weight Change, Litter Sizes, and PND 21 Survival Data	134
Supplementary Table 3.2: Sample Numbers and Statistics	134
Table 4.1: DAVID KEGG pathway enrichment using genes with identified ZAC1 promoter binding	96
Table 4.2: Qiagen IPA canonical pathway enrichment using genes with identified ZAC1 promoter binding	97

LIST OF FIGURES

Figure 2.1: Effects of CdCl ₂ exposure on body weight, liver weight, and liver-to-body-weight percentage at PND 120	28
Figure 2.2: Effects of CdCl ₂ exposure on histological and biochemical markers of MASLD at PND 120.....	30
Figure 2.3: Effects of CdCl ₂ exposure on hepatic transcription of steatosis markers at PND 120	32
Figure 2.4: Effects of CdCl ₂ exposure on hepatic transcription of inflammation and fibrosis markers at PND 120.....	34
Figure 2.5: Effects of CdCl ₂ exposure on hepatic lipids at PND 120.....	36
Figure 2.6: Effects of CdCl ₂ exposure on hepatic transcription of antioxidant markers at PND 120	39
Figure 2.7: Effects of CdCl ₂ exposure on hepatic transcription of select IGN members at PND 120	40
Figure 3.1: Effects of perinatal Cd exposure and systemic <i>H19</i> ablation on hepatic <i>H19</i> expression, body weight, liver weight, and liver-to-body-weight percentage mice at PND 21	62
Figure 3.2: Effects of perinatal Cd exposure and systemic <i>H19</i> ablation on biochemical markers of MASLD at PND 21	64
Figure 3.3: Effects of perinatal Cd exposure and systemic <i>H19</i> ablation on hepatic transcription of MASLD markers at PND 21	66
Figure 3.4: Effects of perinatal Cd exposure and systemic <i>H19</i> ablation on essential trace metal levels in blood at PND 21	68
Figure 3.5: Effects of perinatal Cd exposure and systemic <i>H19</i> ablation on hepatic transcription of select IGN members at PND 21.....	70
Figure 3.6: Effects of prenatal Cd exposure and systemic <i>H19</i> ablation on hepatic <i>H19</i> expression, body weight, liver weight, and liver-to-body-weight percentage in mice at PND 0	72

Figure 3.7: Effects of prenatal Cd exposure and systemic <i>H19</i> ablation on biochemical markers of MASLD at PND 0	74
Figure 3.8: Effects of prenatal Cd exposure and systemic <i>H19</i> ablation on hepatic transcription of MASLD markers at PND 0	75
Figure 3.9: Effects of prenatal Cd exposure and systemic <i>H19</i> ablation on hepatic transcription of select IGN members at PND 0.....	77
Figure 4.1: Identification of genomic regions of ZAC1 binding	93
Figure 4.2: Validation of ZAC1 binding at promoters.....	94
Figure 4.3: Identification of ZAC1 consensus binding motifs at gene promoters using STREME	95

CHAPTER 1:

Introduction

Cadmium

Sources of Release

Cadmium (Cd) is a toxic heavy metal present in the Earth's crust at an abundance of 0.1 to 0.5 parts per million (ppm) and is typically found with zinc (Zn), lead (Pb), and copper (Cu) ores; Cd can also occur naturally in ocean waters with concentrations ranging from less than five ng/L and up to 110 ng/L¹. Natural events – including volcanic activity, forest fires, the weathering of Cd-containing rocks, and sea spray – displace Cd and release it into the air, water, and soil^{2,3}. Human activities have further increased the burden of Cd in the environment. Mining, smelting, the refining of non-ferrous metals, coal and oil combustion, and other industrial practices are major contributors of anthropogenic Cd release³. The use of contaminated phosphate fertilizers on crops has also increased environmental Cd burdens in the soil and water⁴.

Mobility through the Environment

The mobility of Cd through the environment is heavily dictated by the media it contaminates. In the soil, its mobility is influenced by factors such as pH, organic matter content, and the presence of competing ions^{5,6}. Under acidic conditions, Cd remains in its soluble, divalent form (Cd^{2+}), facilitating its leaching into groundwater supplies and increasing its bioavailability for uptake by plants and animals^{2,5}. In aquatic environments, Cd can exist as free ions or form complexes with inorganic and organic ligands⁷. These

complexes increase its solubility and mobility, allowing Cd to be transported over long distances². In the atmosphere, Cd can exist as fine particulate matter or as gaseous species; the fine particulate form is the most common and results from the burning of fossil fuels, industrial emissions, and other combustion processes³. Weather conditions and wind patterns can transport airborne Cd over great distances before it is deposited onto the surface of soil and water⁸.

Routes of Human Exposure

The most common route of exposure to Cd is through the ingestion of contaminated food products³. Crops – especially rice, cereals, and leafy-green vegetables – can readily accumulate Cd from the soil, while fish and shellfish can bioaccumulate Cd from aquatic environments^{9,10}. Cd can also be ingested through the consumption of drinking water contaminated by Cd-rich industrial waste or natural deposits³. The inhalation of cigarette smoke is another significant route of exposure, as tobacco, like many other leafy plants, naturally accumulates Cd from the ground^{11–13}. Inhalation exposure can also occur in occupational settings, such as industries involving welding, mining, and battery manufacturing, where airborne Cd particles are prevalent³. Finally, although less common, dermal exposure to Cd can occur in occupational environments, as well as through the use of products containing Cd, such as contaminated cosmetic products or jewelry^{3,14,15}.

Toxicokinetics

Upon exposure, the absorption of Cd is relatively inefficient, as roughly 25% of inhaled Cd, 1-10% of ingested Cd, and less than 1% of dermally-exposed Cd is absorbed by the lungs, gastrointestinal tract, and skin, respectively³. Once absorbed, Cd is distributed widely throughout the body via the bloodstream with the greatest burden of Cd being deposited in the kidneys, liver, and bone^{16,17}. Cd does not undergo any direct metabolism but binds to albumin and to metallothioneins (MTs), small proteins that play a role in its sequestration, to limit its immediate toxic effects; however, this also contributes to its long-term retention in tissues¹⁶. Cd that is not absorbed into the bloodstream is excreted in feces; due to the long biological half-life of Cd (ranging from 6-38 years), absorbed Cd is removed very slowly and is excreted in both urine and feces³.

Mechanisms of Toxicity

One of the primary mechanisms of Cd toxicity is oxidative stress which is generated by mitochondrial dysfunction and the production of reactive oxygen species (ROS)^{18,19}. The accumulation of ROS can overwhelm cellular antioxidant defenses, leading to lipid peroxidation, protein degradation, and DNA damage. Exposure to Cd can also directly and indirectly disrupt important cellular signaling pathways – including the MAPK, NF- κ B, and p53 pathways – responsible for regulating growth and proliferation, DNA damage responses, and cell death; chronic dysregulation can, ultimately, contribute to cancer development and progression^{17,18}. Another pathway, calcium (Ca) signaling, can be directly impaired by Cd, as Cd can mimic Ca²⁺ ions and compete for Ca binding at proteins to disrupt their normal functions²⁰. In addition to Ca, Cd can more broadly

perturb essential metal homeostasis by interfering with the uptake, distribution, and utilization of metals such as Zn, Cu, and iron (Fe), which are crucial for numerous biological processes²¹⁻²⁴. Cd competes with these essential metals for binding sites on transport proteins and receptors, leading to deficiencies and impairments in enzymatic functions that are dependent on essential metals^{22,25}. Finally, Cd exposure has been shown to induce epigenetic changes, including changes to both DNA methylation and histone modifications, which can lead to long-lasting alterations in gene expression and cellular function^{26,27}.

Transport during Pregnancy

During pregnancy, the placenta serves as a semi-permeable barrier for the exchange of Cd between the mother and fetus. In comparison to other toxic metals like Pb and mercury (Hg), only a small fraction of available Cd enters fetal circulation, as the Cd becomes sequestered in the placental tissue by MTs²⁸⁻³². Various biological and environmental factors – including fetal sex, maternal health, essential metal deficiencies, and others - can influence the amount of Cd that passes through the placenta and into the fetal bloodstream³³⁻³⁵. After birth, an infant's maternal exposure to Cd can continue, as Cd has been detected in breast milk³⁶.

The Liver

Function

The liver is the largest organ in the body, making up around 2% of an individual's total body weight³⁷. It executes a broad range of functions essential for maintaining

homeostasis in the human body. One of its most important roles is to process and store nutrients absorbed from the digestive tract, including glucose, fatty acids, and amino acids³⁸. In addition to metabolic functions, the liver serves as a detoxifying center, breaking down and eliminating toxic compounds - including toxicants, drugs, alcohol, and metabolic byproducts – through enzymes like cytochrome P450³⁹. It also synthesizes proteins vital for systemic Fe homeostasis, blood volume and clotting, and cholesterol transport³⁹. Overall, the liver is indispensable to human health, and its dysfunction can lead to a range of disorders including steatotic liver disease (SLD), cirrhosis, and cancer⁴⁰.

Structure

Structurally, the liver is divided into four lobes – the right, left, caudate, and quadrate (median) lobes – with the right lobe being the largest of the four³⁷. The functional unit of the liver is the hepatic lobule, which is a hexagonal structure composed of hepatocytes arranged in plates or cords radiating from a central vein; a portal triad consisting of a hepatic vein, portal vein, and bile is found at each corner of the hexagon⁴¹. To facilitate exchange of nutrients, waste, and oxygen, blood enters the lobule through the portal triad, flows through specialized capillaries (sinusoids), and drains into the central vein^{37,41}. Bile produced by the hepatocytes flows in the opposite direction through small channels and out the bile ducts⁴¹. This intricate arrangement helps the liver properly support its vital functions.

Cell Types

Hepatocytes, the predominant cell type which account for approximately 70-80% of the liver's mass, are largely responsible for carrying out the diverse metabolic and synthetic functions of the liver^{37,38}. The liver contains various other non-parenchymal cells that have important roles in the livers. Kupffer cells are resident macrophages involved in immune responses, while hepatic stellate cells (HSCs) store vitamin A and play a role in liver fibrosis during injury³⁷. Liver sinusoidal epithelial cells (LSECs) form the blood-liver barrier and regulate the exchange of nutrients and waste between the blood and hepatocytes; cholangiocytes line the bile ducts and are responsible for bile secretion and regulation, ensuring proper bile flow for digestion³⁷.

Metabolic Dysfunction-Associated Steatotic Liver Disease (MASLD)

Pathology and Risk Factors

Metabolic dysfunction-associated steatotic liver disease (MASLD), previously referred to as non-alcoholic fatty liver disease (NAFLD), is characterized by the accumulation of lipids (steatosis) within hepatocytes⁴². To be officially diagnosed, an individual must present with hepatic steatosis, as well as one of five cardiometabolic risk factors (CMRFs) and no history of substantial alcohol consumption⁴³. The CMRFs include obesity, high blood pressure, elevated blood sugar, high blood triglycerides (TAGs), and low HDL cholesterol. Further, a continued increase in fat accumulation can trigger inflammation and cell damage, bringing on metabolic dysfunction-associated steatohepatitis (MASH); MASH, if unresolved, can lead to the formation of scar tissue (fibrosis) which can impair normal liver function^{44,45}. The progression of fibrosis, over time,

can cause cirrhosis. The onset of cirrhosis drastically increases an individual's chance of developing hepatocellular carcinoma (HCC), the most common type of liver cancer⁴⁵. Both cirrhosis and HCC require serious medical intervention to help manage or resolve with most needing a liver transplant^{46,47}. Overall, MASLD is a complex and multi-factorial disease driven by both genetic and environmental factors.

Prevalence in the United States

The prevalence of MASLD in the United States (US) and around the world is a major public health crisis. It is believed that 34% of adults have MASLD in the US; by 2025, the burden of MASLD is forecasted to increase to 41%, translating to nearly 122 million US adults⁴⁸. Despite being a disease associated with aging, the prevalence of MASLD in US adolescents (aged 12-17) is 17%; of those 17%, 6% presented with fibrosis and 2% presented with cirrhosis⁴⁹. These findings demonstrate an urgent need to better understand the underlying etiologies of MASLD in children and adolescents, as MASLD with fibrosis is a significant risk factor for increased mortality⁵⁰.

Molecular and Cellular Mechanisms

The molecular mechanisms underlying MASLD pathogenesis involve complex interactions between lipids, inflammatory mediators, and fibrogenic pathways. Steatosis, the hallmark of MASLD, is primarily driven by the increased influx of free fatty acids (FFAs) from adipose tissue, de novo lipogenesis (DNL) in the liver, and impaired hepatic fatty acid oxidation. FFAs are taken up by hepatocytes via the plasma membrane-associated proteins FA-binding protein (FABPpm), FA translocase (FAT)/CD36, and

caveolin-1 (CAV1)⁵¹. The major regulator of lipid accumulation is the transcription factor sterol regulatory element-binding protein 1c (SREBP-1c) which activates the expression of genes involved in DNL including fatty acid synthase (FASN), acetyl-CoA carboxylase (ACC), and stearoyl-CoA desaturase (SCD1)^{44,51}. The excessive production of fatty acids can exceed the liver's capacity for oxidation and increase intracellular lipid burden; therefore, the peroxisome proliferator-activated receptor alpha (PPAR α), a key regulator of fatty acid oxidation, is often dysregulated in MASLD⁵². Additionally, the liver's ability to export lipids is impaired, due in part to reduced expression of apolipoprotein B (APOB), a crucial component of very low-density lipoprotein (VLDL), which is responsible for lipid export from hepatocytes⁵¹.

The progression of MASLD to MASH is triggered when hepatocytes experience oxidative stress due to the accumulation of ROS generated during incomplete fatty acid oxidation⁵³. These ROS promote the activation of pro-inflammatory signaling pathways, particularly the NF- κ B and inflammasome pathways, which release cytokines such as tumor necrosis factor-alpha (TNF- α) and interleukin-6 (IL-6)^{54,55}. These cytokines recruit and activate Kupffer cells and other immune cells within the liver, perpetuating a pro-inflammatory environment that promote hepatocyte injury and tissue remodeling⁵⁴. Further, the progression of MASH to advanced fibrosis is driven by the release of damage-associated molecular patterns (DAMPs) including high mobility Group Box 1 (HMGB1), which activate HSCs^{56,57}. These activated HSCs transdifferentiate into myofibroblasts, producing excessive extracellular matrix (ECM) components including collagen⁵⁸. The transforming growth factor-beta (TGF- β) signaling pathway plays a

central role in this fibrogenic process, promoting the activation of HSCs and further deposition of ECM to increase fibrosis and, ultimately, cirrhosis and HCC^{57,58}.

Critical Windows of Susceptibility

The Developmental Origins of Health and Disease (DOHaD) Hypothesis

The Developmental Origins of Health and Disease (DOHaD) hypothesis asserts that early-life exposures can significantly influence an individual's long-term health outcomes, including susceptibility to chronic diseases such as cardiovascular disease, diabetes, and obesity⁵⁹. The theory emerged in the early 1990s and was largely influenced by the work of David Barker and colleagues⁶⁰. Overall, this concept is rooted in the idea that exposure to internal and external factors – such as nutrition, stress, metabolic health, and toxicants – during critical windows of susceptibility can program disease later in life⁵⁹.

Perinatal Development

Perinatal development, defined as the period encompassing gestation through the first few months of life, is a critical window of susceptibility to environmental and physiological factors. During this period, the developing fetus and infant undergo rapid cellular differentiation, organogenesis, and physical growth, heightening their sensitivity to stressors⁶¹. Evidence from both human and animal studies shows exposure to stressors during this period influences the trajectory of physical, cognitive, and emotional health later in life^{62–65}. Strikingly, we have demonstrated in our own lab that perinatal

exposure to maternal metabolic syndrome (MetS) and Cd can program MASLD in juvenile mice^{66,67}.

Puberty and Adolescence

Puberty and adolescence, characterized by rapid physical, cognitive, and emotional development, represent a critical window of susceptibility to both biological and environmental influences. During this period, hormonal and metabolic changes trigger a cascade of developmental processes in adolescents including the maturation of the brain, endocrine system, and reproductive organs⁶⁸. These changes increase sensitivity to perturbation by stressors which can affect long-term health and well-being⁶⁹⁻⁷¹. Notably, it is unclear if exposure to Cd during adolescence and young adulthood can induce MASLD later in life. It was a goal of this dissertation to answer that question.

Imprinted Gene Network (IGN)

Imprinted Genes

Imprinted genes are a subset of genes that exhibit parent-of-origin expression, meaning only one allele, either from the mother or father, is actively expressed while the other is silenced⁷². The establishment of genomic imprinting occurs during gametogenesis, where sex-specific epigenetic marks are added to the DNA in either the sperm or the egg; these marks, predominantly DNA methylation patterns, are maintained throughout development and into adulthood⁷³. During development, imprinted genes are essential for regulating the balance of growth between the fetus and the placenta, as well as the allocation of maternal resources. For instance, paternally-expressed genes often

promote growth, while maternally-expressed genes often restrict excessive growth to prevent maternal resource depletion, leading to the so-called "conflict hypothesis" of imprinting⁷³. Strikingly, we and other have shown that imprinted genes are sensitive to environmental perturbations during critical windows of susceptibility⁷⁴⁻⁷⁸.

The IGN

The imprinted gene network is a coordinately-regulated group of both imprinted and biallelically-expressed genes⁷⁹. Upon its original discovery, the IGN consisted of only 15 imprinted genes that functioned to control embryonic development; it was later found to include an additional 70 imprinted genes, as well as hundreds of biallelically-expressed genes that could regulate cell adhesion, cell junction, extracellular matrix (ECM) composition, and growth factor-activated signaling^{79,80}. Notably, we demonstrated in our mouse models of perinatal MetS- and Cd-induced MASLD that the IGN was aberrantly activated, indicating the IGN may play a role in programming MASLD in offspring after developmental exposure to environmental stressors^{66,67}.

Zac1

The imprinted gene *Zac1* (also known as *Plagl11*) encodes a zinc-finger transcription factor that can induce cell cycle arrest and apoptosis, potentially behaving as a tumor suppressor⁸¹⁻⁸⁴. More importantly, it was determined *Zac1* was the master regulator of the IGN and could alter the expression of numerous other imprinted genes including *Igf2*, *H19*, *Cdkn1c*, and *Dlk1*⁸⁰. To investigate further the ability of the IGN to induce phenotypes of MASLD, we artificially activated the IGN by overexpressing *Zac1*

in a mouse hepatoma cell line and observed an increase in the accumulation of neutral lipid and in the expression of pro-fibrotic genes^{66,85}. Notably, we also showed, using targeted chromatin immunoprecipitation (ChIP) quantitative real-time polymerase chain reaction (qRT-PCR) assays, that ZAC1 could bind to promoters of pro-fibrotic genes⁶⁶. It remained unclear, however, the extent of ZAC1 binding at the promoters of genes associated with MASLD pathogenesis. In this dissertation, we aimed to close that knowledge gap by performing ChIP-sequencing.

H19

The imprinted gene *H19* encodes a long non-coding RNA (lncRNA) that negatively regulates cellular growth and proliferation during embryonic development⁸⁶. The regulation of *H19* expression is intricately linked to the imprinted expression of its neighboring gene, the growth factor *Igf2*, via a shared imprinting control region (ICR)⁸⁷. Strikingly, the aberrant activation of *H19* in the liver has been implicated in the pathogenesis of MASLD, as it has been shown to promote key metabolic pathways including lipid metabolism, inflammation, and fibrosis remodeling^{88–92}. In our model of perinatal Cd-induced MASLD, we found that *H19* was one of the most significantly upregulated imprinted genes in the IGN, providing evidence for its potential role in driving MASLD⁶⁷. Another goal of this dissertation was to determine if ablation of *H19* could protect against MASLD phenotypes after perinatal exposure to Cd.

CHAPTER 2:

Cadmium Exposure during Adolescence and Young Adulthood Perturbs Hepatic Lipid Homeostasis and Induces Signatures of Metabolic Dysfunction-Associated Steatotic Liver Disease (MASLD)

The following chapter has been submitted to a peer-reviewed journal.

Logan Dameris^{1,2,3}, Joshua Hartsell⁴, Jessie Chappel^{1,5}, Xiaojing Liu⁴, and Michael Cowley^{1,2,3}

¹Department of Biological Sciences, North Carolina State University, Raleigh, NC, 27695, USA.

²Toxicology Program, North Carolina State University, Raleigh, NC, 27695, USA.

³Center for Human Health and the Environment, North Carolina State University, Raleigh, NC, 27695, USA.

⁴Department of Molecular and Structural Biochemistry, North Carolina State University, Raleigh, NC, 27695, USA.

⁵Bioinformatics Research Center, North Carolina State University, Raleigh, NC, 27606, USA.

Abstract

The heavy metal cadmium (Cd) is ubiquitous in our environment and is one of the top ten chemicals of major public health concern according to the World Health Organization (WHO). We have demonstrated that exposure to Cd during perinatal development programs metabolic dysfunction-associated steatotic liver disease (MASLD), the most prevalent chronic liver disease in the world. Adolescence presents another critical window of susceptibility to environmental stressors; however, the impacts of Cd exposure during this period on the health of the liver are not known. To help bridge this knowledge gap, we exposed juvenile C57BL/6J mice to Cd via their drinking water for 14 weeks. We performed histological, biochemical, and molecular analyses on liver tissue to determine if exposure to Cd during adolescence and young adulthood also induces MASLD. We found that Cd exposure altered hepatic lipid homeostasis via the perturbation of steatosis gene expression and lipid species abundances. Additionally, Cd exposure triggered a hepatic antioxidant response and activated an imprinted gene network (IGN) which we have previously implicated in MASLD. Our results show that adolescence, albeit to a lesser degree than the perinatal period, is a critical window of susceptibility to Cd-induced changes in hepatic lipid homeostasis.

Introduction

Cadmium (Cd) is a toxic heavy metal that has been ranked by the World Health Organization (WHO) as a top ten chemical of major public health concern⁹³. It is ubiquitous in the Earth's crust and can be naturally released via volcanic or erosion events; however, anthropogenic activities – including mining and industrial practices – have greatly increased its presence in our environment³. In the nonsmoking population, the primary source of Cd exposure is through the ingestion of contaminated water and food products^{3,94}; individuals who are exposed to tobacco smoke are at an even greater risk, given the tobacco plant's high affinity for accumulating Cd from the soil^{95–97}. Since Cd is not well excreted, it can persist in the body and cause adverse health effects in multiple organ systems^{3,16}. In the liver, Cd exposure can drive metabolic dysfunction-associated steatotic liver disease (MASLD)^{98–102}.

MASLD is the most common chronic liver disease, impacting 34% of adults in the United States^{103,104}. MASLD is characterized by the accumulation of fat (steatosis) in the liver in conjunction with having at least one cardiometabolic risk factor (CMRF) – obesity, hypertension, hyperglycemia, hypertriglyceridemia, or low HDL cholesterol – and no excess alcohol consumption⁴³. While hepatic steatosis does not pose any immediate threat, its unattenuated progression to metabolic dysfunction-associated steatohepatitis (MASH) and fibrosis increases the probability of developing cirrhosis, hepatocellular carcinoma (HCC), and extrahepatic manifestations^{105–107}. Notably, records from the United States' United Network of Organ Sharing (UNOS) identify MASLD as one of the leading indicators for liver transplant¹⁰³.

Despite being considered a disease of aging, the MASLD prevalence among adolescents and young adults (AYAs) – individuals 12-29 years of age – in the United States is of major concern^{49,108}. A study leveraging data from the National Health and Nutrition Examination Survey 2017–2020 found that approximately 24% of AYAs have MASLD and 11% of those with MASLD have fibrosis⁴⁹. The pervasiveness of MASLD in the AYA population suggests exposure to adverse physiological and environmental stressors during critical windows of susceptibility^{109–113}. These “critical windows” refer to specific periods of development during which individuals are especially vulnerable to perturbations by stressors¹¹⁴. Exposure to Cd during prenatal and early postnatal (perinatal) development induces MASLD and is likely contributing to its incidence in the AYA population^{67,115,116}. Adolescence is another well-defined critical window of susceptibility; however, whether or not exposure to Cd during this period induces MASLD has not been established.

During adolescence, puberty is an important developmental period of physiological and psychological changes⁶⁸; fluctuations in hormones and alterations in body composition increase metabolic strain, making the body more vulnerable to the effects of chemical and non-chemical stressors^{69–71}. The liver plays a central role in metabolism; therefore, it is particularly sensitive to perturbations during puberty^{113,117–120}. There is some limited evidence that Cd exposure during puberty and adolescence can induce MASLD phenotypes. One epidemiological study found that young adults in the highest quartile for toenail Cd concentrations around age 25 had significantly higher odds (odds ratio: 1.43) of developing MASLD at age 50¹⁰⁰. A study in mice showed that oral exposure to Cd during puberty induced hepatic inflammation, indicated by an increase in apoptotic

cells, circulating biomarkers of liver injury, macrophage activation, and protein and transcript markers of pro-inflammatory and anti-inflammatory cytokines¹²¹.

In our study, we aimed to determine if exposure to Cd during adolescence and young adulthood is sufficient to induce MASLD. We leveraged a novel mouse model of AYA cadmium chloride (CdCl₂) exposure to examine the liver for histological, biochemical, and molecular signatures of MASLD. The results of our study provide additional support for adolescence as a critical window of susceptibility to environmental toxicants.

Materials and methods

Ethics statement

Animal work was approved by the North Carolina State University (NCSU) Institutional Animal Care and Use Committee under protocols 19-049-B and 22-162-B. Experiments were conducted in accordance with the Guiding Principles in the Use of Animals in Toxicology. The study is reported in accordance with ARRIVE guidelines.

Cadmium exposure

At 9 weeks of age, C57BL/6J female mice were mated with age matched C57BL/6J males to generate male and female offspring. Mice were maintained on a 14-h/10-h light/dark cycle at 22 ± 4°C and 30%–70% humidity and were housed in Green Line IVC Sealsafe cage housing systems (Tecniplast). At postnatal day (PND) 21, male and female mice were sexed, weaned into cages with 2 to 5 mice per cage, and fed AIN-93G rodent diet (Research Diets, D10012G) *ad libitum* for the duration of the study. Mice were given unrestricted access to filtered drinking water (Millipore RiOs Essential RO water

purification system) containing either 0 or 50 ppm CdCl₂ (Sigma-Aldrich Cadmium chloride 99.99%, 202908) starting at weaning for 14 weeks until PND 120 (4 months old). The duration of exposure captures all of adolescence including pre-pubertal and pubertal development as well as young adulthood. The concentration of CdCl₂ was determined previously to reproduce blood Cd levels of individuals living in Cd-polluted areas²¹.

At the end of the 14-week exposure, mice were fasted for 6 hours early in the morning, weighed, and then euthanized by decapitation. Trunk blood was used for blood glucose readings using a standard glucose meter. Tissues were weighed, flash frozen, and stored at -80°C. A portion of the median liver lobe was fixed in 4% paraformaldehyde (PFA) overnight at 4°C and then transferred to 70% ethanol for short-term storage at 4°C prior to histological staining. All collections were completed by noon each day.

Male and female mice were processed, analyzed, and reported separately. Unless otherwise specified, the number of mice used for each of the analyses described below and the corresponding statistics can be found in Supplementary Table 2.1. If a group contained more mice than needed for a particular analysis, mice were selected by first determining the group's median liver weight and then selecting the mice with the smallest absolute difference from the group's median. No more than two mice from each litter were used in any analysis to control for potential litter effects.

Histology

A portion of the median liver lobe fixed in 4% PFA was delivered to the NCSU Histology Laboratory or to the University of North Carolina – Chapel Hill (UNC-CH) Pathology Services Core (PSC) in 70% ethanol for Hematoxylin and Eosin (H&E) or

Picro-Sirius Red (PSR) staining, respectively. For H&E, the PFA-fixed tissues were paraffin embedded and sectioned onto positively charged slides. Tissues were deparaffinized, rehydrated, and stained following a routine H&E protocol using an autostainer (Leica ST5010 Autostainer XL). Slides were removed from the autostainer, coverslipped with a synthetic mounting media, and stored at room temperature. For PSR, the PFA-fixed liver tissues were paraffin embedded and sectioned onto positively charged slides. Tissue sections were then deparaffinized and hydrated using standard histological procedures. A PSR Stain Kit (PolySciences, 24901-500) was used following the manufacturer's instructions. Briefly, the sections were first treated with phosphomolybdic acid for tissue preparation. After rinsing, they were stained with PSR F3BA to specifically stain collagen fibers and then treated with hydrochloric acid to enhance the contrast of collagen fibers. Following staining, the slides were dehydrated and coverslipped with a xylene-based mounting medium (Leica Surgipath Micromount, 3801730) and stored at room temperature.

A portion of the left liver lobe was flash frozen on dry ice and cryo-embedded in optimal cutting temperature (OCT) compound. The OCT-embedded livers were delivered to the UNC-CH PSC for Oil Red O (ORO) staining. Sections were prepared using standard cryostat procedures onto positively charged slides. Samples were then fixed in formalin, followed by rinsing in tap water. After a rinse in 60% isopropanol, sections were stained for 15 min using a freshly prepared ORO working solution. The working solution was prepared by diluting ORO stock solution made from ORO powder (Sigma, O0625) in isopropanol. Following staining, sections were rinsed in 60% isopropanol and

counterstained lightly with hematoxylin. Slides were coverslipped with an aqueous mounting medium and stored at room temperature.

All stained slides were imaged using a brightfield microscope (Olympus BX41 Microscope with Olympus DP23 Digital Microscope Camera).

Biochemical assays

The triacylglycerides (TAG) assay was performed by digesting a portion of the left liver lobe with 3 M KOH (dissolved in 65% ethanol) solution in a 1:1 ratio with tissue weight (mg) at 70°C for 60 min in a heat block. The samples were vortexed briefly every 20 min. After the 60 min heating period, samples were left to sit overnight. The next day, the total volume of each sample was brought to 250 μ L using 2 M Tris-HCl (pH 7.5) and then vortexed briefly. The samples were diluted 1:250 in 2 M Tris-HCl (pH 7.5) in new tubes. Standards were created using glycerol (Sigma Aldrich Glycerol Standard Solution, G7793) dissolved in 2 M Tris-HCl (pH 7.5) in a 0, 10, 50, 100, 150, and 200 mg/dL serial dilution. All samples and standards were run in duplicate. 100 μ L of each sample and standard was added first to a 96-well plate and then 150 μ L of the TAG detection reagent (Thermo Scientific Triglycerides Reagent, TR22421) was added to each sample or standard. The plate was incubated at 35°C for 10 min and then absorbance was measured at 550 nm using a microplate reader (BMG Labtech FLUOstar Omega). The standards were plotted in Microsoft Excel to determine the equation of the line of best fit. The equation was used to determine the concentration of TAG (mg/dL) in each sample.

The hydroxyproline (Hyp) assay (QuickZyme Sensitive Tissue Collagen Assay Kit, QZBTISCOL) was performed using a portion of the median liver lobe according to the manufacturers' instructions.

RNA isolation

Total RNA was isolated from a portion of the left liver lobe using a mini bead mill homogenizer (VWR) and was purified (Macherey-Nagel NucleoSpin RNA Mini Kit, 740955) according to the manufacturer's instructions. RNA was quantified on a spectrophotometer (Thermo Fisher Nanodrop 2000), and quality was assessed using the 260/280 and 260/230 ratios of absorbance.

qRT-PCR

Total RNA from the left liver lobe was diluted to 500 ng and used to synthesize first-strand cDNA (Promega M-MLV Reverse Transcriptase, M170) according to the manufacturer's instructions. A 1/10 cDNA dilution was created for each sample. Standards were created using pooled cDNA in a 1/5, 1/10, 1/20, 1/40, and 1/80 serial dilution. Water was used as a no template control (NTC). Quantitative real-time (qRT)-PCR was performed in a 96-well plate using SYBR Green chemistry (Bio-Rad SsoAdvanced Universal SYBR Green Supermix, 1725271) with a real-time PCR system (Thermo Fisher QuantStudio 3). The cycling conditions were as follows: a hold stage at 95°C for 30 s; a PCR stage at 40 cycles of 95°C for 15 s and 60°C for 30 s; a melt curve stage at 95°C for 15 s, 60°C for 60 s, and 95°C for 1 s (dissociation). All samples,

standards, and NTCs were run in duplicate. Primer sequences are presented in Supplementary Table 2.2.

Dissociation curves showed that there was no contamination in the NTC wells and that the primers only amplified a single product. Amplification efficiencies were calculated in Microsoft Excel using the standard dilutions. *B2m* was used as the housekeeping gene for males, while *Polr2a* was used as the housekeeping gene for females. Neither *B2m* ($p > 0.1$) nor *Polr2a* ($p > 0.1$) were significantly differentially expressed between treatment groups. Gene expression for all target genes was analyzed using the $\Delta\Delta C_t$ method¹²². All gene expression data are visualized as a percentage of the 0 ppm CdCl₂ group for each sex.

Lipid extraction

Lipid extraction was described in a previous publication¹²³. Briefly, ice cold extraction solvent (250 μ L 80% methanol/water, v/v) and 10 μ L of fatty acid internal standard (50 ng/ μ L of ¹³C₁₆-palmitic acid, Sigma-Aldrich) were added to 20-40 mg of caudate liver lobe tissue in a 1.7 mL Eppendorf tube. Geno/Grinder homogenizer was used (1500 rpm, 1 to 2 min) to further break down the tissue chunk and form an even suspension. The sample was then centrifuged at 20,000 \times g at 4°C for 10 min, and 50 μ L of supernatant containing free fatty acids (FFAs) was removed and transferred to a vial for free FFA analysis by liquid chromatography-mass spectrometry (LC-MS).

The remaining 200 μ L of solvent and insoluble pellet were briefly homogenized using Geno/Grinder again (1500 rpm, 30 s) to loosen the bottom pellet, followed by the addition of 480 μ L MTBE and 10 μ L of lipid internal standards. Lipid standards were

obtained from Avanti Polar Lipids individually and combined to make the internal standard mix to evaluate the system performance and stability. This internal standard mix contains: 15:0–18:1(d7) PC, 15:0–18:1(d7) PE, 15:0–18:1(d7) PS, 15:0–18:1(d7) PG, 15:0–18:1(d7) PI, 15:0–18:1-d7-PA, 18:1(d7) LPC, 18:1(d7) LPE, 18:1(d7) Chol Ester, 18:1(d7) MG, 15:0–18:1(d7) DG, 15:0–18:1(d7)-15:0 TG, 18:1(d9) SM, and Cholesterol (d7). After vigorous vortexing, 120 μ L of water was added to initiate phase separation. All samples were centrifuged at 20,000 \times g at 4°C for 10 min. The supernatant containing lipids was transferred to a new Eppendorf tube, dried using a speed vacuum, and stored at –80°C. Prior to LC-MS analysis, the dry pellets were dissolved in 300 μ L of a 1:1 (v/v) isopropanol:ethyl acetate solvent.

Lipidomic LC-MS

LC-MS was performed using a Vanquish UHPLC (Thermo Fisher Scientific) coupled to Orbitrap Exploris 480 mass spectrometer (Thermo Fisher Scientific). LC-MS methods were described in a previous publication¹²³. Briefly, the measurement of FFAs was achieved by using a hydrophilic interaction chromatography method (HILIC) with an Xbridge amide column (100 \times 2.1 mm i.d., 3.5 μ m; Waters) for compound separation at 25°C. Mobile phase A: water with 5 mM ammonium acetate (pH 6.8), and mobile phase B: 100% acetonitrile. Linear gradient is: 0 min, 85% B; 1.5 min, 85% B; 5.5 min, 35% B; 6.9 min, 35% B; 10.5 min, 35% B; 10.6 min, 10% B; 12.5 min, 10% B; 13.5 min, 85% B; 17.9 min, 85% B; 18 min, 85% B; 20 min, 85% B. The flow rate is: 0-5.5 min, 0.110 mL/min; 6.9-10.5, .130 mL/min; 10.6-17.9 min, .250 mL/min; 18.0-20.0 min, .110 ml/min. The parameters of Orbitrap Exploris 480 were as listed: vaporizer temperature, 350°C;

ion transfer tube temperature, 300°C; sheath gas, 35; auxiliary gas, 7; sweep gas, 1; spray voltage, 3.5 kV for positive mode and 3.0 kV for negative mode; RF-lens (%), 30; resolution was set at 60,000 (at m/z 200); scan range, 70-900 (m/z); positive/negative switching mode. FFA analysis was performed using Sieve (Thermo Fisher Scientific) based on theoretical m/z and retention time.

The measurement of all other lipids was achieved by using a reversed phase chromatography method with Xbridge BEH C18 column (2.1 × 100 mm, Column XP; 130 Å; Waters) for compound separation at 40°C. Mobile phase A: water:acetonitrile (8:2, v/v) with 0.1% formic acid and 10 mM ammonium formate, and mobile phase B: isopropanol:acetonitrile (9:1, v/v) with 0.1% formic acid and 10 mM ammonium formate. Linear gradient was: 0 min, 40% B; 1.5 min, 40% B; 5.0 min, 85% B; 12.0 min, 97% B; 16.0 min, 97% B; 16.5 min, 40% B; 21.0 min, 40% B. The flow rate was: 0.15 ml/min. The parameters of Orbitrap Exploris 480 were as listed: vaporizer temperature, 350°C; ion transfer tube temperature, 300°C; sheath gas, 35; auxiliary gas, 7; sweep gas, 1; spray voltage, 3.5 kV for positive mode and 2.5 kV for negative mode; RF-lens (%), 45; resolution was set at 120,000 (at m/z 200); scan range, 200-1600 (m/z); positive/negative switching mode. The MS/MS condition for positive or negative ion mode was set as follows: precursor isolation window was set at 1 (m/z), HCD collision energy was set at 25%, orbitrap resolution MS/MS scan was set at 15,000. Intensity threshold was set at 10,000. Lipid peak extraction and integration were performed using MS-DIAL. Lipids identified by MS-DIAL were exported and subjected to further processing: (1) Mass error was calculated in an excel sheet and ions with mass error larger than 4 ppm were

excluded from further analysis; (2) Redundant lipid identifications were removed from the result of MS-DIAL analysis.

Lipidomic data analysis

All computational analyses were conducted using R software (v4.2.1). Prior to statistical analysis, lipidomic data was assessed for normality, individual lipid outliers, and sample outliers. Lipid abundances were initially visualized using density plots. This revealed a strong left skew, which is a common hallmark of lipidomic data¹²⁴. To alleviate this skew, abundances were total ion chromatogram (TIC) normalized and \log_2 transformed. Individual lipid outliers were identified by evaluating the coefficient of variation (CV) and interquartile range (IQR) for each group. Acceptable CV values were defined as those within the median CV plus or minus two times the median absolute deviation. CV values outside this range were flagged as outliers. For the IQR, outliers were defined as values less than the first quartile minus two times the IQR or greater than the third quartile plus two times the IQR. Lipids flagged by both methods were removed from downstream analyses, resulting in the removal of 43 out of 665 detected lipids. Sample outliers were evaluated by applying both principal component analysis and hierarchical clustering using a Euclidean distance metric and looking for samples with outlying distributions. Based on this assessment, no samples were excluded.

To identify differentially abundant lipids, statistical analyses were conducted separately for each sex using the Linear Models for Microarray and RNA-seq Data (limma) package¹²⁵. This method was chosen over traditional hypothesis tests, such as the t-test, because it accounts for the correlation structure among individual lipids and

across samples, making it particularly well-suited for “omics” datasets with limited sample sizes. P-values were adjusted using the Benjamini-Hochberg method to control false discovery rates. Two sets of significant lipids were identified based on “stringent” ($p_{\text{adj}} < 0.05$ and $|\log_2\text{fold-change}| > 1$) and “less stringent” ($p_{\text{adj}} < 0.1$ and $|\log_2\text{fold-change}| > 0.5849$) thresholds. Enriched lipid classes were then identified using a chi-squared test ($p_{\text{adj}} < 0.05$ and $\log_2\text{fold-change} > 1$). Asterisks represent chi-square test p_{adj} -values as follows: * $p < 0.05$, ** $p < 0.01$, *** $p < 0.001$, **** $p < 0.0001$. The statistical results for the limma and enrichment analyses can be found in Supplemental Table 2.3. Overlap of significant lipids between males and females was visualized using the eulerr proportional Venn diagram tool¹²⁶. The breakdown of significant lipid classes was visualized using a stacked bar chart generated using the package ‘ggplot2’ (v3.3.6)¹²⁷. A lipid class key can be found in Supplemental Table 2.4.

Statistical analyses

Unless otherwise specified, statistical analyses were performed using a two-tailed Student’s t-test using GraphPad Prism (version 10) software. Outliers were removed using Grubbs’ Test ($\alpha = 0.05$). Data are presented as the mean \pm the standard error of the mean. A p-value of less than 0.05 was considered statistically significant. Asterisks represent p-values as follows: * $p < 0.05$, ** $p < 0.01$, *** $p < 0.001$, **** $p < 0.0001$.

Results

CdCl₂ exposure alters organ weights and organ-to-body-weight percentages

Epidemiological and rodent studies have shown that exposure to Cd can cause reduced body weight³. In our model, CdCl₂ exposure during AYA development is associated with a trend for reduced body weight at PND 120 compared to control mice, although this difference was not statistically significant (Fig. 2.1a-b, Supplementary Table 2.1). Exposure did not significantly affect the raw weights of liver, brain, heart, kidneys, gonadal white adipose tissue (gWAT), retroperitoneal white adipose tissue (rWAT), or quadricep muscles in males or females; however, it did significantly decrease the raw weight of the gonads in males (Fig. 2.1c-d, Supplementary Table 2.1).

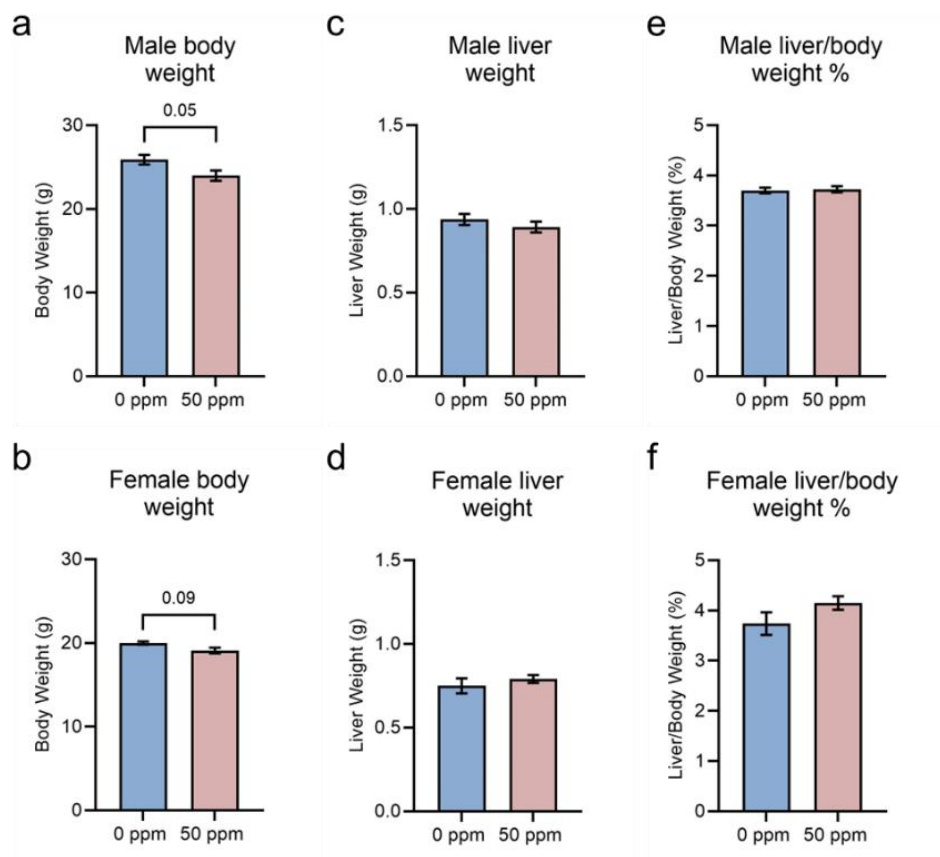


Figure 2.1. Effects of CdCl₂ exposure on body weight, liver weight, and liver-to-body-weight percentage at PND 120. (a) Male and (b) female body weight. (c) Male and (d) female liver weight. (e) Male and (f) female liver-to-body-weight percentage. Abbreviations: CdCl₂, cadmium chloride; PND, postnatal day.

Given the trending decrease in body weight, organ-to-body-weight percentages were also calculated to investigate sparing and wasting phenotypes. Exposed male mice showed significantly increased brain-to-body-weight and kidney-to-body-weight percentages; exposed female mice showed significantly increased brain-to-body-weight and rWAT-to-body-weight percentages but a significantly decreased quadriceps muscle-to-body-weight percentage (Supplementary Table 2.1). Notably, exposure to CdCl₂ does

not affect the liver-to-body-weight percentages in males or females (Fig. 2.1e-f, Supplementary Table 2.1).

CdCl₂ exposure does not induce overt MASLD phenotypes

MASLD is characterized by an elevated abundance of hepatic TAG, and, at more advanced stages, by excess deposition of collagen indicative of fibrosis¹⁰⁵. Histology was performed to qualitatively examine the liver for MASLD phenotypes after CdCl₂ exposure. Exposure did not induce histological changes at PND 120 in either males or females. H&E staining showed both exposure groups have normal microscopic morphology including regularly-shaped hepatocytes with centralized nuclei and well-organized sinusoids (Fig. 2.2a-b). ORO and PSR staining, which stain neutral lipid droplets and collagen fibers, respectively, showed no visual indication of lipid accumulation or collagen deposition in the exposed mice when compared to controls (Fig. 2.2a-b).

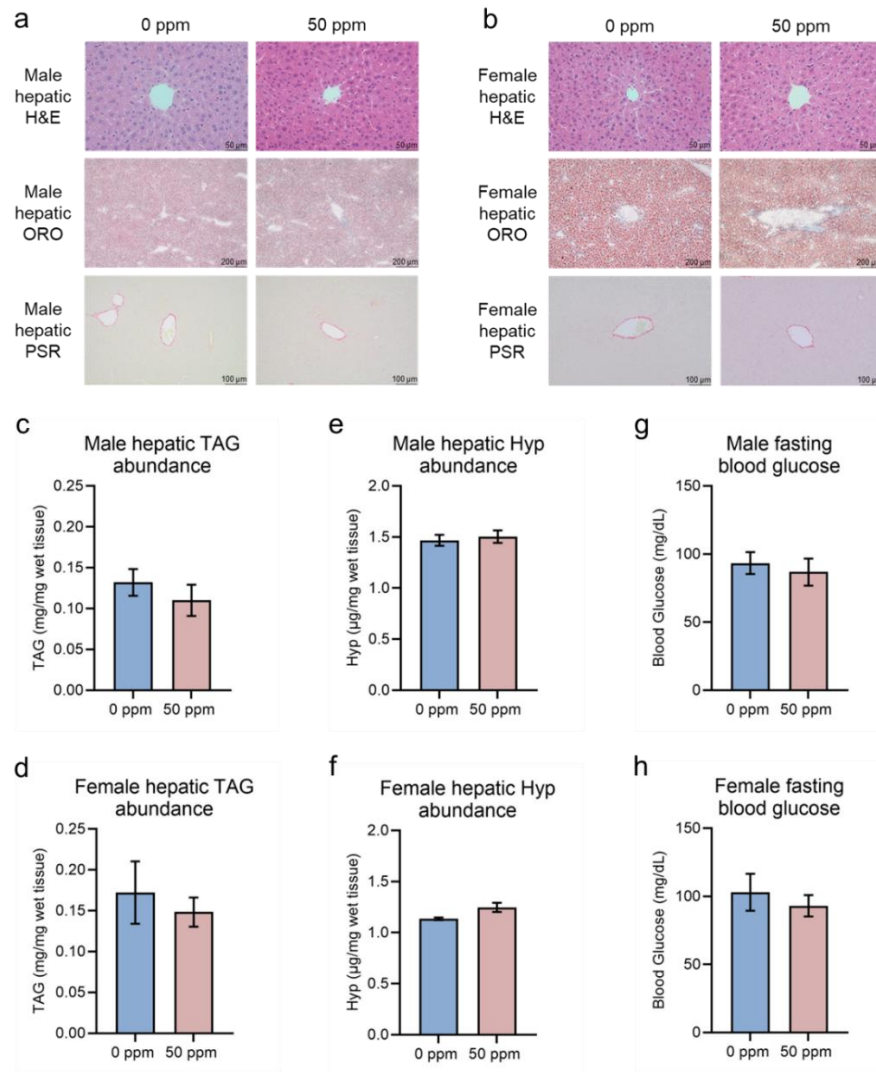


Figure 2.2. Effects of CdCl₂ exposure on histological and biochemical markers of MASLD at PND 120. Representative photomicrographs of (a) male and (b) female liver sections centered around a vein. First row: H&E liver staining (scale bar = 50 μm). Second row: ORO liver staining (scale bar = 200 μm). Third row: PSR liver staining (scale bar = 100 μm). (c) Male and (d) female hepatic TAG abundance. (e) Male and (f) female hepatic Hyp abundance. (g) Male and (h) female fasting blood glucose levels. Abbreviations: CdCl₂, cadmium chloride; PND, postnatal day; H&E, Hematoxylin & Eosin; ORO, Oil Red O; PSR, Picro-Sirius Red; TAG, triacylglyceride; Hyp, hydroxyproline.

Consistent with our observations at the histological level, a TAG assay identified no change in TAG abundance between exposed and unexposed mice, while an assay for Hyp – a major component of collagen fibers – also found no changes (Fig. 2.2c-f, Supplementary Table 2.1). In addition to a fatty liver, individuals with MASLD must have at least one CMRF; therefore, fasting blood glucose levels were measured to screen for metabolic dysfunction and for the presence of a CMRF⁴³. Exposure had no effect on fasting blood glucose levels between exposed and unexposed mice in either sex (Fig. 2.2g-h, Supplementary Table 2.1). Overall, exposure to 50 ppm CdCl₂ during adolescence and young adulthood did not induce overt MASLD phenotypes at PND 120.

CdCl₂ exposure activates hepatic gene expression signatures of MASLD

The manifestation of MASLD is associated with perturbed expression of steatosis-, inflammation-, and fibrosis-related genes^{128–130}. Males exposed to CdCl₂ had marked alterations in the abundance of transcripts associated with fatty acid (FA) uptake and transport including a significant increase in *Pparg*, *Slc27a5* (also known as *Fatp5*), *Cd36*, and *Fabp4* expression and a significant decrease in *Fabp1* expression (Fig. 2.3a, Supplementary Table 2.1). Exposed males also showed significantly increased expression of *Srebf1*, a major driver of *de novo* lipogenesis (DNL), as well as *Dgat2*, an enzyme that catalyzes the final step in TAG synthesis, when compared to the unexposed males (Fig. 2.3a, Supplementary Table 2.1). Notably, exposed female mice presented with only minimal changes in the expression of steatosis genes including a significant increase in *Fabp4* expression; other genes associated with FA uptake and transport and

DNL showed some indications of changes in expression, but these were not statistically significant (Fig. 2.3b, Supplementary Table 2.1).

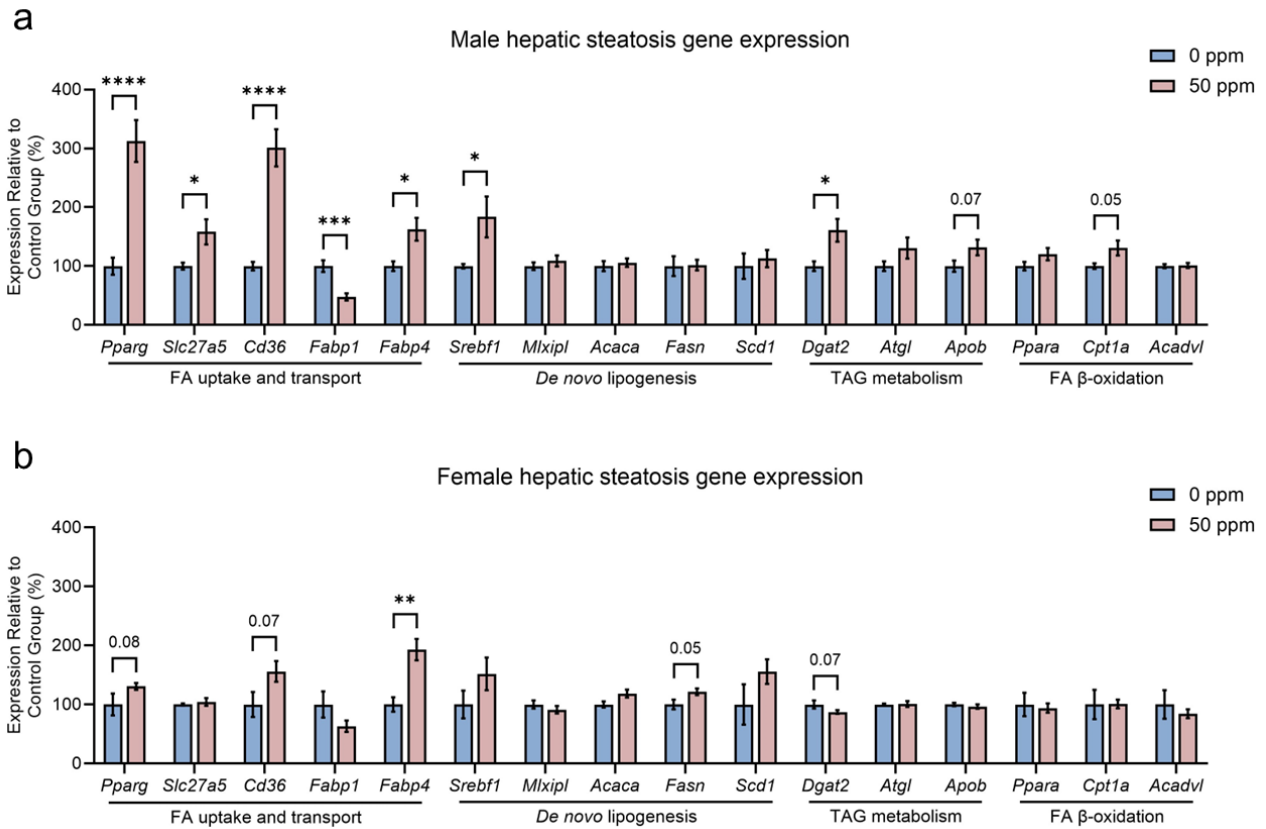


Figure 2.3. Effects of CdCl₂ exposure on hepatic transcription of steatosis markers at PND 120. (a) Male and (b) female hepatic transcript abundance for genes related to steatosis. Left to right: FA uptake and transport genes; *De novo* lipogenesis genes; TAG metabolism genes; FA β -oxidation genes. Asterisks represent p-values as follows: * $p < 0.05$, ** $p < 0.01$, *** $p < 0.001$, **** $p < 0.0001$. Abbreviations: CdCl₂, cadmium chloride; PND, postnatal day; FA, fatty acid; TAG, triacylglycerides.

Exposed males had significantly increased expression of the inflammation markers *Tnfrsf1a*, a membrane-bound receptor for the cytokine TNF α , and *Hmgb1*, a hepatic damage-associated molecular pattern (DAMP) molecule (Fig. 2.4a, Supplementary Table 2.1). Exposed males also showed significantly increased expression of *Tgfb1*, a major driver of fibrosis, as well as *Col6a1*, a component of type VI collagen; two other components of collagen, *Col1a1* and *Col3a1*, showed a non-significant trend towards increased expression (Fig. 2.4a, Supplementary Table 2.1). On the other hand, exposed females had significant decreases in expression of *Il6ra*, a membrane-bound receptor for the cytokine IL6, and *Tgfb1* (Fig. 2.4b, Supplementary Table 2.1). Despite the absence of histological or biochemical markers of MASLD, these results show that exposure to 50 ppm CdCl₂ during adolescence and young adulthood is associated with hepatic gene expression signatures of MASLD at PND 120, a result that is more pronounced in males than females.

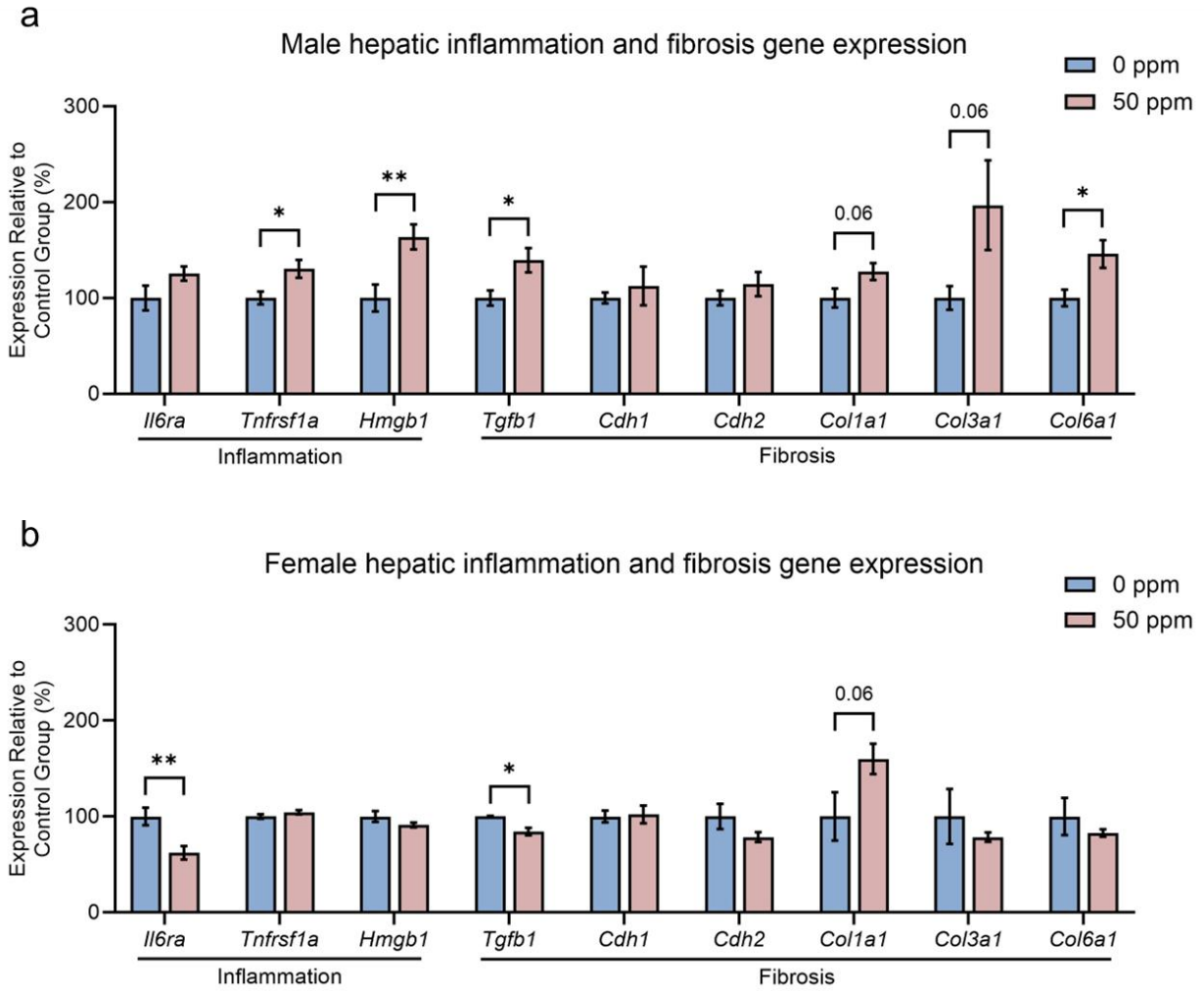


Figure 2.4. Effects of CdCl₂ exposure on hepatic transcription of inflammation and fibrosis markers at PND 120. **(a)** Male and **(b)** female hepatic transcript abundance for genes related to inflammation and fibrosis. Left to right: Inflammation genes; Fibrosis genes. Asterisks represent p-values as follows: **p* < 0.05, ***p* < 0.01. Abbreviations: CdCl₂, cadmium chloride; PND, postnatal day.

CdCl₂ exposure modulates hepatic lipid homeostasis

Considering the changes observed in steatosis gene expression, lipidomics was performed to measure Cd-induced changes in hepatic lipid species abundances at PND 120. A total of 622 lipids were detected for each sex (Supplementary Table 2.3). Of those detected, 12 lipids (1.93%) from 6 classes were found to be significantly altered ($p_{\text{adj}} < 0.05$ and $|\log_2\text{fold-change}| > 1$) in exposed males, and 18 lipids (2.89%) from 9 classes were found to be significantly altered in exposed females. Only 4 of the significantly altered lipids were shared between males and females (Supplementary Table 2.3).

After seeing only a small number of significantly altered lipids for each sex, a less stringent threshold ($p_{\text{adj}} < 0.1$ and $|\log_2\text{fold-change}| > 0.5849$) was leveraged to explore more nuanced changes in lipid species abundances. Of the 622 lipids detected, the less stringent threshold determined that 47 lipids (7.56%) from 14 classes were significantly altered in exposed males, and 74 lipids (11.9%) from 14 classes were significantly altered in exposed females (Fig. 2.5a, Supplementary Table 2.3). There were 22 significantly altered lipids shared between males and females (Fig. 2.5b, Supplementary Table 2.3).

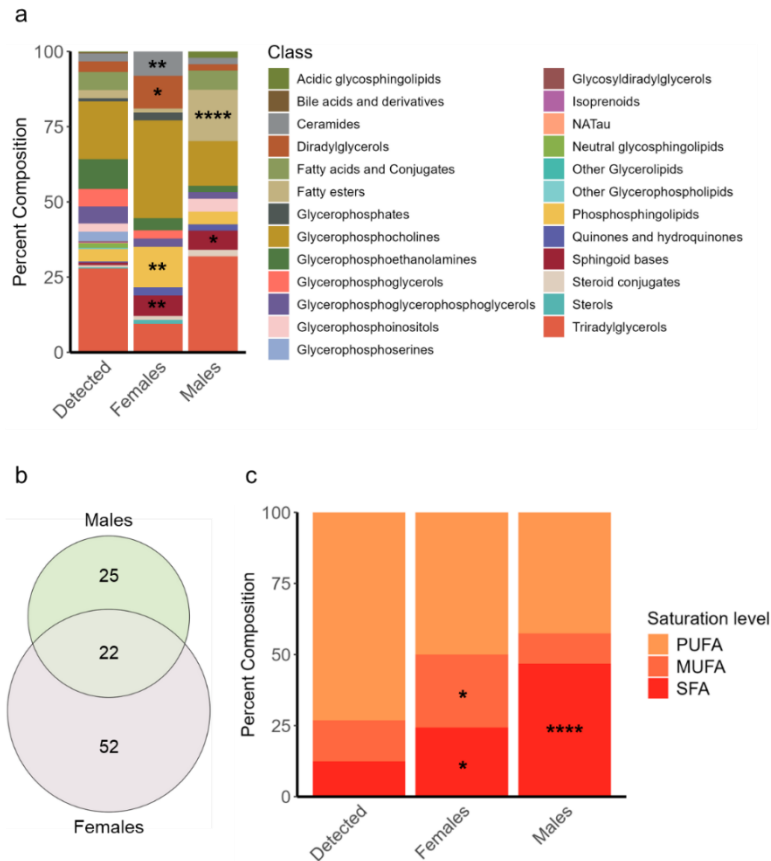


Figure 2.5. Effects of CdCl₂ exposure on hepatic lipids at PND 120. **(a)** Lipid class composition (%) of all detected lipids and of the significant lipids ($p_{adj} < 0.1$ and $|\log_2 \text{fold-change}| > 0.5849$) for males and females. Significantly enriched lipid classes ($p_{adj} < 0.05$ and $\log_2 \text{fold-change} > 1$) are denoted with asterisks. **(b)** Venn diagram showing the number of significant lipids ($p_{adj} < 0.1$ and $|\log_2 \text{fold-change}| > 0.5849$) shared between males and females. **(c)** Fatty acyl saturation level composition (%) of all detected lipids and of the significant lipids for males and females. Significantly enriched saturation levels ($p_{adj} < 0.05$ and $\log_2 \text{fold-change} > 1$) are denoted with asterisks. Asterisks represent chi-square test p_{adj} -values as follows: * $p < 0.05$, ** $p < 0.01$, **** $p < 0.0001$. Abbreviations: CdCl₂, cadmium chloride; PND, postnatal day; PUFA, polyunsaturated fatty acyl; MUFA, monounsaturated fatty acyl; SFA, saturated fatty acyl.

We next looked for shifts in lipid class compositions. Lipid class enrichment analyses were performed using the significantly altered lipid species obtained using the less stringent threshold to determine lipid classes that were significantly enriched in males and females relative to the number of detected lipids for each class. In exposed males, fatty esters and sphingoid bases were significantly enriched ($p_{\text{adj}} < 0.05$ and $\log_2\text{fold-change} > 1$); in exposed females, sphingoid bases, ceramides, phosphosphingolipids, and diradylglycerols were significantly enriched (Fig. 2.5a, Supplementary Table 2.3). Notably, sphingoid bases were significantly enriched in both exposed males and females.

The pathogenesis of MASLD is associated with a shift in the saturation level of lipids from polyunsaturated fatty acyls (PUFAs) and monosaturated fatty acyls (MUFAs) to saturated fatty acyls (SFAs), as DNL primarily creates SFAs^{131,132}. In addition, a diet high in SFAs can further exacerbate the shift by increasing the burden of SFAs in the liver^{133,134}. Lipid saturation level enrichment analyses were performed using the significantly altered lipid species obtained using the less stringent threshold to determine significantly enriched saturation levels of lipids in males and females relative to the saturation levels of all detected lipids. In exposed males, SFAs were significantly enriched ($p_{\text{adj}} < 0.05$ and $\log_2\text{fold-change} > 1$), comprising nearly 50% of all significantly altered lipids (Fig. 2.5c, Supplementary Table 2.3). In exposed females, SFAs and MUFAs were significantly enriched with SFAs making up nearly 25% of significantly altered lipids (Fig. 2.5c, Supplementary Table 2.3). Overall, the lipidomic analyses show that exposure to CdCl₂ during adolescence and young adulthood can perturb lipid homeostasis in males and females at PND 120, including the composition of lipid classes and saturation levels.

CdCl₂ exposure activates hepatic antioxidant gene expression

Oxidative stress is a major factor in the development and progression of MASLD^{135,136}. Exposure to Cd can induce oxidative stress in the liver, triggering a robust antioxidant response to mitigate adverse effects¹³⁷. To determine if the hepatic antioxidant response was activated in exposed mice, we measured mRNA transcripts associated with Cd-induced antioxidants. We found that expression of *Mt1* and *Mt2*, the primary hepatic metallothionein (MT) isoforms, was significantly increased in both males and females exposed to CdCl₂ (Fig. 2.6a-b, Supplementary Table 2.1). Exposed males also showed significantly increased expression of *Gss* and *Gpx1*, enzymes involved in glutathione (GSH) synthesis and detoxification pathways, as well as *Nfe2l2* (also known as *Nrf2*), a transcription factor that regulates antioxidant protein expression, when compared to unexposed controls (Fig. 2.6c, Supplementary Table 2.1). Exposed females, on the other hand, showed a significant decrease in the expression of *Sod1*, an enzyme that neutralizes superoxide radicals, when compared to unexposed controls (Fig. 2.6b, Supplementary Table 2.1). These results show that 50 ppm CdCl₂ exposure during adolescence and young adulthood activates antioxidant response transcripts in males and females at PND 120.

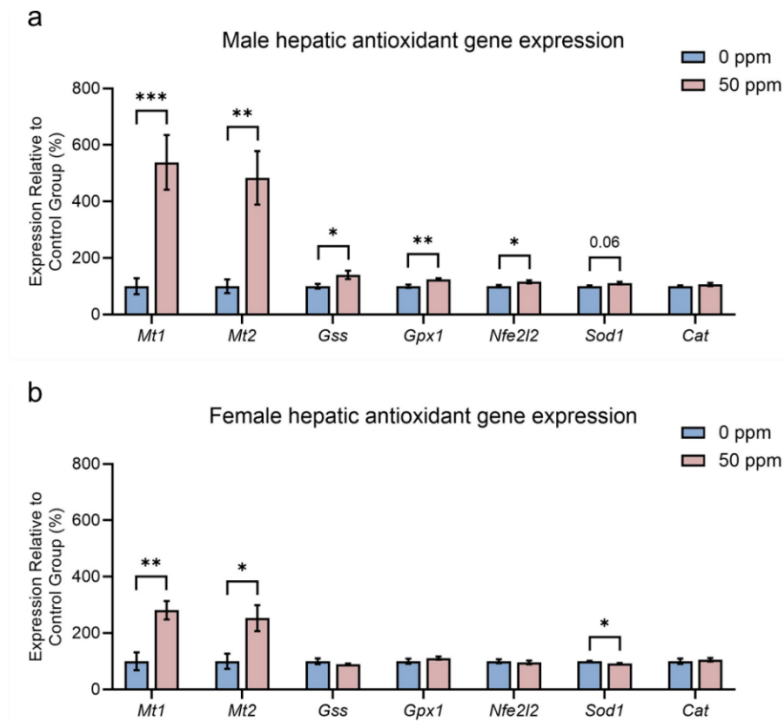


Figure 2.6. Effects of CdCl₂ exposure on hepatic transcription of antioxidant markers at PND 120. (a) Male and (b) female hepatic transcript abundance for genes related to the antioxidant response. Asterisks represent p-values as follows: **p* < 0.05, ***p* < 0.01, ****p* < 0.001. Abbreviations: CdCl₂, cadmium chloride; PND, postnatal day.

CdCl₂ exposure activates hepatic IGN gene expression

We previously showed that exposure to CdCl₂ during perinatal development activates an imprinted gene network (IGN) – a coordinately-expressed group of imprinted and biallelically-expressed genes – in the liver to drive MASLD phenotypes^{66,67}. In our current study of AYA exposure, we noted that *Cd36*, *Col1a1*, *Col3a1*, and *Col6a1*, which are members of the IGN, were all up-regulated in response to Cd (Fig. 2.3, Fig. 2.4). We therefore screened a panel of imprinted and biallelically-expressed IGN members that have previously been shown to be sensitive to Cd exposure⁶⁷. Exposed males showed

significantly increased expression of *Plagl1* (also known as *Zac1*), *Grb10*, *Mest*, *Ccdc80*, *Pcolce*, *Tgfbi*, and *Ak3*, while exposed females showed only a non-significant, trending increase in the expression of *Grb10* and *Ccdc80* (Fig. 2.7a-b, Supplementary Table 2.1). These results show that exposure to Cd during adolescence and young adulthood can significantly upregulate IGN genes in exposed males.

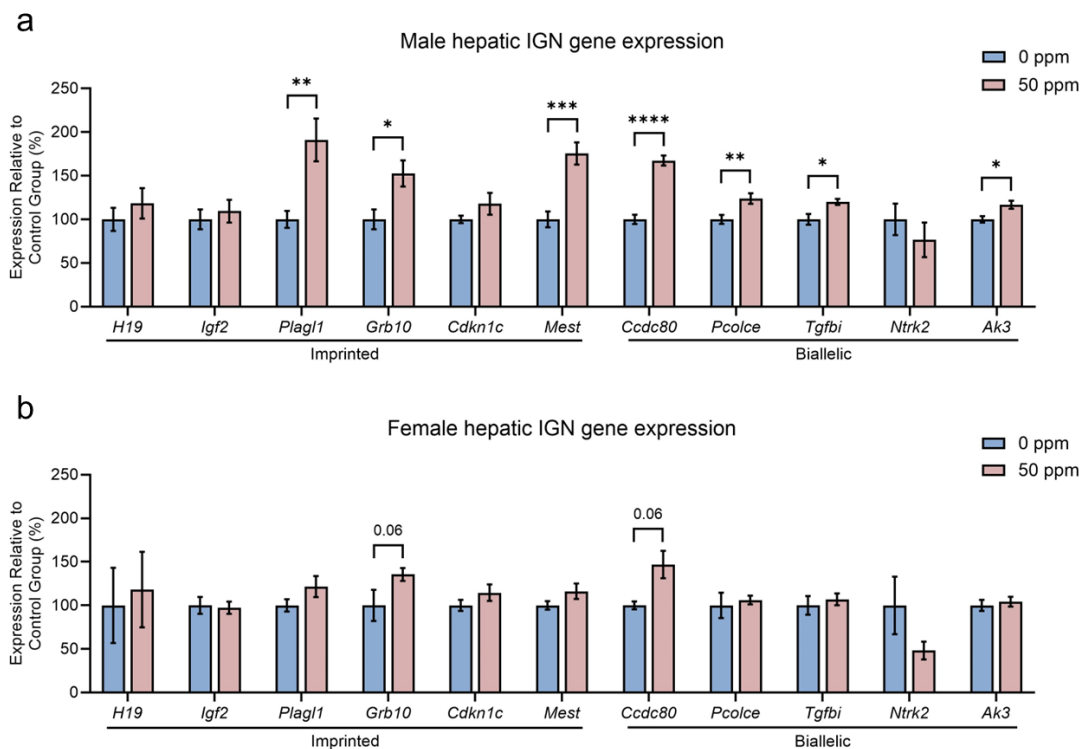


Figure 2.7. Effects of CdCl₂ exposure on hepatic transcription of select IGN members at PND 120. (a) Male and (b) female hepatic transcript abundance for members of the IGN. Left to right: Imprinted genes; Biallelically expressed genes. Asterisks represent p-values as follows: **p* < 0.05, ***p* < 0.01, ****p* < 0.001, *****p* < 0.0001. Abbreviations: CdCl₂, cadmium chloride; IGN, Imprinted Gene Network; PND, postnatal day.

Discussion

In our study, we established a model of AYA Cd exposure to investigate adolescence and young adulthood as a critical window of susceptibility in the development of MASLD. Male and female mice were exposed to 0 or 50 ppm CdCl₂ starting at weaning (PND 21) for 14 weeks until 4 months of age (PND 120) to capture the entirety of adolescence in mice including pre-pubertal, pubertal, and early adulthood development. CdCl₂ exposure did not significantly alter body weight, liver weight, or liver-to-body-weight percentage in males or females; H&E, ORO, and PSR staining of liver tissue showed no qualitative evidence of MASLD phenotypes including no abnormal histomorphology, increase in TAGs, or increase in collagen fibers. Biochemical assays used to quantify intrahepatic TAGs and collagen deposition showed Cd exposure did not significantly increase TAG or collagen fiber accumulation in liver tissue, consistent with the histological observations. In addition, blood glucose levels, one of five CMRFs for MASLD and a key marker for systemic metabolic function, showed no change due to Cd exposure.

Despite observing no overt MASLD phenotypes, CdCl₂ exposed mice showed activation of transcriptional signatures of MASLD in the liver, characterized by the upregulation of key genes related to steatosis, inflammation, and fibrosis. Most notably, markers of FA uptake showed changes in expression including increased expression of *Pparg*, *Slc27a5*, and *Cd36*. Increased lipid uptake is a major driver of hepatic steatosis, as dietary (exogenous) lipids contribute the most to TAG production¹³⁸. There was also a noticeable switch in the transcript abundance of the fatty acid transport genes *Fabp1* and *Fabp4*. *Fabp1*, the isoform primarily active in the liver, was decreased, while *Fabp4*, the

isoform primarily active in adipose tissue, was increased. This shift in expression may be indicative of an adipogenic transformation of the liver, as FABP4 plays a major role in fatty acid transport, lipid accumulation, and adipogenesis in adipocytes¹³⁹. A study in mice found that high-fat diet (HFD)-induced MASLD significantly increased *Fabp4* expression in liver sinusoidal endothelial cells (LSECs), while inhibition of FABP4 decreased liver injury and inflammation¹⁴⁰. In addition to fatty acid uptake and transport, exposed male mice showed an increase in *Srebf1* expression, which encodes a key transcriptional regulator of DNL lipogenesis. Increased DNL is a key feature of MASLD that contributes to TAG synthesis and hepatic steatosis¹³⁸. A study in rats found that oral subacute exposure to Cd increased DNL in the liver which was associated with a significant increase in hepatic SREBP-1C, a protein isoform encoded by *Srebf1*¹⁴¹.

The onset of hepatic inflammation is a crucial step in the progression of MASLD to MASH and fibrosis. Remarkably, males exposed to CdCl₂ had increased *Hmgb1* expression when compared to unexposed males. *Hmgb1* is an important hepatic DAMP produced by injured hepatocytes to activate an inflammatory response¹⁴². A study showed that FFA exposure in cultured hepatocytes increased HMGB1 secretion, as well as proinflammatory cytokines TNF- α and IL-6 secretion; the treatment of the FFA-infused hepatocytes with anti-HMBG1 antibodies significantly reduced TNF- α and IL-6 secretion¹⁴³. Chronic liver injury and inflammation, if unmitigated, typically leads to fibrosis which is largely mediated by TGF- β 1, the TGF- β isoform that is primarily responsible for fibrosis signaling. TGF- β 1 can activate hepatic stellate cells (HSC) or initiate epithelial-to-mesenchymal transition (EMT), leading to the increased production and deposition of collagen fibers and other extracellular matrix (ECM) proteins¹⁴⁴. In our study, exposed

males showed increased expression of *Tgfb1* along with increased expression of the collagen components *Col1a1*, *Col3a1*, and *Col6a1* which may indicate the activation of fibrosis signaling.

The observed changes in lipid metabolism genes prompted a deeper exploration into the effects of Cd exposure on hepatic lipid species abundance and composition of the lipidome. While TAGs are the primary lipid associated with MASLD, the accumulation of other lipid species, especially those that are bioactive, can contribute to hepatic lipotoxicity and the pathogenesis of MASLD¹³¹. In our study, lipidomic analyses showed that CdCl₂ exposure enriched several lipid classes including sphingoid bases in both males and females. Sphingoid bases are the backbone of sphingolipids, which are highly complex lipids that serve as both structural components of cellular membranes and as bioactive signaling molecules in numerous cellular response pathways¹⁴⁵. There is growing evidence that implicates sphingolipids and their metabolites in metabolic diseases including MASLD^{146–148}. Notably, ceramides – precursors to a wide variety of more complex sphingolipids – have received a lot of attention, as their abundance has been found to increase during hepatic steatosis; they can also be predictive markers for the transition of MASLD to MASH^{149,150}. In our study, ceramides were significantly enriched in Cd-exposed females. A different study using adult male rats found that Cd exposure primarily altered hepatic sphingolipid pathways with changes in the metabolism of ceramides being the most significant; *in vitro* experiments using Cd-exposed BRL-3A cells showed that the inhibition of ceramide synthesis attenuated Cd-induced hepatocyte damage including a reduction in pro-apoptotic signaling and oxidative stress¹⁵¹. Taken

together, these data suggest a possible mechanism of action for Cd-induced lipotoxicity via perturbed sphingolipid and ceramide metabolism.

Among the significantly altered lipid species, our analyses also detected a significant enrichment of SFAs in exposed males and SFAs and MUFAs in exposed females. SFAs contain no double bonds in their carbon chains, making them more lipotoxic and disruptive to intracellular membranes than MUFAs and PUFAs, which contain one or more double bond in their carbon chains¹⁵²⁻¹⁵⁴. DNL and a diet high in SFAs drastically increases the presence of SFAs in the liver, leading to a shift in the composition of the hepatic lipidome from unsaturated to saturated which increases lipotoxicity¹³¹⁻¹³⁴. The lipotoxicity associated with increased SFA accumulation includes dysregulated mitochondrial function, increased oxidative stress, impaired autophagy, increased endoplasmic reticulum (ER) stress, and increased pro-apoptotic signaling^{152,153}. A study using a streptozotocin with high-fat diet (STAM) mouse model of MASH showed CdCl₂ exposure significantly exacerbated MASH phenotypes and impaired FA desaturation, leading to increased SFA accumulation; the increased SFAs were associated with heightened inflammation and cell death¹⁵⁵. Another study using AML12 cells found Cd exposure in conjunction with SFA exposure increased pro-inflammatory M1 polarization of macrophages in the liver; the results observed *in vitro* were recapitulated *in vivo* leveraging the same STAM MASH model with CdCl₂ exposure as the previous study¹⁵⁶. Additional research is needed to better understand the role SFAs play in Cd-induced lipotoxicity in AYAs.

Antioxidants play an important role in maintaining redox balance by eliminating harmful reactive oxygen species (ROS) and reducing oxidative stress¹⁵⁷. Although the

liver has a robust antioxidant defense system in place to combat ROS, acute and chronic exposure to Cd can induce oxidative stress by overwhelming and depleting key hepatic antioxidants^{137,158}. Oxidative stress is a major driver of MASLD; therefore, it is likely Cd-induced oxidative stress contributes substantially to the onset and progression of MASLD^{135,136}. In our study, we assessed several transcripts – including genes related to MT, GSH, and antioxidant enzymes – to determine if CdCl₂ exposure could perturb the hepatic antioxidant response. Notably, both exposed males and females had significantly increased MT expression, while males alone had increased GSH-related gene and antioxidant enzyme expression, indicating males may have experienced more oxidative stress than females. GSH and MT are considered the primary lines of defense against Cd toxicity; Cd first complexes with GSH to be neutralized and then is sequestered by MT for long-term storage¹³⁷. Additional antioxidant enzymes are produced to eliminate ROS and free radicals created by mitochondrial dysfunction and essential metal displacement¹³⁷. With the exception of *Sod1* in females, we did not detect a significant decrease in the expression of any antioxidant genes. These results suggest the antioxidant defense system was activated at the gene expression level. More experiments examining antioxidant protein concentrations, mitochondrial function, lipid peroxidation products, and essential metals abundances will provide additional insight into the overall redox status of the liver in our model.

We previously showed that CdCl₂ exposure during perinatal development is sufficient to program MASLD in the livers of juvenile mice, and that this is associated with activation of a coordinately-regulated network of imprinted and biallelically-expressed genes, the IGN, in the liver⁶⁷. Artificial activation of the IGN through over-expression of

Plagl1 – an imprinted member of the IGN and its master regulator – in cultured hepatocytes induced intracellular lipid accumulation and activated profibrotic signaling pathways^{66,67}. Strikingly, several of the steatosis and fibrosis genes that were significantly upregulated in males in our model of peripubertal exposure are members of the IGN; therefore, we screened a panel of IGN members that were perturbed by CdCl₂ exposure in the perinatal study to assess the IGN after AYA Cd exposure⁶⁷. We found additional IGN members that were significantly activated in the exposed males but not the exposed females including both imprinted (*Plagl1*, *Grb10*, and *Mest*) and biallelically-expressed (*Ccdc80*, *Pcolce*, *Tgfb1*, and *Ak3*) genes. All of these upregulated genes have been implicated in hepatic steatosis, inflammation, or fibrosis pathways^{159–168}. For example, increased expression of *Mest* – one of the most significantly altered IGN panel genes in the exposed males – has been shown to attenuate carbon tetrachloride (CCl₄)-induced hepatic collagen deposition in rats and has also been found to decrease lipid accumulation in 3T3-L1 mouse adipocytes, indicating *Mest* may be a useful target for impairing MASLD progression^{161,162}. Overall, these findings provide evidence that the IGN may play a role in driving MASLD after Cd exposure during AYA development.

Finally, the limitations of this study should be discussed. First, our mouse model may not perfectly recapitulate the effects of Cd exposure on the liver and metabolic homeostasis in humans. Second, the lack of any collection timepoints beyond PND 120 allows only for speculation of potential MASLD manifestation later in life. Future studies using this dosing paradigm will leverage additional time points to determine if mice exposed to CdCl₂ during adolescence and young adulthood have more advanced MASLD phenotypes during later adulthood. Lastly, conclusions drawn from this study rely heavily

on changes in transcript abundances; therefore, future studies will include experiments that quantify protein abundances in tandem with transcript abundances.

Conclusions

The results of our study show that adolescence is a critical window of susceptibility to Cd-induced MASLD signatures in young adult mice, as evidenced by the activation of genes related to steatosis, inflammation, and fibrosis in the liver. Additionally, the detected changes in the composition and saturation of bioactive hepatic lipids is suggestive of lipotoxicity, a key contributor to the development and progression of MASLD. We also found that members of the IGN – which have been implicated in the pathogenesis of MASLD – were upregulated in exposed male mice. We hypothesize that the IGN may be activated by Cd exposure during critical windows of susceptibility to drive MASLD. Additional studies investigating the perturbed lipids and IGN members will be necessary to explore these underlying mechanisms empirically.

Acknowledgements

The authors thank Lily Wai of the UNC-CH PSC for expert technical assistance with the histology. The authors also thank members of the Cowley Lab for their helpful discussion of the manuscript.

CHAPTER 3:

Systemic Deletion of the Imprinted Long Non-Coding RNA *H19* does not Mitigate the Developmental Cadmium Exposure-Induced Transcriptional Signatures of MASLD in Juvenile Mice

The following chapter will be submitted to a peer-reviewed journal.

Logan Dameris^{1,2,3}, Hannah Klossner¹, Rebecca Lichtler^{1,3}, Sierra D. Riegl^{1,2,3}, Claudia Gebert⁴, Karl Pfeifer⁴, and Michael Cowley^{1,2,3}

¹Department of Biological Sciences, North Carolina State University, Raleigh, NC, 27695, USA.

²Toxicology Program, North Carolina State University, Raleigh, NC, 27695, USA.

³Center for Human Health and the Environment, North Carolina State University, Raleigh, NC, 27695, USA.

⁴Division of Intramural Research, Eunice Kennedy Shriver National Institute of Child Health and Human Development (NICHD), National Institutes of Health (NIH), Bethesda, MD, USA.

Abstract

The heavy metal cadmium (Cd) has been denoted a top ten chemical of major public health concern by the World Health Organization (WHO), given its ubiquity in the environment, long biological half-life, and association with numerous adverse health effects including liver disease. We have demonstrated that exposure to Cd during perinatal development is sufficient to program metabolic dysfunction-associated steatotic liver disease (MASLD) – the most prevalent chronic liver disease in the world – in juvenile mice. The manifestation of MASLD is also associated with the activation of the imprinted gene network (IGN), a group of coordinately-regulated imprinted and biallelically-expressed genes, in the liver. One of the most significantly upregulated imprinted genes in our model, *H19*, has been previously implicated in the pathogenesis of MASLD. *H19* encodes a long non-coding RNA (lncRNA) that activates transcriptional programs underlying hepatic steatosis, fibrosis, and metabolic homeostasis. We therefore hypothesized that systemic deletion of *H19* would protect against developmental Cd-induced MASLD. To test this hypothesis, wild type and *H19* knockout mice were exposed to 0 or 30 ppm CdCl₂ during perinatal development and then collected at PND 0 or PND 21. We found that Cd exposure was sufficient to induce molecular but not biochemical signatures of MASLD at PND 21. Notably, the deletion of *H19* did not protect against the activation of steatosis and fibrosis genes in our model. We also showed that members of the IGN – including a dramatic increase in *Igf2* expression – were activated in mice perinatally exposed to Cd at PND 21. Overall, our results do not support a role for *H19* in programming MASLD at PND21 in response to developmental Cd exposure.

Introduction

Cadmium (Cd) is a non-essential heavy metal found ubiquitously in the Earth's crust. While natural processes contribute largely to its presence in the environment, human activities have significantly increased the burden of Cd in the atmosphere, water, and soil³. This is especially true in urban areas, where anthropogenic sources of Cd are more prevalent¹⁶⁹. Human exposure to Cd occurs primarily through the consumption of contaminated food items; leafy green vegetables, in particular, have greater levels of Cd, as they readily accumulate Cd from the soil⁹⁴. Individuals who smoke tobacco products, reside near Cd-emitting industries, or participate in occupations that handle Cd are at an even greater risk of exposure³. Cd is not well excreted after exposure and can persist in tissues, especially the kidneys and liver, for years or even decades¹⁷⁰. Chronic exposure to Cd is associated with numerous adverse health effects, impacting nearly every major organ system in the body^{3,171}. Given its pervasiveness in the environment, long biological half-life, and broad negative health effects, the World Health Organization (WHO) has designated cadmium (Cd) a top ten chemical of major public health concern.

Human and rodent data have shown Cd exposure can induce hallmarks of metabolic dysfunction-associated steatotic liver disease (MASLD)^{99–102}. MASLD is the most common chronic liver disease, burdening nearly 34% of adults and 17% of adolescents in the United States^{48,49}. It is characterized by having increased lipid accumulation (steatosis) in hepatocytes, at least one of five possible cardiometabolic risk factors (CMRFs), and no history of significant alcohol consumption⁴³. The simple steatosis associated with MASLD is often considered benign; however, if allowed to persist, MASLD has the potential to cause hepatic inflammation and fibrosis and progress

to metabolic dysfunction-associated steatohepatitis (MASH)¹⁰⁵. This, ultimately, can lead to cirrhosis, hepatocellular carcinoma (HCC), and even extrahepatic manifestations, all of which require significant medical intervention to resolve¹⁰⁷. Despite a precedence existing for Cd-induced MASLD, there has been a paucity of research investigating the effects of prenatal and early postnatal (perinatal) Cd exposure on the incidence of MASLD during childhood and adolescence. This is especially concerning, given Cd has been detected in both fetal cord blood and breast milk with significantly higher concentrations being measured in women who smoked throughout their pregnancy^{36,172,173}.

To address this knowledge gap, we previously created a mouse model of developmental Cd exposure and found that juvenile mice perinatally exposed to 50 ppm cadmium chloride (CdCl₂) had signatures of MASLD at postnatal day (PND) 21⁶⁷. This timepoint coincides with the transition from the early postnatal to adolescence stage in mouse development. In addition, juvenile mice at PND 21 concomitantly had aberrant activation of a coordinately-regulated network of imprinted and biallelically-expressed genes in the liver, the imprinted gene network (IGN)⁶⁷. Imprinted genes – defined by their expression from either the paternal or maternal allele – are particularly sensitive to environmental stressors during perinatal growth and development^{74–78}. Evidence from our lab has shown that overexpression of *Plagl1* (also known as *Zac1*) – the master regulator of the IGN – in *in vivo* and *in vitro* models can induce markers of MASLD^{66,67}. Among the IGN genes upregulated at PND 21, the imprinted gene, *H19*, had one of the largest fold changes in expression in both sexes⁶⁷. *H19* is maternally-expressed and encodes a long non-coding RNA (lncRNA) that negatively regulates growth and cellular proliferation during gestational development⁸⁶. Strikingly, the aberrant expression of *H19* has been

implicated in the pathogenesis of MASLD; these studies reveal *H19* can activate transcriptional networks underlying hepatic steatosis and fibrosis and regulate metabolic homeostasis and liver remodeling^{88–92}.

In this study, we aimed to determine if the ablation of *H19* can protect against the onset or progression of perinatal Cd exposure-induced MASLD, making it a potential therapeutic target. We leveraged a novel *H19* knockout mouse model of developmental Cd exposure to examine the liver for histological, biochemical, and molecular signatures of MASLD, as well as for the activation of the IGN at PND 0 and PND 21. The results of this study offer a better understanding of the molecular mechanisms underlying Cd-induced liver disease and provide new evidence of *H19*'s role in regulating metabolic homeostasis after exposure to a pertinent environmental stressor.

Materials and methods

Generation of *H19*^Δ mouse model

All mouse studies were performed according to NIH and PHS guidelines and only after protocols were reviewed and approved by the Eunice Kennedy Shriver National Institute of Child Health and Human Development Animal Care and Use Committee.

To generate conditional *H19*^{fllox/+} mutant mice, loxP sequences (ATA ACT TCG TAT AGC ATA CAT TAT ACG AAG TTA T) were inserted at +3,156-bp 5' and at -1,033-bp 3' of the mouse *H19* gene using CRISPR/Cas9 technology¹⁷⁴. These sites were positioned to remove the entire *H19* gene body while leaving the nearby *H19/Igf2* imprinting control region (ICR) intact. Guide RNAs (gRNAs) were designed using the open access software crispr.mit.edu. Only gRNAs with a score above 80 were chosen to

minimize off-target mutations. The designed sense- and antisense gRNAs targeted 20-bp at the 5' end (GTC CGT CAG TAT CAT AAC TT on mouse chr. 7, 142,579,177-bp - 142,579,196-bp, UCSC Genome Browser) and 3' end (CCT TGC AGT AAG GCT CGT AA on mouse chr. 7, 142,574,970-bp – 142,574,989-bp, UCSC Genome Browser) and carried the adapter sequences CACC and AAAC, respectively. Next, the gRNAs were cloned into the vector pX330-U6- Chimeric_BB-CBh-hSpCas9 (Addgene, #42230). The repair plasmid was generated by cloning gBlocks fragments (Integrated DNA Technologies, IDT) spanning the entire *H19* gene from the *Xba*I site 5' and the *Sa*II site 3' of *H19* into the Bluescript SK vector using the In-Fusion HD Cloning kit (Takara Bio USA Inc., #639650). Prior to nucleofection of mouse embryonic stem cells (ES cells) both plasmids were sequenced to ensure correct targeting and mutagenesis. Mouse R1 ES cells were subject to nucleofection with the gRNAs and repair plasmid using the Amaxa Mouse Embryonic Stem Cell Nucleofector Kit (Lonza, #VPH-1001). ES cell clones were picked 7-8 days post nucleofection and expanded. Correctly targeted clones were identified by PCR genotyping and injected into B6(Cg)-*Tyr^{c-2J}/J* blastocysts (The Jackson Laboratory, #000058)^{175,176}. To genotype correctly targeted ES cell clones, we used the primer sequences 5'-CAA CCA CCA CAA GGT GAC AG-3' and 5'-TGG CAG ATC CTC AGC CTA GT-3' at the 5' end and 5'-GTC CTG CCT GGA TGA CTC TG-3' and 5'-TAC GCA GCC TCA TGT GTA GC-3' at the 3' end.

To generate mice carrying a systemic deletion of the *H19* gene (*H19*^Δ), *Ella-cre* transgenic female mice (The Jackson Laboratory, #003724) were mated with *H19*^{fllox/+} males. Female offspring carrying the *H19*^{+Δ} deletion were then mated with C57BL6/J (The Jackson Laboratory, #000664) males to breed out the Cre. After generating *H19*^{Δ/+}

female offspring, $H19^{\Delta/+}$ females were backcrossed ten times to B6.129(Cg)-Gt(ROSA)26Sor^{tm4(ACTB-tdTomato,-EGFP)Lox/J} (The Jackson Laboratory, #007676) males to generate $H19^{\Delta/+}$ mice with the ROSA^{mT/mG} reporter in the paternal allele. Primer sequences to genotype $H19^{\Delta}$ animals were 5'-GTA TGG CAA GGG GTA TGG TG-3' and 5'-TGG CAG ATC CTC AGC CTA GT-3' to detect the wild type (WT) allele (511-bp) and 5'-GTA TGG CAA GGG GTA TGG TG-3' and 5'-ACC ATG GGC CTC TTT ATG TG-3' to detect the $H19$ deletion allele (425-bp).

Developmental cadmium exposure mouse model

All animal work was authorized by the NCSU Institutional Animal Care and Use Committee under protocols 19-049-B and 22-162-B. Experiments were performed in accordance with the Guiding Principles in the Use of Animals in Toxicology. Mice were maintained on a 14-h/10-h light/dark cycle at $22 \pm 4^{\circ}\text{C}$ and 30%–70% humidity and were housed in Green Line IVC Sealsafe cage housing systems (Tecniplast). Drinking water was filtered via reverse osmosis (RO) (Millipore RiOs Essential RO water purification system).

Three male $H19^{\Delta/+}$ mice with the ROSA^{mT/mG} reporter in the paternal allele were delivered to the North Carolina State University (NCSU) Toxicology Animal facility. After acclimation, the males were mated with C57BL6/J (The Jackson Laboratory, #000664) females to generate $H19^{+/Δ}$ males for colony maintenance and to breed out the ROSA^{mT/mG} reporter. Sanger sequencing was performed by the NCSU Genomic Sequencing Laboratories (GSL) using genomic DNA isolated from 2 mm ear tissue punches of $H19^{+/Δ}$ and $H19^{+/+}$ mice to confirm the location of the deletion in $H19^{\Delta}$ mice.

The sequencing primer sequence 5'-CAA CCA CCA CAA GGT GAC AG-3' was used for both genotypes.

To establish a maternal body burden of Cd, five-week-old, *H19*^{+Δ} dams received 0 ppm or 30 ppm CdCl₂ (Sigma-Aldrich, 202908) in drinking water *ad libitum* for five weeks prior to mating, throughout mating and gestation, and until PND 10. A prior study performed by our lab leveraging the developmental Cd exposure mouse model exposed dams to 50 ppm CdCl₂ in drinking water; however, this resulted in the death of nearly 50% of offspring by PND 21⁶⁷. A lower dose of 30 ppm CdCl₂ was instead adopted to avoid significant mortality in offspring mice while still sufficiently manifesting MASLD phenotypes by PND 21. In this study, the lower dose did not significantly alter dam water consumption, chow consumption, weight gain, litter sizes, or the survivability of offspring by PND 21 (Supplementary Table 3.1). Mice were fed a standard-source AIN-93G Growing Rodent Diet (Research Diets Inc., D10012G) to standardize trace metal exposure from chow. At the end of the five weeks, the *H19*^{+Δ} dams were mated with age matched unexposed C57BL/6J males to generate male and female offspring with a 1:1 ratio of *H19*^{+/+} and *H19*^{Δ/+}. Since *H19* is a maternally-expressed gene, deletion on the maternal allele is equivalent to a null genotype; therefore, *H19*^{Δ/+} mice are herein referred to as knockout (KO) mice; *H19*^{+/+} mice are herein referred to as wild type (WT) mice.

Male and female offspring were sacrificed at PND 0 (day of birth) and PND 21. At PND 0, pups were weighed and then euthanized via decapitation. Blood glucose levels of trunk blood were tested using a blood glucose meter. The liver, brain, heart, kidneys, quadricep muscles, and a 4 mm tail snip (for genotyping) were weighed and flash frozen on dry ice. Prior to freezing, the liver was sectioned into four pieces. One of the four pieces

was soaked in 4% paraformaldehyde (PFA) for 24 hours at 4°C and then stored in 70% ethanol for histological analyses. At PND 21, pups were fasted for 6 hours early in the morning, weighed, and then euthanized by decapitation. Blood glucose levels of trunk blood were determined using a blood glucose meter. Trunk blood (approximately 20 µL) was also collected for metallomics. The liver, brain, heart, kidneys, quadriceps muscles, gonadal white adipose tissue (gWAT), retroperitoneal white adipose tissue (rWAT), and a 2 mm ear punch (for genotyping) were weighed and flash frozen on dry ice. Prior to freezing, the liver was sectioned into eight pieces. A portion of the median lobe was soaked in 4% PFA for 24 hours at 4°C and then stored in 70% ethanol for histological analyses. All collections were completed by noon each day.

After all collections were completed, pups were genotyped using tail (PND 0) or ear (PND 21) tissue genomic DNA isolated via the HotSHOT method¹⁷⁷. A three-primer PCR genotyping assay was performed by leveraging a shared forward primer (5'-CAA CCA CCA CAA GGT GAC AG-3') with a unique WT reverse primer (5'- TGG CAG ATC CTC AGC CTA GT-3) and unique KO reverse primer (5'-GCT GCC TAC TTA CGA GCC TA-3) to produce a 218 bp WT PCR product or 149 bp KO PCR product. The PCR products were loaded onto a 1.3% agarose (Apex BioResearch Products, 20-102) gel and ran for 40 min at 160 V for visualization. WT mice have a single gel band per lane, while KO mice have two gel bands per lane. After genotyping, mice were sorted into 4 groups per sex: 0 ppm WT, 0 ppm KO, 30 ppm WT, and 30 ppm KO. Male and female mice were processed, analyzed, and reported separately. Unless stated otherwise, the number of mice used for each analysis and the corresponding statistical results can be found in Supplementary Table 3.2. If a treatment group contained more mice than needed

for a specific analysis, mice were selected by calculating the group's median liver weight and then choosing mice with the smallest absolute difference from the group's median. No more than three mice per litter were used in any analysis to control for possible litter effects.

Metallomics

Trunk blood was collected and delivered to the NCSU Molecular Education, Technology and Research Innovation Center (METRIC). Approximately 20 mg of blood was aliquoted into 15 mL digestion tubes (SCP Science) and digested roughly according to procedures described previously¹⁷⁸. Briefly, to the 20 μ L of blood, 200 μ L of concentrated nitric acid (SCP Science) and 25 μ L of a 10,000 ppb internal standard (containing germanium, indium, yttrium, and praseodymium) were added. This mixture was heated to 95°C for 30 min (with a 15 min ramp up to temperature) and then allowed to cool to room temperature. Notably, digestion times were decreased compared to previous methods due to the low volumes of samples used here. After the initial heating and cooling step, 100 μ L of 30% hydrogen peroxide (SCP Science Plasma Pure Plus) was added and the mixture was again heated to 95°C for 30 min (again with a 15 min ramp to temperature). After cooling to room temperature, 100 μ L of additional concentrated nitric acid was added to each sample which were then diluted to the 5 mL mark with ultrapure water (Elga PURELAB Flex Water Purification System) and vortexed. Samples were analyzed on a mass spectrometer (Thermo iCAP RQ ICP-MS) using triplicate main runs and incorporating an autosampler (ESI SC-2DX autosampler). The instrument was optimized and calibrated daily for all elements analyzed. Calibration

curves ranged from 0.01 ppb to 500 ppb. Limits of quantitation (LOQ) were determined on a batch-by-batch basis, and results below the LOQ are not reported as quantitative values.

Biochemical assays

A portion of the left liver lobe at PND 21 was used to perform the triacylglyceride (TAG) assay. Briefly, liver tissue was submerged in a 3 M KOH (dissolved in 65% ethanol) solution in a 1:1 ratio with tissue weight (mg) for digestion at 70°C for 60 min in a heat block. Every 20 minutes, the samples were removed from the heat block, vortexed briefly, and then placed back into the heat block. At the end of the 60 min, samples were removed from the heat and left to sit overnight at room temperature. The following day, each sample was brought to a total volume of 250 μ L using 2 M Tris-HCl (pH 7.5) and then vortexed briefly. The samples were then diluted 1:151 in 2 M Tris-HCl (pH 7.5). A 0, 10, 50, 100, 150, and 200 mg/dL dilution series was created using glycerol (Sigma Aldrich Glycerol Standard Solution, G7793) dissolved in 2 M Tris-HCl (pH 7.5) for standards. 100 μ L of each standard and sample was added to a 96-well plate and then 150 μ L of the TAG detection reagent (Thermo Scientific Triglycerides Reagent, TR22421) was added to each well. The standards and samples were run in duplicate. Prior to measuring the absorbance at 550 nm using a microplate reader (BMG Labtech FLUOstar Omega), the plate was incubated at 35°C for 10 min. The outputs for the glycerol standards were plotted in Microsoft Excel to calculate the equation of the line of best fit. The equation (factoring in the dilutions) was used to determine the TAG concentration (mg/dL) in each sample.

A portion of liver at PND 0 or a portion of the median liver lobe at PND 21 was used to perform the hydroxyproline (Hyp) assay (QuickZyme Sensitive Tissue Collagen Assay Kit, QZBTISCOL) according to the manufacturers' instructions.

RNA isolation

Total RNA was obtained from a portion of liver at PND 0 or from a portion of the right liver lobe at PND 21 using a mini bead mill homogenizer (VWR). The RNA was purified (Macherey-Nagel NucleoSpin RNA Mini Kit, 740955) according to the manufacturer's instruction and then quantified using a spectrophotometer (Thermo Fisher Nanodrop 2000). RNA quality was determined using the 260/280 and 260/230 ratios of absorbance from the spectrophotometer.

qRT-PCR

500 ng of total RNA was used to synthesize first-strand cDNA (Promega M-MLV Reverse Transcriptase, M170) according to the manufacturer's instructions. The cDNA was diluted to 1/10 for each sample. A 1/5, 1/10, 1/20, 1/40, and 1/80 dilution series was created using pooled cDNA for standards. Water served as a no template control (NTC) to ensure there was no contamination. Quantitative real-time (qRT)-PCR was executed using SYBR Green chemistry (Bio-Rad SsoAdvanced Universal SYBR Green Supermix, 1725271) with a real-time PCR system (Thermo Fisher QuantStudio 3) in 96-well plates. The qRT-PCR cycling conditions were as follows: hold stage at 95°C for 30 s; PCR stage at 40 cycles of 95°C for 15 s and 60°C for 30 s; melt curve stage at 95°C for 15 s, 60°C

for 60 s, and 95°C for 1 s (dissociation). The NTC, standards, and samples were run in duplicate for each reaction. Primer sequences can be found in Supplementary Table 2.2.

Dissociation curves confirmed that target primers amplified only a single qRT-PCR product. The standard dilutions were plotted in Microsoft Excel to monitor amplification efficiencies. *Actb* was used as the housekeeping gene for the PND 0 and PND 21 samples and was not differentially expressed between treatment groups. Target gene expression was analyzed using the $\Delta\Delta C_t$ method¹²². Expression data are visualized as a percentage of the 0 ppm WT group for each sex.

Statistical analyses

Unless otherwise specified, datasets were analyzed with an ordinary two-way analysis of variance (ANOVA) using GraphPad Prism software. Outliers were removed prior to ANOVA testing using Grubbs' Test ($\alpha = 0.05$). The CdCl₂ concentration ("Cadmium") and genotype of the mice ("Genotype") were the two independent variables. Šídák's multiple comparison tests were performed between relevant groups when the ANOVA found a significant effect. Asterisks represent significant multiple comparison p-values for the Cadmium factor as follows: * $p < 0.05$, ** $p < 0.01$, *** $p < 0.001$, **** $p < 0.0001$. Pound signs represent significant multiple comparison p-values for the Genotype factor as follows: # $p < 0.05$, ## $p < 0.01$, ### $p < 0.001$, #### $p < 0.0001$. Data are presented as the mean \pm the standard error of the mean. Dam water consumption, dam food consumption, dam body weight, and survival percentage of PND 21 litters were analyzed using a repeated-measures two-way ANOVA with the Geisser-Greenhouse correction.

The CdCl₂ concentration and the week or postnatal day were the two independent variables. 0 ppm and 30 ppm CdCl₂ litter sizes were analyzed using an unpaired t-test.

Results

Perinatal exposure to Cd and systemic deletion of *H19* elicit morphometric effects at PND 21

The deletion of *H19* in the livers of KO offspring at PND 21 was verified by performing qRT-PCR using bulk liver tissue which confirmed that *H19* was significantly decreased in male and female KO offspring compared to their WT counterparts (Fig. 3.1A-B). Previous studies have shown that a reduction in *H19* expression can perturb gross phenotypes in mice^{179,180}. To determine if the ablation of *H19* had similar effects in our model, body weights and the absolute and relative organ weights of the liver, brain, heart, kidneys, gonadal white adipose tissue (gWAT), retroperitoneal white adipose tissue (rWAT), and quadricep muscles were assessed at PND 21. Males but not females presented with significantly increased body weights (Fig. 3.1C-D). Males and females both had unchanged liver weights, while males alone showed a significant decrease in liver-to-body-weight percentage (Fig. 3.1E-H). The effect of *H19* ablation on the absolute and relative weights of the other organs measured in this study can be found in Supplementary Table 3.2.

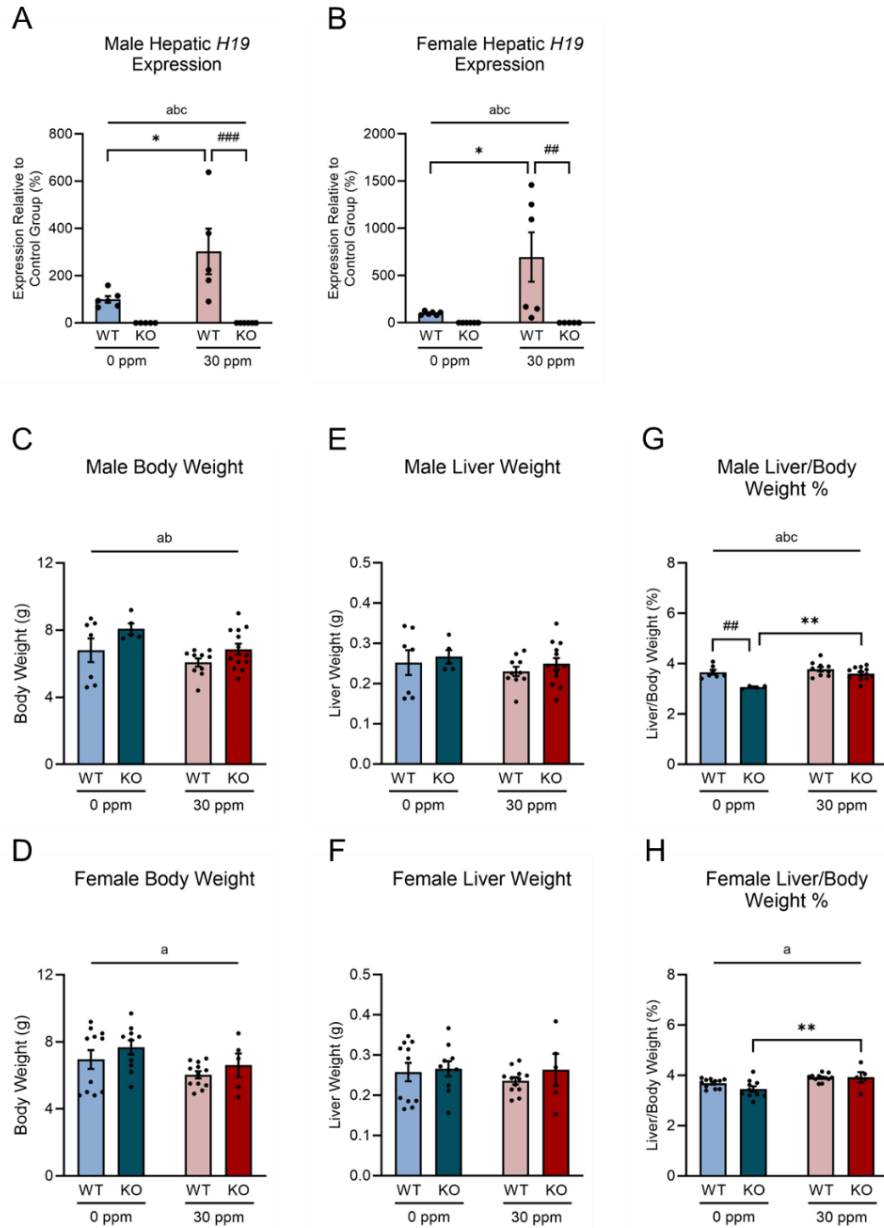


Figure 3.1: Effects of perinatal Cd exposure and systemic *H19* ablation on hepatic *H19* expression, body weight, liver weight, and liver-to-body-weight percentage mice at PND 21. (A,B) Male and female *H19* transcript abundance. (C,D) Male and female body weight. (E,F) Male and female liver weight. (G,H) Male and female liver-to-body-weight percentage. Lowercase letters represent significant two-way ANOVA factors as follows: a, Cadmium effect; b, Genotype effect; c, Interaction effect. Asterisks represent significant

Šídák's multiple comparison test p-values for the Cadmium factor as follows: * $p < 0.05$, ** $p < 0.01$. Pound signs represent significant Šídák's multiple comparison test p-values for the Genotype factor as follows: ## $p < 0.01$, ### $p < 0.001$. Abbreviations: CdCl₂, cadmium chloride; PND, postnatal day; WT, wild type; KO, knockout.

Our previous study found perinatal exposure to Cd perturbed body weight and the weights of numerous organs at PND 21⁶⁷. In this study, we recapitulated similar outcomes including a significant decrease in the body weights of both males and females (Fig. 3.1C-D). Males and females also presented with unchanged liver weights but had significantly increased liver-to-body-weight percentages (Fig. 3.1E-H). The impact of perinatal Cd exposure on the weights of the other organs analyzed can be found in Supplementary Table 3.2. Consistent with our previous observations, we demonstrated a significant increase in the expression of *H19* in the livers of male and female offspring exposed to Cd (Fig. 3.1A-B).

Perinatal exposure to Cd does not induce overt MASLD phenotypes at PND 21

We have previously demonstrated that perinatal exposure to 50 ppm CdCl₂ increases TAG accumulation in hepatocytes, as well as increases collagen fiber deposition at PND 21⁶⁷. To determine if these biochemical phenotypes were present in this study, which used 30 ppm CdCl₂, we performed TAG and Hyp – the main component of collagen – assays to quantify total hepatic TAGs and hepatic collagen, respectively. We found that Cd exposure did not significantly alter TAG or Hyp abundances in males or females at PND 21 (Fig. 3.2A-D). Males did, however, show a trend for increased TAG

(Cadmium: $F [1, 18] = 3.102$, $P = 0.0952$) and Hyp (Cadmium: $F [1, 19] = 3.851$, $P = 0.0645$) deposition, which may be indicative of potential MASLD onset (Supplementary Table 3.2). Notably, *H19* ablation also had no effect on TAG or Hyp abundances in the liver (Fig. 3.2A-D).

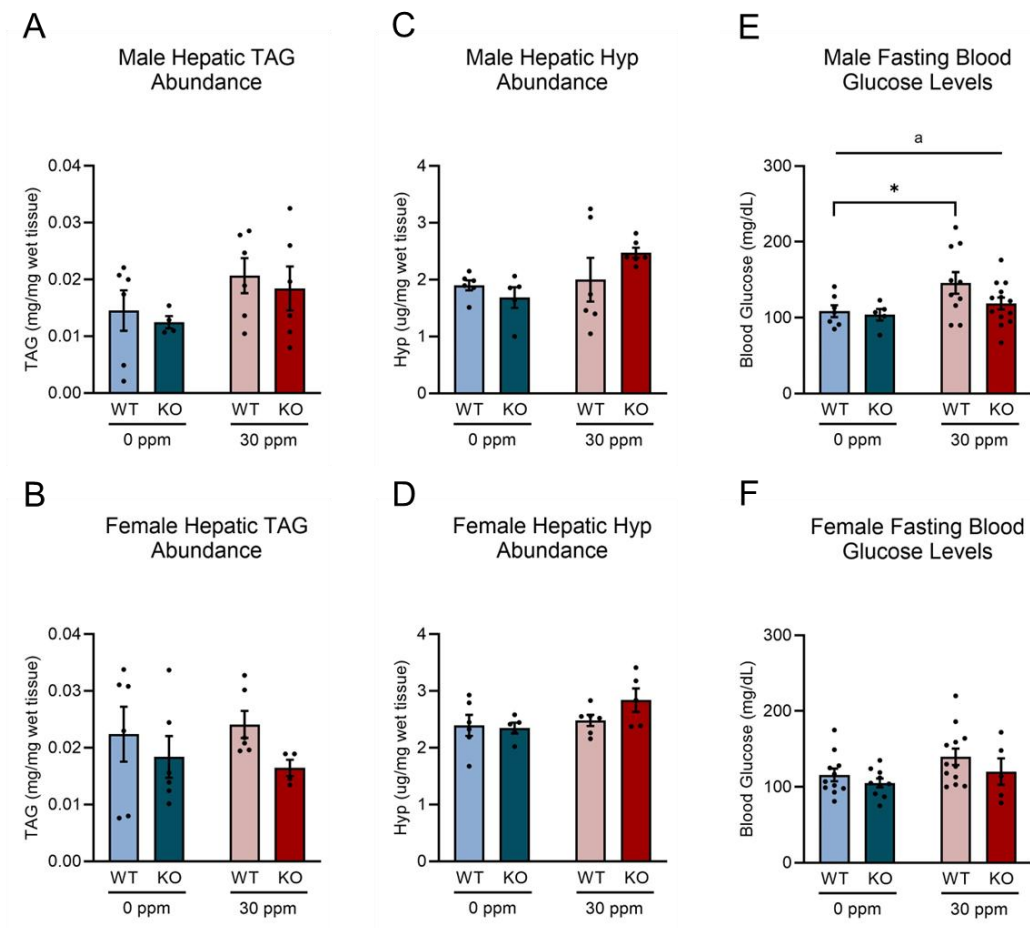


Figure 3.2: Effects of perinatal Cd exposure and systemic *H19* ablation on biochemical markers of MASLD at PND 21. **(A,B)** Male and female hepatic TAG abundance. **(C,D)** Male and female hepatic Hyp abundance. **(E,F)** Male and female fasting blood glucose levels. Lowercase letters represent significant two-way ANOVA factors as follows: a, Cadmium effect. Asterisks represent significant Šídák's multiple comparison test p-values

for the Cadmium factor as follows: $*p < 0.05$. Abbreviations: CdCl₂, cadmium chloride; PND, postnatal day; TAG, triacylglyceride; Hyp, hydroxyproline; WT, wild type; KO, knockout.

To be diagnosed with MASLD, an individual must have hepatic steatosis along with at least one CMRF; therefore, we measured fasting blood glucose to determine if perinatal Cd exposure could increase fasting blood glycemia levels. We found that males but not females had significantly increased fasting blood glucose levels at PND 21 (Fig. 3.2E-F). Females did, however, show a trending increase for blood glycemia (Cadmium: $F [1, 34] = 3.378, P = 0.0748$) (Supplementary Table 3.2). As observed with the TAG and Hyp assays, the ablation of *H19* had no effect on fasting blood glucose levels (Fig. 3.2E-F).

Perinatal exposure to Cd perturbs MASLD-related transcripts at PND 21

Our previous study showed that perinatal Cd exposure could alter the expression of MASLD-related transcripts at PND 21⁶⁷. In this study, a panel of steatosis (*Fabp4*, *Cd36*, *Dgat2*, and *Ppara*), inflammation (*Hmgb1* and *Il6ra*), and fibrosis (*Tgfb1* and *Col6a1*) genes were leveraged to interrogate the liver for molecular changes indicative of MASLD pathogenesis. In males, perinatal exposure to Cd caused a significant increase in *Fabp4*, *Tgfb1*, and *Col6a1* expression but a significant decrease in *Dgat2*, *Ppara*, and *Hmgb1* expression (Fig. 3.3A). In females, similar results were observed with exposure causing a significant increase in *Fabp4* and *Col6a1* expression but a significant decrease

in *Dgat2*, *Hmgb1*, and *Il6ra* expression (Fig. 3.3B). Notably, *H19* ablation had no effect on any of the MASLD genes in males or females at PND 21 (Fig. 3.3A-B).

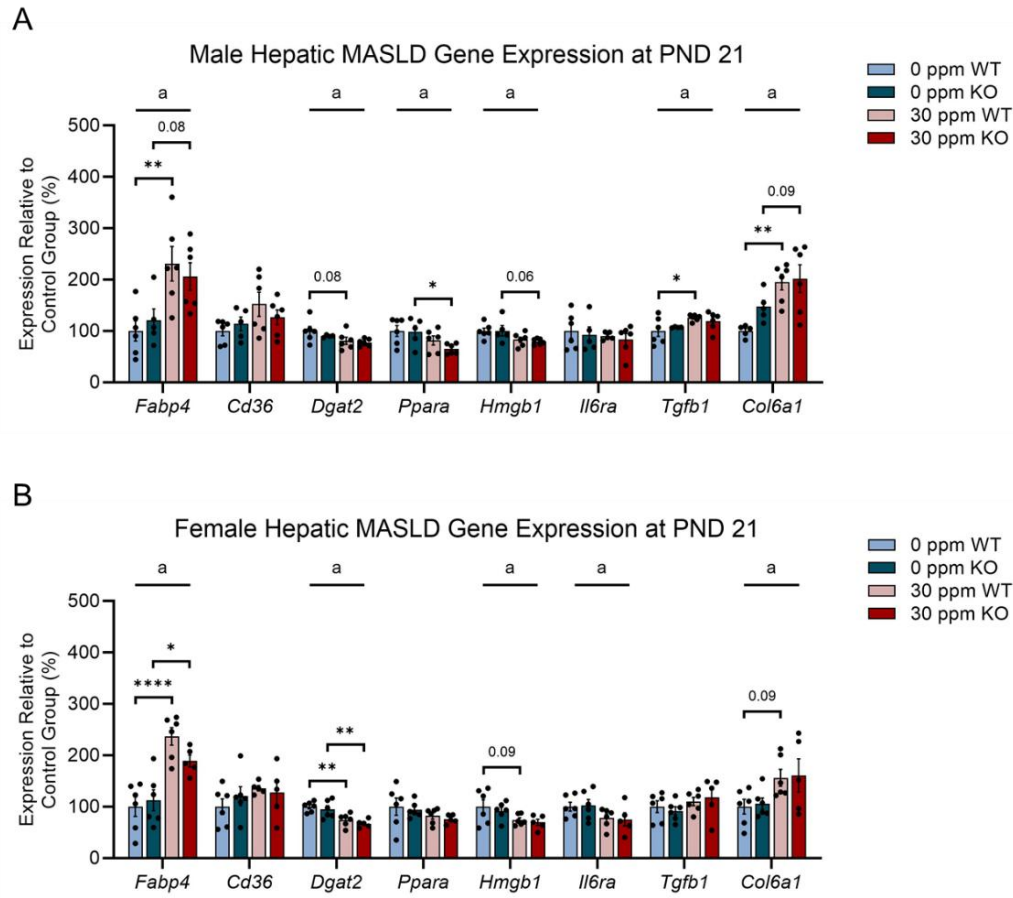


Figure 3.3: Effects of perinatal Cd exposure and systemic *H19* ablation on hepatic transcription of MASLD markers at PND 21. (A,B) Male and female hepatic transcript abundance of MASLD markers. Lowercase letters represent significant two-way ANOVA factors as follows: a, Cadmium. Asterisks represent significant Šídák's multiple comparison test p-values for the Cadmium factor as follows: * $p < 0.05$, ** $p < 0.01$, **** $p < 0.0001$. Abbreviations: CdCl₂, cadmium chloride; PND, postnatal day; WT, wild type; KO, knockout.

Perinatal exposure to Cd displaces essential trace metals in the blood at PND 21

In vivo studies have shown that Cd exposure can disrupt essential trace metal homeostasis in the blood and other tissues²¹⁻²⁴. There is growing evidence that essential trace metal imbalances contribute to metabolic disease pathology including MASLD^{181,182}. In this study, metallomics were performed to examine the blood for essential trace metal levels after perinatal Cd exposure. Both males and females presented with a significant decrease in the concentration of iron (Fe) (Fig. 3.4A-B). Males alone had significantly decreased copper (Cu) and magnesium (Mg) levels, while females alone had significantly decreased zinc (Zn) levels (Fig. 3.4A-B). Strikingly, the ablation of *H19* significantly decreased the concentrations of Fe and Zn in female offspring, indicative of a role for *H19* in regulating essential trace metal homeostasis (Fig. 3.4A-B).

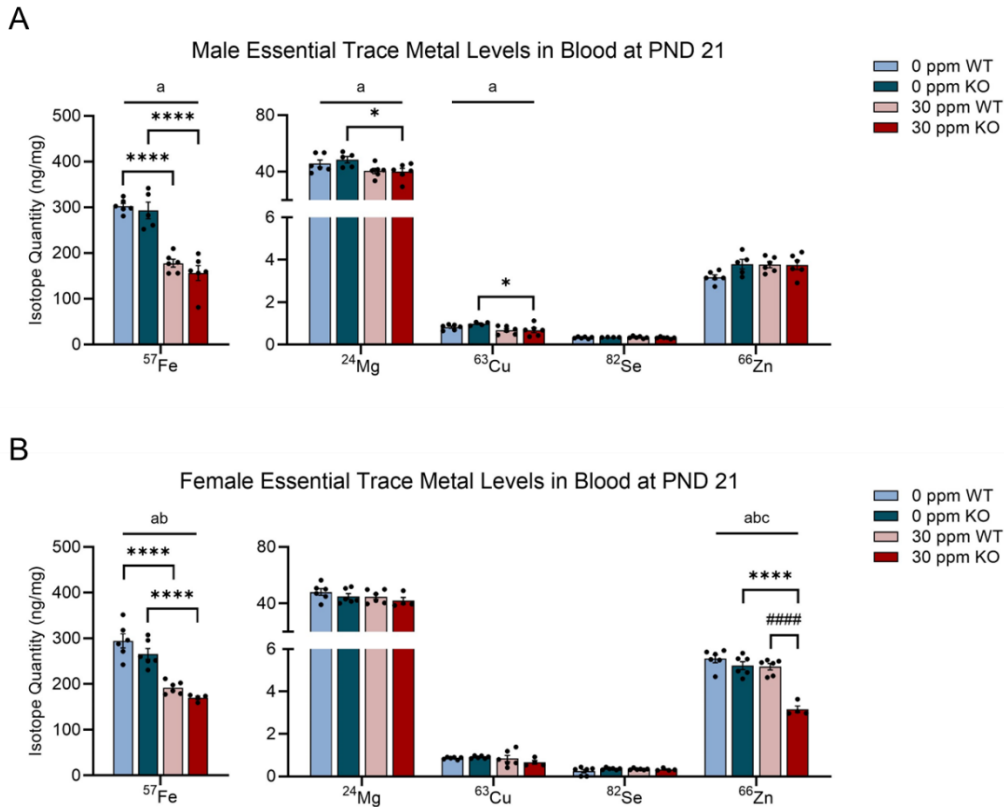


Figure 3.4: Effects of perinatal Cd exposure and systemic *H19* ablation on essential trace metal levels in blood at PND 21. **(A,B)** Male and female isotope quantities of trace essential metals in blood. Lowercase letters represent significant two-way ANOVA factors as follows: a, Cadmium effect; b, Genotype effect; c, Interaction effect. Asterisks represent significant Šídák's multiple comparison test p-values for the Cadmium factor as follows: * $p < 0.05$, **** $p < 0.0001$. Pound signs represent significant Šídák's multiple comparison test p-values for the Genotype factor as follows: ##### $p < 0.0001$. Abbreviations: CdCl₂, cadmium chloride; PND, postnatal day; Fe, iron; Mg, magnesium; Cu, copper; Se, selenium; Zn, zinc; WT, wild type; KO, knockout.

Perinatal exposure to Cd activates IGN transcripts at PND 21

We demonstrated previously that Cd exposure during perinatal development was sufficient to activate IGN genes at PND 21⁶⁷. In this study, we assessed a targeted panel of imprinted (*H19*, *Igf2*, *Plagl1*, and *Grb10*) and biallelically-expressed (*Ccdc80* and *Pcolce*) members of the IGN to determine if Cd exposure induced the same outcomes. Strikingly, both males and females showed upregulation of *Igf2*; however, this increase was only significant in females (Fig. 3.5A-B). Males and females also had significantly increased *H19* and *Grb10* expression. (Fig. 3.1A-B; Fig. 3.5A-B). Additionally, the ablation of *H19* had no significant effect on the expression of other IGN genes in both males and females at PND 21 (Fig. 3.5A-B).

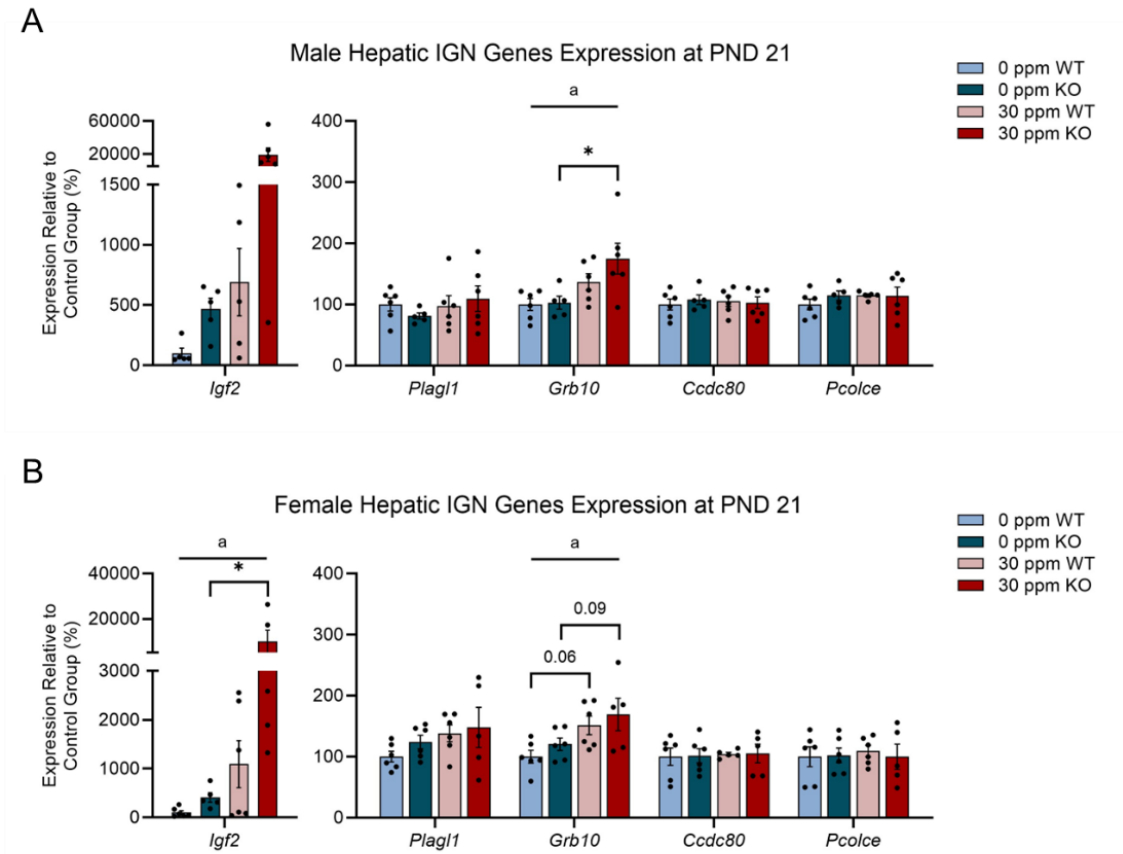


Figure 3.5: Effects of perinatal Cd exposure and systemic *H19* ablation on hepatic transcription of select IGN members at PND 21. **(A,B)** Male and female hepatic transcript abundance for members of the IGN. Lowercase letters represent significant two-way ANOVA factors as follows: a, Cadmium effect. Asterisks represent significant Šídák's multiple comparison test p-values for the Cadmium factor as follows: * $p < 0.05$. Abbreviations: CdCl₂, cadmium chloride; IGN, Imprinted Gene Network; PND, postnatal day; WT, wild type; KO, knockout.

Prenatal exposure to Cd and systemic deletion of *H19* induce morphometric effects at PND 0

To determine if any of the phenotypes observed at PND 21 were present at birth, male and female mice were collected and examined at PND 0. The ablation of *H19* in the liver was validated via qRT-PCR using bulk liver RNA. As expected, the transcript abundance of *H19* was significantly decreased in male and female KO mice (Fig. 3.6A-B). The loss of *H19* expression altered the body weights, as well as the absolute and relative organ weights of neonatal mice. Males presented with significantly increased body weight and liver weight, while females had unaffected body weight but significantly increased liver weight (Fig. 3.6C-F). The liver-to-body-weight percentage was unchanged in both males and females (Fig. 3.6G-H). The effect of *H19* ablation on the absolute and relative tissues weights of the brain, heart, kidneys, and quadriceps muscles can be found in Supplementary Table 3.2.

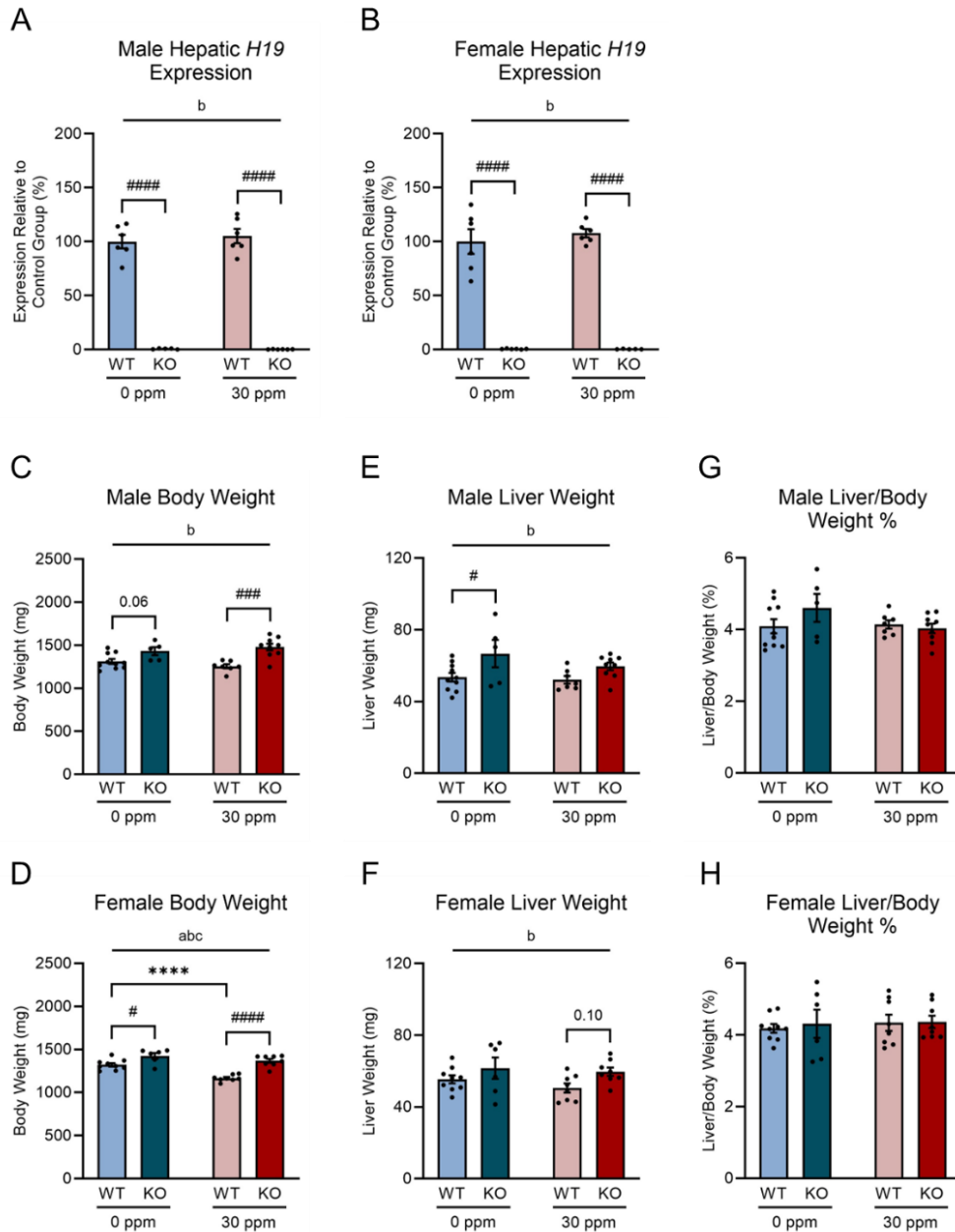


Figure 3.6: Effects of prenatal Cd exposure and systemic *H19* ablation on hepatic *H19* expression, body weight, liver weight, and liver-to-body-weight percentage in mice at PND 0. (A,B) Male and female *H19* transcript abundance. (C,D) Male and female body weight. (E,F) Male and female liver weight. (G,H) Male and female liver-to-body-weight percentage. Lowercase letters represent significant two-way ANOVA factors as follows:

a, Cadmium effect; b, Genotype effect; c, Interaction effect. Asterisks represent significant Šídák's multiple comparison test p-values for the Cadmium factor as follows: **** $p < 0.0001$. Pound signs represent significant Šídák's multiple comparison test p-values for the Genotype factor as follows: # $p < 0.05$, ### $p < 0.001$, #### $p < 0.0001$. Abbreviations: CdCl₂, cadmium chloride; PND, postnatal day; WT, wild type; KO, knockout.

We and others have shown that prenatal Cd exposure can cause fetal growth restriction (FGR) and reduced body weight at birth^{67,183–185}. In this study, we found that females but not males presented with significantly decreased body weights when compared to controls at PND 0 (Fig. 3.6C-D). The liver weights and liver-to-body-weight percentages were unaffected in both males and females (Fig. 3.6E-H). The effect of prenatal Cd exposure on the absolute and relative weights of the other tissues measured can be found in Supplementary Table 3.2. Notably, the expression of *H19* in the liver was not affected by Cd exposure in males or females (Fig. 3.6A-B).

Prenatal exposure to Cd and systemic deletion of *H19* do not elicit molecular or biochemical signatures of MASLD at PND 0

Our previous study found that prenatal exposure to Cd, overall, did not induce histological markers of MASLD or perturb the expression of MASLD-related genes at PND 0⁶⁷. In this study, the Hyp assay and fasting blood levels were performed to investigate the effect perinatal Cd exposure had on hepatic collagen deposition and the presence of a CMRF at PND 0, respectively. We found that males had no change in the abundance of collagen, while females presented with a slight interaction effect for collagen deposition

(Fig. 3.7A-B). Males but not females had significantly increased fasting blood glucose levels, indicative of possible metabolic dysfunction in males at PND 0 (Fig. 3.7D-C). The ablation of *H19* had no effect on either assay in males or females at PND 0 (Fig. 3.7A-D).

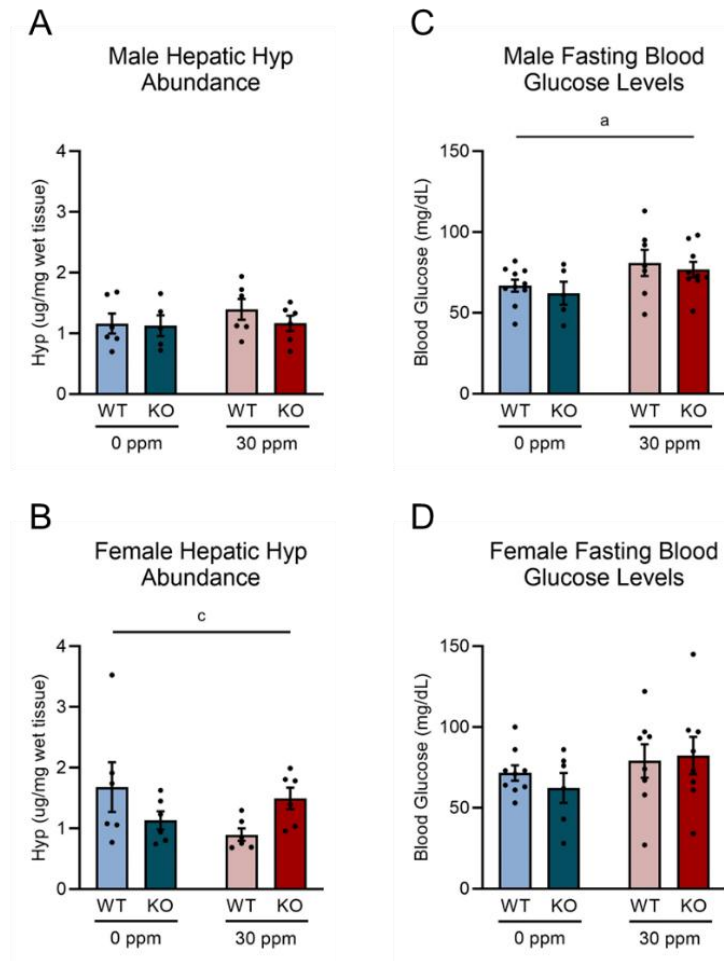


Figure 3.7: Effects of prenatal Cd exposure and systemic *H19* ablation on biochemical markers of MASLD at PND 0. **(A,B)** Male and female hepatic Hyp abundance. **(C,D)** Male and female fasting blood glucose levels. Lowercase letters represent significant two-way ANOVA factors as follows: a, Cadmium effect; c, Interaction effect. Abbreviations: CdCl₂, cadmium chloride; PND, postnatal day; TAG, triacylglyceride; Hyp, hydroxyproline; WT, wild type; KO, knockout.

In addition to the biochemical tests, a panel of steatosis (*Pparg*, *Fabp4*, *Cd36*, *Dgat2*, and *Ppara*), inflammation (*Hmgb1*, *Il6ra*, and *Tnfrsf1a*), and fibrosis (*Tgfb1*, *Col1a1*, *Col3a1*, and *Col6a1*) genes was examined via qRT-PCR to determine if there was molecular evidence of MASLD pathogenesis. Both males and females showed a significant increase in *Fabp4* expression, while females alone showed a significant increase in *Col6a1* expression at PND 0 (Fig. 3.8A-B). All other transcripts assessed were unchanged. Notably, *H19* ablation had no effect on the expression of any of the MASLD-related genes at PND 0 (Fig. 3.8A-B).

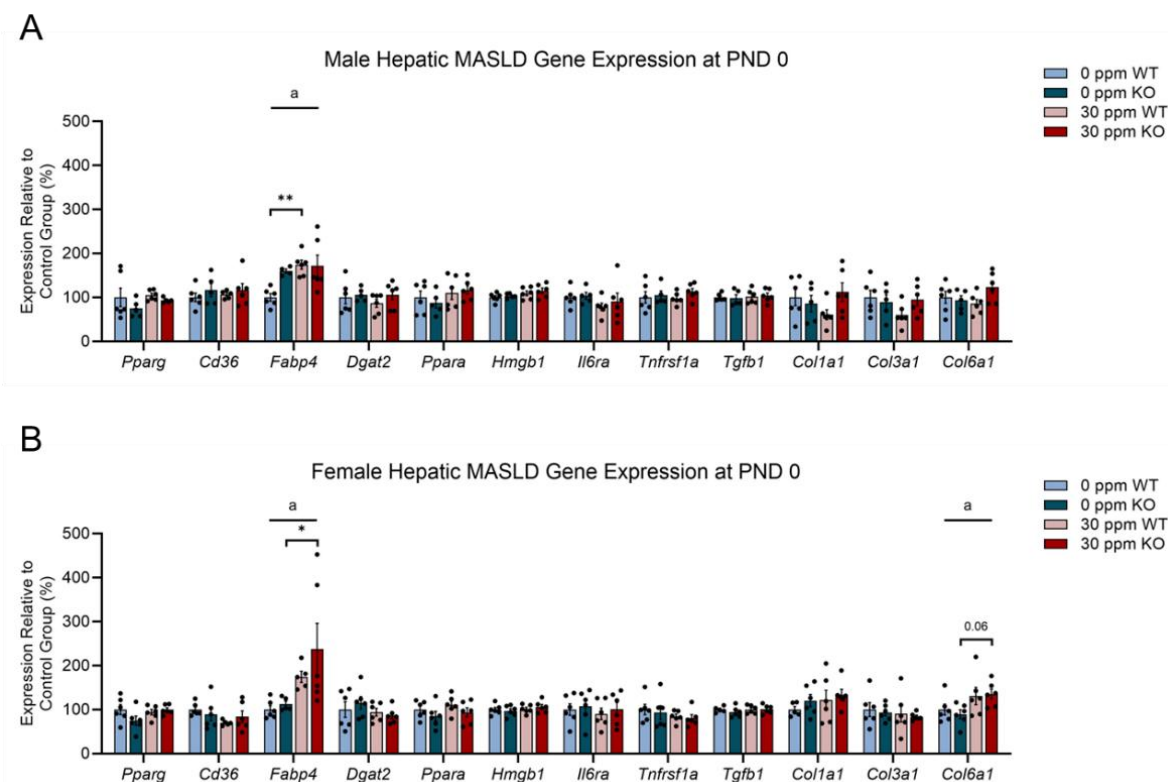


Figure 3.8: Effects of prenatal Cd exposure and systemic *H19* ablation on hepatic transcription of MASLD markers at PND 0. (A,B) Male and female hepatic transcript

abundance of MASLD markers. Lowercase letters represent significant two-way ANOVA factors as follows: a, Cadmium. Asterisks represent significant Šídák's multiple comparison test p-values for the Cadmium factor as follows: * $p < 0.05$, ** $p < 0.01$. Abbreviations: CdCl₂, cadmium chloride; PND, postnatal day; WT, wild type; KO, knockout.

Systemic deletion of H19 activates IGN transcripts at PND 0

We previously demonstrated that prenatal exposure to Cd did not dysregulate the expression of imprinted genes at birth⁶⁷. In this study, we examined a panel of imprinted (*H19*, *Igf2*, *Plagl1*, *Grb10*, *Cdkn1c*, and *Mest*) and biallelically-expressed (*Ccdc80*, *Pcolce*, and *Tgfb1*) members of the IGN. We found that Cd did not affect the expression of any of the IGN genes at PND 0 (Fig. 3.6A-B; Fig. 3.9A-B). Strikingly, the ablation of *H19* significantly increased the expression of nearly every IGN gene assessed in males including *Igf2*, *Plagl1*, *Grb10*, *Cdkn1c*, *Mest*, and *Pcolce* (Fig. 3.9A). Notably, there was an interaction effect in the expression of *Tgfb1* in males (Fig. 3.9A). Females, on the other hand, showed only a significant increase in the expression of *Plagl1* and *Mest* (Fig. 3.9B).

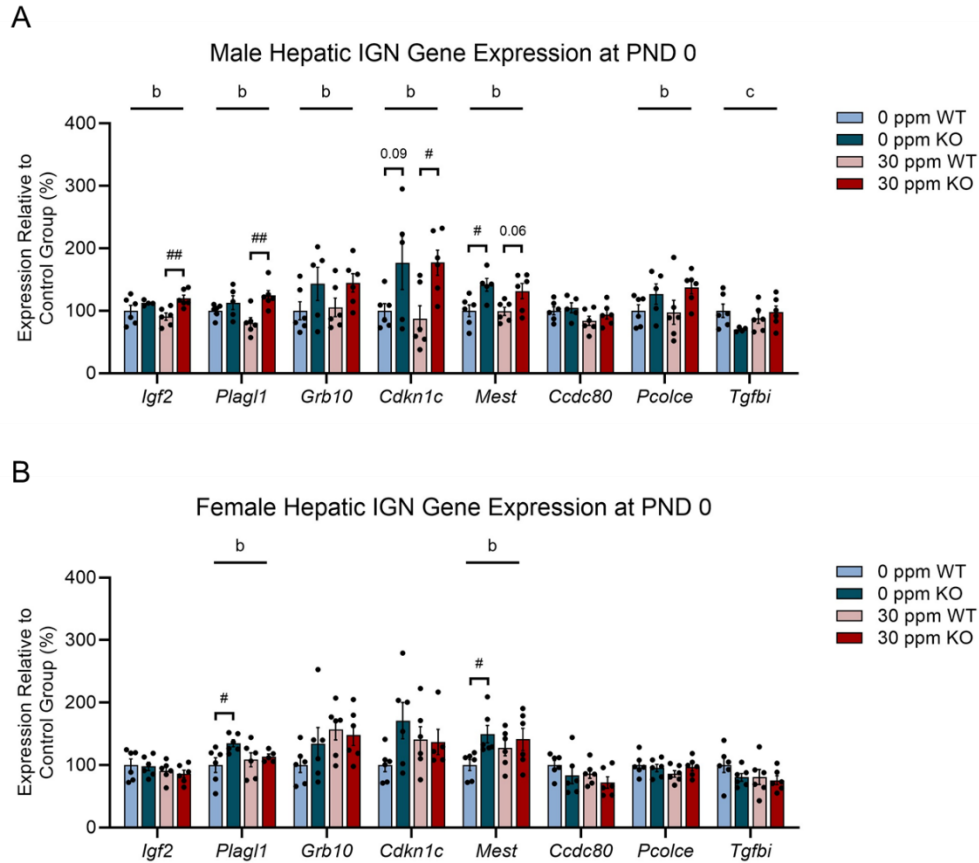


Figure 3.9: Effects of prenatal Cd exposure and systemic *H19* ablation on hepatic transcription of select IGN members at PND 0. (A,B) Male and female hepatic transcript abundance for members of the IGN. Lowercase letters represent significant two-way ANOVA factors as follows: b, Genotype effect; c, Interaction effect. Pound signs represent significant Šídák's multiple comparison test p-values for the Genotype factor as follows: # $p < 0.05$, ## $p < 0.01$. Abbreviations: CdCl₂, cadmium chloride; IGN, Imprinted Gene Network; PND, postnatal day; WT, wild type; KO, knockout.

Discussion

Although efforts have been made to minimize human exposure to the heavy metal Cd, natural processes and anthropogenic activities have increased its presence in the air, soil, and water. Prolonged exposure to Cd can negatively impact the function of numerous organs and tissues including the liver. Evidence from epidemiological and animal studies have found that Cd exposure can drive MASLD, the most common chronic liver disease in the world⁹⁹⁻¹⁰². Strikingly, MASLD burdens nearly 17% of adolescents in the United States⁴⁹. Considering Cd has been detected in fetal cord blood, breast milk, and foods commonly consumed by infants and children, it is plausible that exposure to Cd during prenatal and early postnatal development is contributing to the prevalence of MASLD among adolescents^{172,173,186}. We recently demonstrated that perinatal exposure to Cd is sufficient to program MASLD phenotypes in the livers of juvenile mice concomitantly with the activation of the hepatic IGN, a network of coordinately-regulated imprinted and biallelically-expressed genes, including the imprinted lncRNA *H19*⁶⁷. Recent evidence suggests that the aberrant activation of *H19* in the liver can drive networks of steatosis and fibrosis, making it a potential therapeutic target for alleviating or even preventing MASLD progression^{89,91,92}.

In this study, we leveraged our developmental Cd exposure mouse model to determine if the systemic ablation of *H19* could protect against Cd-induced MASLD in offspring. WT and *H19* KO mice born to mothers exposed to 0 or 30 ppm CdCl₂ in drinking water for five-weeks prior to mating, during gestation, and until PND 10 were collected at PND 0 and PND 21 to assess the liver for MASLD pathologies. At PND 21, perinatal Cd exposure did not induce overt MASLD phenotypes in the liver, as evidenced by unaltered

hepatic TAG and collagen abundances. This finding is contrary to what was observed at PND 21 in our previous study; however, the differing genetic backgrounds of the mice, as well as the lower concentration of Cd used in the exposure paradigm could be contributing to these discrepancies. Mice at PND 0, similarly, presented with no quantitative increase in the abundance of collagen in the liver due to prenatal Cd exposure. Strikingly, Cd exposure increased fasting blood glucose levels in male offspring at PND 21, a phenotype that was also observed in male offspring at PND 0. Elevated blood glycemia is closely linked to MASLD progression and is one of five CMRFs used in its diagnosis⁴³. These findings suggest males may be more sensitive to Cd-induced metabolic dysfunction than females after developmental exposure to Cd. Since developmental Cd exposure was unable to induce overt MASLD phenotypes at PND 0 or PND 21 in our model, the role *H19* ablation plays in mitigating those outcomes is not clear.

Despite observing no biochemical evidence of MASLD manifestation, the expression of hepatic steatosis, inflammation, and fibrosis genes was perturbed by perinatal exposure to Cd at PND 21. Males and females had a noticeable increase in the expression of *Fabp4*, a fatty acid transport protein that is primarily active in adipose tissue. The activation of *Fabp4* may be indicative of increased hepatic lipid abundances and inflammation, as well as an adipogenic shift in hepatocyte function^{139,140}. Noticeably, males and females also presented with a marked decrease in the expression of hepatic TAG metabolism and inflammation genes including *Dgat2*, *Ppara*, and *Hmgb1* in males and *Dgat2*, *Hmgb1*, and *I6ra* in females. This may signify a stress response by the liver to combat against MASLD progression which may explain why overt phenotypes were not observed in the liver. Despite a decrease in steatosis and inflammation markers,

perinatal Cd exposure caused an increase in fibrosis transcripts, as evidenced by the upregulation of *Tgfb1* – the TGF β isoform largely responsible for fibrosis signaling – expression in males and *Col6a1* – a component of Type VI collagen – expression in males and females, indicative of potential disease progression. Further, our previous study demonstrated that prenatal exposure to Cd did not, overall, alter the expression of MASLD-related genes in offspring at PND 0⁶⁷. The current study similarly observed only an increase in *Fabp4* expression in males and females and an increase in *Col6a1* expression in females alone. Strikingly, the ablation of *H19* had no effect on the expression of any of the steatosis, inflammation, and fibrosis transcripts assessed in males or females at either timepoint, suggesting *H19* may not play a role in driving Cd-induced MASLD. It is possible, however, that a more comprehensive approach could uncover relevant molecular targets in our model.

Evidence from our lab and others have shown developmental exposure to Cd can elicit morphometric effects in offspring including reduced body weight^{67,183,184}. At PND 21, both males and females presented with decreased body weights but unaltered liver weights. Despite an overall decrease in body weight, the relative weights of the liver were increased in the Cd exposed offspring in both male and females, illustrating a potential sparing phenotype. Interestingly, only females exposed to Cd experienced a reduced body weight at PND 0, while both males and females presented with unaffected liver and relative liver weights. A study performed using CD-1 mice found that Cd preferentially crossed placental barrier of female fetuses¹¹⁵. This may explain why a reduction in body weight was only observed in females at PND 0, albeit males do eventually manifest the phenotype at PND 21. Further, there is evidence that the loss of *H19* expression during

development can also induce morphometric effects^{179,180}. The expression of *H19* during early-life is co-regulated with another imprinted gene, the growth factor *Igf2*. *H19* functions to negatively regulate growth and cellular proliferation, in part, by suppressing *Igf2* expression; therefore, the deletion of *H19* causes increased *Igf2* expression which can, ultimately, lead to overgrowth phenotypes in offspring. At PND 21, KO males but not females had increased body weight. The liver weights of both males and females were unaltered, but males had a decreased relative liver weight. Notably, both KO males and females had overgrowth phenotypes at PND 0, as evidenced by increased body weights and liver weights. These findings demonstrate that some of the overgrowth phenotypes induced by *H19* ablation at PND 0 can stabilize over time and return to within a normal range, an outcome more prominently observed in the female offspring at PND 21.

It is well-known that Cd can displace essential trace metals in the blood, liver, and other tissues²¹⁻²⁴. At PND 21, perinatal Cd exposure caused a substantial decrease in blood Fe levels in males and females, a decrease in blood Cu and blood Mg levels in males, and a decrease in blood Zn levels in females. Epidemiological studies have found that deficiencies in essential trace metals – including Fe, Cu, Zn, Selenium (Se), and Mg – are prevalent in individuals diagnosed with MASLD; however, the relationship between the two is complex¹⁸⁷⁻¹⁹⁰. It is not always clear whether an essential trace metal deficiency can cause MASLD or if it is a side effect of MASLD pathology. In either case, perinatal Cd exposure likely exacerbates those issues and increases metabolic stress in the liver. The deletion of *H19* also caused a decrease in blood Fe and blood Zn in females at PND 21. Exposure to Cd and *H19* ablation, together, induced a larger decrease in blood Zn levels. Currently, there is limited evidence that *H19* can impact Fe or Zn homeostasis.

One study using lung cancer cells showed *H19* upregulation was able to enhance the expression of *FTH1*, a subunit of the Fe storage protein ferritin¹⁹¹. Another study using mice found the deletion of *Zip14* – a Zn transport protein – in the small intestine caused a marked increase in *H19* expression¹⁹².

Evidence from our lab has shown perinatal exposure to stressors can activate the expression of the IGN in the livers of juvenile mice^{66,67}. At PND 21, the expression of *H19* and *Grb10* were increased in both male and female offspring. A study in mice demonstrated that a liver-specific deletion of *Grb10*, an imprinted growth factor receptor bound protein, suppressed acute endoplasmic reticulum (ER) stress-induced steatosis phenotypes¹⁵⁹. Strikingly, the expression of *Igf2* was dramatically increased in males and females, albeit only significantly so in females; exposure to Cd and *H19* ablation, together, appear to induce an even larger increase in the hepatic expression of *Igf2*. There is growing evidence that aberrant *Igf2* activation can contribute to elevated hepatic steatosis and fibrosis, as well as hepatic mitochondrial dysfunction^{193–196}. Given *Igf2*'s similar metabolic function to *H19* in liver disease pathology, it is possible that the marked increase in *Igf2* was able to inhibit the protective effects of *H19* ablation in our model. Additional studies will be performed to explore this relationship. Further, as observed in our previous study, the current study did not show activation of the IGN at birth due to prenatal Cd exposure. The ablation of *H19*, on the other hand, increased the expression of numerous IGN members at PND 0, an outcome more prominent in male offspring. Males and females had increased *Plagl1* and *Mest* expression, while males alone had increased *Igf2*, *Grb10*, *Cdkn1c*, and *Pcolce* expression. Similarly to *Plagl1*, the master regulator of the IGN, *H19* has been shown to control the expression of other genes in the

IGN¹⁹⁷. As observed at PND 21, the effect of *H19* ablation on IGN gene expression is lost, as KO mice no longer differ from their WT counterparts.

Finally, the limitations of this study should be considered. First, the outcomes observed in our mouse model may not all be recapitulated in humans. Second, the ablation of *H19* in our model was not liver specific. Future studies will explore liver cell type-specific knockouts of *H19* and other IGN genes of interest. Third, there are no collection timepoints beyond PND 21. Future studies will explore later timepoints to see if more advanced MASLD phenotypes are present as a result of developmental exposure. Lastly, the conclusions drawn from this study rely largely upon gene expression data. Future studies will incorporate experiments that quantify protein abundances to help support the gene expression data.

Conclusions

The results of our study show developmental exposure to 30 ppm CdCl₂ was sufficient to program molecular signatures of MASLD at PND 21 but not at PND 0; however, the ablation of *H19* did not reduce the expression of steatosis and fibrosis genes at PND 21. A more global gene expression approach may reveal larger molecular changes driven by *H19* deletion. Additionally, genes of the IGN were activated by developmental Cd exposure at PND 21 and by the ablation of *H19* at PND 0. Future studies will explore the roles *Igf2*, and other pertinent IGN members have on the onset and progression of MASLD after developmental exposure to environmental stressors.

Acknowledgements

The authors thank Jeffrey Enders for his expert guidance and assistance with the metallomics experiment.

CHAPTER 4:

The Imprinted Transcription Factor ZAC1 Binds Directly to the Promoters of Genes Enriched in Pathways Implicated in MASLD

This chapter will be submitted to a peer-reviewed journal as part of a larger study.

Logan Dameris^{1,2,3}, Marine Baptissart^{1,3}, Dereje D. Jima³, and Michael Cowley^{1,2,3}

¹Department of Biological Sciences, North Carolina State University, Raleigh, NC, 27695, USA.

²Toxicology Program, North Carolina State University, Raleigh, NC, 27695, USA.

³Center for Human Health and the Environment, North Carolina State University, Raleigh, NC, 27695, USA.

Abstract

The imprinted gene *ZAC1* encodes a zinc-finger transcription factor that regulates the expression of the imprinted gene network (IGN), a group of coordinately-regulated imprinted and biallelically-expressed genes. We have demonstrated previously that perinatal exposure to environmental stressors can activate the IGN in the liver, while simultaneously eliciting hepatic signatures of metabolic dysfunction-associated steatotic liver disease (MASLD). The artificial activation of the IGN via *ZAC1* overexpression in hepatoma cells showed *ZAC1* could enhance lipid and collagen deposition and could also bind to the promoters of the pro-collagen gene *COL6A2*; however, the full extent of *ZAC1* binding in hepatocytes and the associated downstream effects, especially those related to MASLD, remain unknown. To address this knowledge gap, we performed chromatin immunoprecipitation sequencing (ChIP-seq) using *ZAC1*-overexpressing hepatoma cells to identify global binding coordinates of *ZAC1*, as well as consensus binding sequences. We found that nearly 50% of called *ZAC1* peaks overlapped the promoter regions of genes. Among those genes included 45 members of the IGN, indicating *ZAC1* can directly interact with those genes to influence their expression. Pathway enrichment analyses revealed significant enrichment of biological pathways associated with MASLD including PI3K/AKT signaling, insulin resistance, and regulation of epithelial-mesenchymal transition (EMT). We were also able to identify GC-rich consensus binding motifs, a feature of zinc-finger transcription factors. These findings provide new insights into our understanding of *ZAC1*'s ability to regulate the expression of IGN in the liver and drive transcriptional networks of MASLD.

Introduction

Imprinted genes, characterized by their expression from only one of the parental alleles, play a crucial role in proper growth and development during early life. Upon its initial discovery in the late 1990s and early 2000s, the imprinted *ZAC1* gene (also known as *PLAGL1*), which encodes a C2H2 zinc-finger transcription factor with both transactivation and repressor functions, was characterized as a biallelically-expressed tumor suppressor gene, as it was found to induce apoptosis and cell cycle arrest^{81–84}. Years later, it was determined *ZAC1* was maternally-imprinted and could also regulate the expression of a network of imprinted genes that was responsible for controlling embryonic growth⁸⁰; the imprinted gene network (IGN) was later updated to include additional imprinted genes, as well as biallelically-expressed genes that govern extracellular matrix (ECM) composition, cell-adhesion, and more⁷⁹.

Notably, imprinted genes have been found to be sensitive to perturbations by environmental stressors, especially during development^{74–78,198}. We have shown that exposure to maternal metabolic syndrome (MetS) and the heavy metal cadmium (Cd) during perinatal development can facilitate the aberrant activation of the IGN in the livers of juvenile mice^{66,67}. This, concomitantly, occurred with the manifestation of hepatic steatosis and fibrosis which are phenotypes associated with metabolic dysfunction-associated steatotic liver disease (MASLD), the most common chronic liver disease in the world. To further explore the role *ZAC1* and the IGN play in facilitating MASLD, we overexpressed *ZAC1* in a human hepatoma cell line to artificially activate the IGN and observed a significant increase in the uptake of neutral lipids after oleic acid exposure, as well as increased collagen deposition per elevated pro-COL1A1 – a precursor to Type

I collagen – levels^{66,67}. Given ZAC1's function as a transcription factor, we also performed chromatin immunoprecipitation (ChIP) and leveraged targeted quantitative real-time polymerase chain reaction (qRT-PCR) assays for predicted ZAC1 binding sites at the pro-fibrotic genes *TGFB1*, *SNAI1*, *COL6A2*, and *COL1A1*. We found ZAC1 binding was significantly enriched at the promoter regions of *TGFB1* and *COL6A2*⁶⁶. Still, the magnitude and overall consequences of ZAC1 binding at MASLD-related genes was not clear.

In this study, we performed ChIP-sequencing (ChIP-seq) in ZAC1-overexpressing hepatoma cells to discover the global genomic binding coordinates of ZAC1 with a particular interest in the promoter regions of genes associated with MASLD and the IGN. Pathway enrichment analyses were conducted to identify enriched biological pathways associated with steatosis, inflammation, and fibrosis signaling. We also performed binding motif discovery to determine ZAC1 consensus binding sequences. Overall, these results offer a greater understanding of ZAC1's ability to activate transcriptional networks of MASLD.

Materials and Methods

ZAC1 ChIP

The ZAC1 ChIP was described in a previous study⁶⁶. Briefly, HEK293T cells were plated and transfected with a pLenti-CMV-ZAC1-FLAG construct and three lentiviral plasmid constructs to produce a Zac1-FLAG lentiviral media. The ZAC1-FLAG lentiviral particles were transduced into plated HepG2 cells (a hepatoma cell line) to overexpress ZAC1. ChIP was performed using magnetic beads coupled with antibodies against ZAC1-

FLAG or IgG to immunoprecipitate DNA. The IgG was used as a control for non-specific binding.

ChIP-seq

Three ZAC1-FLAG and IgG replicates were delivered to the University of North Carolina-Chapel Hill (UNC) High Throughput Sequencing Facility (HTSF) for library preparation and sequencing.

Peak assembly was performed in consultation with the Bioinformatics Core at the NCSU Center for Human Health and the Environment (CHHE). An average of ~50 million paired-end raw ChIP-Seq data was generated with three replicates with treatment and mock samples. The quality of sequenced data was assessed using the *fastqc*¹⁹⁹ application, and seven poor-quality bases were trimmed from the 5'-end. The remaining good-quality reads were aligned to the Human reference genome (hg38) using a *bowtie2*²⁰⁰ aligner. The alignment files were sorted, and the uniquely aligned reads were retained and indexed using *sambamba* version 0.7²⁰¹. Model-based ChIP-seq data analysis (MACS2, version 2.2.7.1)²⁰² was used to call the peaks between the ZAC1 treatment and mock IGG samples in the three replicates. The default settings were used except for setting the minimum false discovery rate (FDR) cut-off (q value) to 0.05. We obtained 0, 71,331, and 5,703 peaks for replicates 1, 2, and 3, respectively. Replicate 1 was removed from all analyses moving forward. To assess the concordance of peak intervals between replicates 2 and 3, we used the Galaxy²⁰³ platform to intersect replicate 2 peaks onto replicate 3 peaks (5,127 intervals) and then replicate 3 peaks onto replicate 2 peaks (4,767 intervals). The peak intervals had to overlap by at least 1 base pair (bp).

We then merged the overlapping intervals of the two files generated in the previous step to create a single interval file for the two replicates. This produced a total of 4,647 peak intervals for downstream analyses.

ZAC1 genome binding

Transcript chromosomal coordinates from the National Center for Biotechnology Information (NCBI) Reference Sequence (RefSeq) Select²⁰⁴ database – which consists of a representative transcript for every protein-coding gene in the genome – were downloaded from the University of Santa Cruz (UCSC) Table Browser²⁰⁵ tool using the GRCh38/hg38 human genome build. Of the total 22,320 genes in the database, 2,998 “chr_alt” and “chr_fix” transcript coordinates were removed to generate a final list of 19,322 representative genes. These coordinates were then modified to explore specific gene regions including the gene promoter (the transcription start site plus and minus 40 bp), the gene body, the gene body plus one kilobase (kb) upstream, the gene body plus three kb upstream, the gene body plus five kb upstream, and the gene body plus ten kb upstream. The 4,647 peak intervals were then overlapped with the various gene region coordinates using the Galaxy²⁰³ platform to determine if ZAC1 was bound to a gene region. The gene names (2,381 genes) and ZAC1 peak coordinates (2,275 intervals) from the promoter region file were used for additional analyses. ZAC1 peak binding at promoters was visualized using the Integrative Genomics Viewer (IGV) desktop application²⁰⁶.

ZAC1 IGN binding

The gene names from the promoter region file were compared to a list of human IGN genes assembled by Al Adhami et al., 2015⁷⁹. Any of the IGN genes not present in the NCBI RefSeq Select database were removed from the assembled list of human IGN members. After trimming, there was a total of 297 IGN genes: 61 imprinted and 236 biallelically-expressed genes.

Consensus binding motif

The ZAC1 peak coordinates from the promoter region file were converted to their corresponding DNA sequences using the Galaxy²⁰³ platform. The sequences were uploaded to the MEME Suite for input into the Sensitive, Thorough, Rapid, Enriched Motif Elicitation (STREME)²⁰⁷ motif identification software. The average length of the DNA sequences was 1,416 bp. An e-value < 0.05 was considered significant.

DAVID pathway analysis

The gene names from the promoter region file were uploaded to the National Institutes of Health (NIH) Database for Annotation, Visualization, and Integrated Discovery (DAVID)^{208,209} tool as input for Functional Annotation. The Kyoto Encyclopedia of Genes and Genomes (KEGG) pathway function annotation chart was selected to assess enriched pathways. A p-value < 0.05 was considered significant.

Qiagen Ingenuity Pathway Analysis

The gene names from the promoter region file were uploaded to the Qiagen Ingenuity Pathway Analysis²¹⁰ (IPA) software as input for a Core Analysis. Biological filters were adjusted to include molecules and/or relationships related only to humans and the HepG2 cell line. The Canonical Pathways function was used to assess enrichment. A p-value > 1.3 was considered significant.

Results

Identification of ZAC1 genomic binding regions

To assess regions of the genome where ZAC1 binding was present, the 4,647 ZAC1 peak intervals were overlapped with defined coordinates near genes including gene promoters, gene bodies, and gene bodies plus increasing distances upstream from the TSS. We found that approximately 85% of the ZAC1 peaks were within a 10kb region upstream from the TSS of genes and that nearly 50% of the ZAC1 peaks were bound at gene promoters (Fig. 4.1A). Of the total 19,322 representative genes used to generate the varying coordinates, ZAC1 was bound at the promoters of 2,381 genes (Fig. 4.1B).

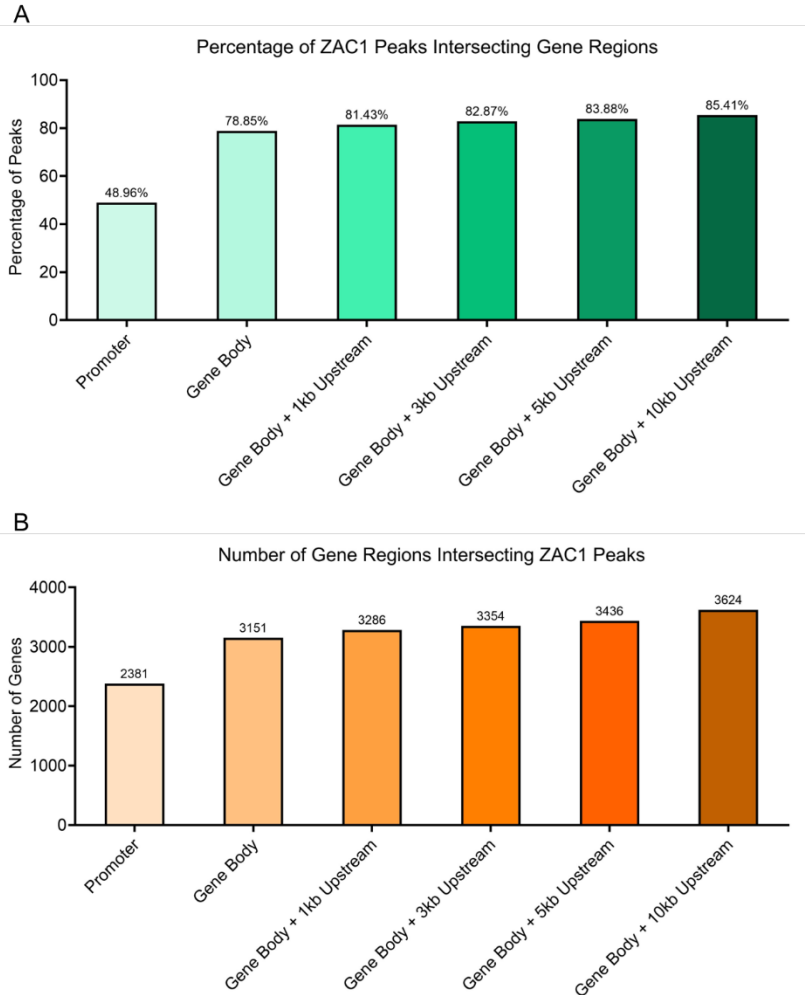


Figure 4.1: Identification of genomic regions of ZAC1 binding. **(A)** Percentage of ZAC1 peaks overlapping regions near genes. **(B)** Number of regions near genes that overlap ZAC1 peaks.

We demonstrated previously that ZAC1 binds to the promoters of *TGFB1* and *COL6A2*⁶⁶. In this study, we used IGV to visually confirm these findings and again showed ZAC1 was bound to the *TGFB1* and *COL6A2* promoters (Fig. 4.2A-B). Further, since ZAC1 is the master regulator of the IGN, we wanted to determine which IGN genes ZAC1 directly interacts with at their promoters. We found that ZAC1 could bind to the promoters

of 45 (15%) IGN members. Eight of those 45 genes (*TP73*, *PPP1R9A*, *PLAGL1* [ZAC1], *IGF2*, *PHLDA2*, *UBE3A*, *ATP10A*, and *ANKRD11*) were imprinted.

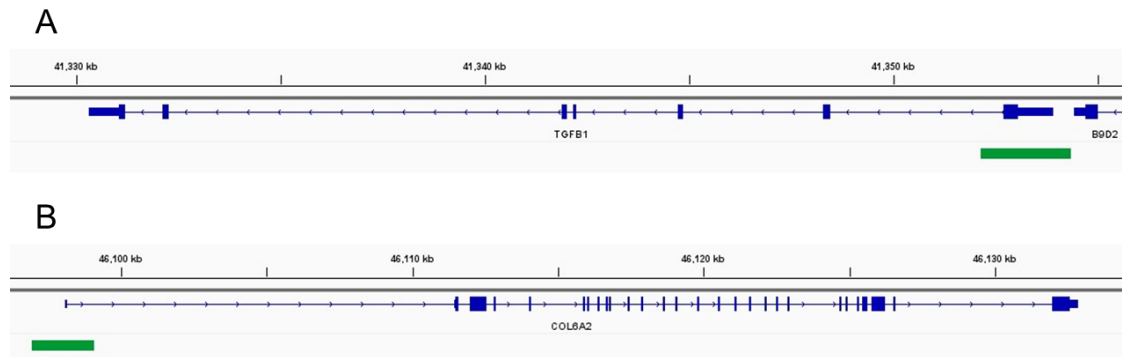


Figure 4.2: Validation of ZAC1 binding at promoters. **(A)** ZAC1 binding at the promoter of *TGFB1*. **(B)** ZAC1 binding at the promoter of *COL6A2*. Green rectangles depict the ZAC1 peak interval coordinates.

Identification of ZAC1 binding motifs

It has been shown that ZAC1 preferentially binds to GC-rich motif sequences²¹¹. Using the motif discovery tool STREME, we identified consensus binding motifs for ZAC1 peaks bound to gene promoters. The top three most significant motifs similarly contain GC-rich sequences (Fig. 4.3). Motif #1 was found in 41% of ZAC1 peaks with a sequence of CGCCGCCGCCGCCGC. Motif #2 and motif #3 were observed in 43% and 33% of ZAC1 peaks, respectively, and both shared a nearly identical sequence of CCC(C/G)GCCCC(G/C)CCCC.

Motif	Sequence Logo	Reverse Complement Logo	P-Value	E-Value	Sites
1-CGCCGCCGCCGCCGC			8.0e-020	5.9e-018	924 (40.6%)
2-CCCGGCCGCCGCC			4.8e-015	3.5e-013	983 (43.2%)
3-CCCCRCCCCWCCC			3.5e-014	2.6e-012	751 (33.0%)
4-GGAGGAGGAGGAGGA			1.7e-011	1.2e-009	331 (14.5%)
5-AAGDTGADKA			1.3e-009	9.6e-008	692 (30.4%)

Figure 4.3: Identification of ZAC1 consensus binding motifs at gene promoters using STREME. An e-value < 0.05 was considered significant. The figure shows the top five most significant motifs.

ZAC1 enriches pathways related to MASLD

We have demonstrated that *ZAC1* overexpression can increase steatosis and fibrosis in liver cells, hallmark manifestations associated with MASLD^{66,67}. To determine if *ZAC1* binds to the promoters of genes involved in MASLD pathogenesis, pathway enrichment analyses were performed using the names of genes that *ZAC1* binds at their promoters. The DAVID KEGG pathway enrichment analysis found several pathways associated with MASLD including hepatocellular carcinoma (HCC), insulin resistance, and MAPK signaling (Table 4.1). Similarly, the IPA canonical pathway enrichment

determined several pathways with links to MASLD including the regulation of the epithelial-mesenchymal transition (EMT) pathway and PI3K/AKT signaling (Table 4.2).

Table 4.1: DAVID KEGG pathway enrichment using genes with identified ZAC1 promoter binding. A p-value < 0.05 was considered significant. The ratio reveals the percentage of ZAC1 promoter genes that overlap the genes of the specific pathway. The table includes the top ten most significantly enriched terms.

Pathway Term	P-Value	Ratio
Hippo signaling pathway	5.44E-10	2.02%
Proteoglycans in cancer	1.73E-09	2.35%
Bacterial invasion of epithelial cells	7.24E-08	1.18%
Yersinia infection	7.43E-08	1.68%
MAPK signaling pathway	2.52E-07	2.81%
Hepatocellular carcinoma	4.41E-07	1.85%
Rap1 signaling pathway	5.73E-07	2.14%
Shigellosis	6.73E-07	2.39%
Insulin resistance	1.32E-06	1.34%
Pathways in cancer	2.18E-06	4.16%

Table 4.2: Qiagen IPA canonical pathway enrichment using genes with identified ZAC1 promoter binding. A p-value > 1.3 was considered significant. The ratio reveals the percentage of ZAC1 promoter genes that overlap the genes of the specific pathway. The table includes the top ten most significantly enriched terms.

Pathway Term	P-Value	Ratio
IL-4 Signaling	3.40	56%
BEX2 Signaling Pathway	3.26	48%
PI3K/AKT Signaling	3.26	43%
Role of WNT/GSK-3 β Signaling in the Pathogenesis of Influenza	3.15	64%
IL-13 Signaling Pathway	3.12	57%
Glioblastoma Multiforme Signaling	3.06	46%
Pulmonary Fibrosis Idiopathic Signaling Pathway	3.03	35%
Interleukin-4 and Interleukin-13 signaling	2.66	40%
Transcriptional Regulatory Network in Embryonic Stem Cells	2.66	40%
Regulation of the Epithelial-Mesenchymal Transition Pathway	2.66	40%

Discussion

In this study, we were interested in determining where ZAC1 binds in the genome and if those regions were near the promoters of genes associated with the activation of MASLD-related transcriptional networks. We performed ChIP-seq using a hepatoma cell line overexpressing ZAC1 and identified 4,647 ZAC1 peaks, of which nearly 50% were bound to promoter regions of genes. This amounted to 2,381 genes. We validated our previous findings and confirmed ZAC1 peaks were present at the promoters of *TGFB1* and *COL6A2*. Further, we obtained the DNA sequences from the ZAC1 peaks bound to promoters and performed motif discovery analyses to identify consensus binding motifs. The top three most significant results yielded GC-rich sequences which were present in 41%, 43%, and 33% of ZAC1 peaks, respectively. Another study exploring ZAC1 consensus binding sequences similarly obtained GC-rich motifs²¹¹. These findings are to be expected, as it is well-established that C2H2 transcription factors, like ZAC1, tend to bind to GC-rich motifs in the genome²¹².

We have shown previously that artificial activation of the IGN via ZAC1 overexpression can facilitate steatosis and fibrosis phenotypes in liver cells^{66,67}. Using the 2,381 genes with identified ZAC1 binding at their promoter, we performed KEGG and IPA pathway enrichment analyses to discover enriched transcriptional pathways, especially those related to MASLD pathogenesis. Both enrichment analyses, together, yielded several pathways with direct relationships to MASLD among their top ten most significantly enriched terms including HCC, insulin resistance, MAPK signaling, regulation of the EMT pathway, and PI3K/signaling^{213,214}. The Hippo signaling pathway, the most significantly enriched pathway identified by KEGG, has also been implicated in the

pathogenesis of MASLD, as it plays an important role in maintaining liver homeostasis by regulating liver size, metabolism, and regeneration²¹⁵. Studies have shown that perturbing the expression of the core components of the Hippo pathway – including LATS1/2, MST1/2, and SAV – can promote or mitigate MASLD progression²¹⁶. Further, the most significantly enriched pathway identified by IPA, IL-4 signaling, has a complex relationship with MASLD, as IL-4 has been shown to both reduce and promote hepatic inflammation and fibrosis^{217,218}.

In addition to MASLD-related genes and pathways, we set out to elucidate which IGN members ZAC1 directly bound to at their promoters. We overlapped the 2,381 ZAC1 promoter genes with a list of IGN members and found that ZAC1 could directly bind to 45 IGN genes: 37 biallelically-expressed and eight (*TP73*, *PPP1R9A*, *PLAGL1* [*ZAC1*], *IGF2*, *PHLDA2*, *UBE3A*, *ATP10A*, and *ANKRD11*) imprinted genes. Among those eight imprinted genes was *ZAC1*, illustrating it can bind to its own promoter to potentially activate or repress its expression. In the context of MASLD, the growth factor, *IGF2*, has been implicated in its pathogenesis; studies have shown aberrant *IGF2* activation can increase steatosis, fibrosis, and mitochondrial dysfunction in the liver^{193–196}. Two of the other imprinted genes, *UBE3A* and *ATP10A*, among the eight also have connections to MASLD; however, the evidence is limited^{219,220}.

Finally, limitations for this study should be considered. First, ZAC1 ChIP-seq was performed in a human hepatoma cell line which may not perfectly recapitulate outcomes observed in humans. Future studies will explore performing ChIP-seq and other experiments using primary hepatocytes for more accurate translation to humans. Second, ChIP-seq was performed in an overexpression model, so the findings may not fully reflect

the binding sites obtained at endogenous levels of *ZAC1* expression. This was necessary due to the poor quality of *ZAC1* antibodies available, particularly for ChIP, so we had to overexpress *ZAC1* with a FLAG-tag. Future work will involve making a cell line in which endogenous *ZAC1* is replaced with *ZAC1*-FLAG so that endogenous levels of expression are maintained while still having the FLAG-tag for ChIP. Lastly, a fold-change metric was not included in the pathway enrichment analyses; therefore, we were unable to determine positive or negative enrichment of pathways.

CHAPTER 5:

Conclusions and Future Directions

In the Constitution of the World Health Organization (WHO), it is stated that “health is a state of complete physical, mental and social well-being and not merely the absence of disease or infirmity”²²¹. Exposure to emerging and legacy contaminants is of major concern and jeopardizes our attempts to secure health for individuals of all ages around the world. It has been estimated that the global burden of disease attributable to environmental and occupational risk factors is 15-25%; in 2021, these factors were responsible for 19% (13 million) of global deaths and 14% of all disability-adjusted life years²²². Despite best efforts to regulate the release of hazardous chemicals into the environment to mitigate our exposure, our contact is inevitable; therefore, it is of paramount importance to identify the most prominent environmental contaminants, determine their impacts to human health, and find means to alleviate the associated adverse outcomes.

The WHO has compiled a list of the top ten chemicals of major public health concern which include arsenic, asbestos, benzene, cadmium, dioxins (and dioxin-like substances), inadequate or excess fluoride, lead, mercury, and highly-hazardous pesticides²²³. Among those chemicals, the heavy metal cadmium (Cd) has been designated a top ten chemical due to its widespread presence in the environment, its prolonged biological half-life in body tissues, and its link to harmful effects across nearly all organ systems³. Once absorbed, Cd is poorly excreted and can remain in the body for years or even decades. The kidneys, liver, and bones are primary sites of Cd

accumulation and are especially vulnerable to its toxic effects³. Research has shown that Cd exposure can contribute to the development of metabolic dysfunction-associated steatotic liver disease (MASLD), a condition marked by excessive fat accumulation in hepatocytes^{99–102}. If left unchecked, MASLD can progress to metabolic dysfunction-associated steatohepatitis (MASH), cirrhosis, and eventually even hepatocellular carcinoma (HCC)^{44,45}. MASLD is currently the most prevalent chronic liver disease globally, affecting both adults and adolescents^{48,49}.

We have shown that exposure to Cd during the perinatal period – a highly-sensitive developmental window during prenatal and early postnatal life – can program features of MASLD in juvenile mouse livers, including steatosis and fibrosis⁶⁷. Although perinatal development is widely recognized as the most influential period of growth and maturation, adolescence is another crucial developmental period marked by increased sensitivity, yet it has been less thoroughly investigated^{109–113}. Strikingly, imprinted genes are particularly responsive to environmental influences during these critical windows, positioning themselves as potential drivers of long-term adverse health outcomes^{74–78}. In our perinatal Cd exposure mouse model, we observed MASLD phenotypes alongside the activation of a network of imprinted and biallelically expressed genes in the liver⁶⁷. Experimentally inducing this imprinted gene network (IGN), through upregulation of its master regulator ZAC1, enhanced hepatic steatosis and upregulated genes associated with fibrosis, supporting the idea that the IGN can promote MASLD during vulnerable developmental periods^{66,67}. Among the IGN members, the imprinted long non-coding RNA (lncRNA) H19 showed a dramatic increase in expression following perinatal Cd

exposure; notably, *H19* has previously been linked to MASLD pathogenesis, making it a potential therapeutic target^{88–92}.

In **Chapter 2**, we investigated how Cd exposure during adolescence and young adulthood affects the development of MASLD in mice. While no overt MASLD phenotypes were observed – including changes in liver weight, triacylglyceride (TAG) levels, or collagen deposition – Cd exposure activated transcriptional networks associated with steatosis, inflammation, and fibrosis, particularly in males. Key lipid metabolism genes and markers of fibrosis were upregulated, alongside a shift in fatty acid transport gene expression suggestive of an adipogenic transformation of the liver. Lipidomic analyses revealed enrichment of lipotoxic lipid species including sphingoid bases, ceramides, and saturated fatty acids (SFAs) with stronger effects observed in females. Males also showed increased oxidative stress response gene expression and activation of the IGF1R, providing evidence of potential mechanisms of action for Cd-induced MASLD. Overall, these findings suggest that Cd exposure during adolescence and young adulthood can prime the liver for MASLD later in life, especially in males. Future studies will explore including additional collection timepoints to determine if the molecular and biochemical signatures of MASLD induced by Cd can manifest into overt phenotypes at later life stages.

In **Chapter 3**, we examined the impact of developmental Cd exposure and the role of the imprinted lncRNA *H19* in the programming of MASLD in juvenile mice. Considering the evidence of *H19*'s involvement in the pathogenesis of MASLD, we hypothesized that systemic ablation of *H19* could protect against MASLD in mice exposed to Cd during perinatal development. Contrary to our previous study, offspring did not display overt Cd-

induced MASLD phenotypes at postnatal day (PND) 0 (birth) or PND 21. This discrepancy could be contributed to differences in Cd concentration and mouse strain. At PND 0, developmental Cd exposure also did not significantly alter MASLD-related gene expression, aside from increases in *Fabp4* in both sexes and *Col6a1* in females. Males did, however, present with Cd-related elevated fasting blood glucose which was also present in males at PND 21. At PND 21, male and female offspring showed Cd-induced perturbations in the expression of key genes involved in lipid metabolism, inflammation, and fibrosis, indicating early molecular signs of liver stress and MASLD. Notably, the ablation of *H19* did not alter the MASLD-related gene expression changes caused by developmental Cd exposure. At PND 0 and PND 21, mice exhibited reductions in body and organ weights due to Cd and overgrowth phenotypes due to systemic ablation *H19*, outcomes that were to be expected. Males and females also presented with changes in essential metal trace concentrations in their blood including iron (Fe). Further, *H19* ablation activated IGN genes at PND 0, especially in males, while perinatal Cd exposure activated IGN genes at PND 21. Of importance, the expression of the imprinted gene *Igf2* was dramatically increased in *H19* knockout (KO) males and females exposed to Cd. We hypothesize that the marked increase in *Igf2*, a gene also implicated in MASLD, may inhibit the protective effects of *H19* ablation. Future work will investigate the relationship between *H19* and *Igf2* in this model.

In **Chapter 4**, we explored the genomic binding sites of the transcription factor ZAC1 to better understand its role in perturbing transcriptional networks associated with MASLD. Using chromatin immunoprecipitation-sequencing (ChIP-seq) in a hepatoma cell line overexpressing ZAC1, we identified 4,647 binding peaks, nearly half of which were

at gene promoters including the pro-fibrotic genes *TGFB1* and *COL6A2*. Motif analysis showed that ZAC1 preferentially binds GC-rich sequences, consistent with its classification as a C2H2 transcription factor. Enrichment analyses of the 2,381 genes with promoter-bound ZAC1 highlighted key MASLD-related pathways, including insulin resistance, HCC, MAPK signaling, epithelial-mesenchymal transition (EMT), and PI3K signaling. ZAC1 was also shown to bind to 45 IGN members including itself and *IGF2*. These findings offer insight into ZAC1's potential regulatory role in MASLD. Future studies will work to leverage primary hepatocytes and physiological ZAC1 expression levels.

Collectively, this body of work advances our understanding of adolescence and the perinatal period as sensitive windows during which exposure to Cd can contribute to the development of MASLD. It may be of great interest to explore other pertinent chemicals, especially those highlighted by the WHO, for their ability to program liver diseases such as MASLD during critical windows of susceptibility. Further, this dissertation offers novel insights into the regulatory roles of the imprinted genes *H19* and *ZAC1*, demonstrating how they can modulate the expression of genes associated with the IGN and MASLD to influence the trajectory and severity of disease progression. Considering the interconnected nature of the IGN, exploring the functions of other pertinent imprinted genes – including *Igf2* – in disease pathology may identify new therapeutic targets in the treatment of prevalent diseases.

REFERENCES

1. Morrow, H. Cadmium and Cadmium Alloys. in *Kirk-Othmer Encyclopedia of Chemical Technology* 1–36 (John Wiley & Sons, Ltd, 2010). doi:10.1002/0471238961.0301041303011818.a01.pub3.
2. Kubier, A., Wilkin, R. T. & Pichler, T. Cadmium in soils and groundwater: A review. *Appl Geochem* **108**, 1–16 (2019).
3. Faroon, O. *et al. Toxicological Profile for Cadmium*. (Agency for Toxic Substances and Disease Registry (US), Atlanta (GA), 2012).
4. Suci, N. A., De Vivo, R., Rizzati, N. & Capri, E. Cd content in phosphate fertilizer: Which potential risk for the environment and human health? *Current Opinion in Environmental Science & Health* **30**, 100392 (2022).
5. Autier, V. & White, D. Examination of cadmium sorption characteristics for a boreal soil near Fairbanks, Alaska. *Journal of Hazardous Materials* **106**, 149–155 (2004).
6. Elinder, C. G. Cadmium as an environmental hazard. *IARC Sci Publ* 123–132 (1992).
7. *Cadmium and Health: A Toxicological and Epidemiological Appraisal*. vol. Volume 1: Exposure, Dose, and Metabolism (CRC Press, Boca Raton, 2019).
8. Shevchenko, V., Lisitzin, A., Vinogradova, A. & Stein, R. Heavy metals in aerosols over the seas of the Russian Arctic. *Science of The Total Environment* **306**, 11–25 (2003).
9. Qing, Y. *et al.* Assessment of Cadmium Concentrations in Foodstuffs and Dietary Exposure Risk Across China: A Metadata Analysis. *Expo Health* **15**, 951–961 (2023).
10. Kim, K. *et al.* Dietary Cadmium Intake and Sources in the US. *Nutrients* **11**, 2 (2018).

11. Mei, S. *et al.* Cadmium Accumulation in Cereal Crops and Tobacco: A Review. *Agronomy* **12**, 1952 (2022).
12. Scherer, G. & Barkemeyer, H. Cadmium concentrations in tobacco and tobacco smoke. *Ecotoxicology and Environmental Safety* **7**, 71–78 (1983).
13. Wróblewski, K., Wojnicka, J., Tutka, P., Szmagara, A. & Błażewicz, A. Measurements of cadmium levels in relation to tobacco dependence and as a function of cytosine administration. *Sci Rep* **14**, 1883 (2024).
14. Arshad, H., Mehmood, M. Z., Shah, M. H. & Abbasi, A. M. Evaluation of heavy metals in cosmetic products and their health risk assessment. *Saudi Pharm J* **28**, 779–790 (2020).
15. Kern, M. S., Boron, M. L. & Weidenhamer, J. D. Buyer beware: Inexpensive, high cadmium jewelry can pose severe health risks. *Science of The Total Environment* **764**, 142926 (2021).
16. Godt, J. *et al.* The toxicity of cadmium and resulting hazards for human health. *J Occup Med Toxicol* **1**, 22 (2006).
17. Qu, F. & Zheng, W. Cadmium Exposure: Mechanisms and Pathways of Toxicity and Implications for Human Health. *Toxics* **12**, 388 (2024).
18. Liu, J., Qu, W. & Kadiiska, M. B. Role of oxidative stress in cadmium toxicity and carcinogenesis. *Toxicol Appl Pharmacol* **238**, 209–214 (2009).
19. Das, S. C. & Al-Naemi, H. A. Cadmium Toxicity: Oxidative Stress, Inflammation and Tissue Injury. *Occupational Diseases and Environmental Medicine* **7**, 144–163 (2019).

20. Choong, G., Liu, Y. & Templeton, D. M. Interplay of calcium and cadmium in mediating cadmium toxicity. *Chemico-Biological Interactions* **211**, 54–65 (2014).
21. Hudson, K. M., Belcher, S. M. & Cowley, M. Maternal cadmium exposure in the mouse leads to increased heart weight at birth and programs susceptibility to hypertension in adulthood. *Sci Rep* **9**, 13553 (2019).
22. Cirovic, A., Cirovic, A., Yimthiang, S., Vesey, D. A. & Satarug, S. Modulation of Adverse Health Effects of Environmental Cadmium Exposure by Zinc and Its Transporters. *Biomolecules* **14**, 650 (2024).
23. Guo, W. *et al.* Environmental cadmium exposure perturbs systemic iron homeostasis via hemolysis and inflammation, leading to hepatic ferroptosis in common carp (*Cyprinus carpio* L.). *Ecotoxicology and Environmental Safety* **275**, 116246 (2024).
24. Kusak, R., Nasiadek, M., Stragierowicz, J., Hanke, W. & Kilanowicz, A. Changes in Endogenous Essential Metal Homeostasis in the Liver and Kidneys during a Six-Month Follow-Up Period after Subchronic Cadmium Exposure. *Int J Mol Sci* **25**, 3829 (2024).
25. Moulis, J.-M. Cellular mechanisms of cadmium toxicity related to the homeostasis of essential metals. *Biometals* **23**, 877–896 (2010).
26. Wang, B., Li, Y., Shao, C., Tan, Y. & Cai, L. Cadmium and its epigenetic effects. *Curr Med Chem* **19**, 2611–2620 (2012).
27. Vilahur, N., Vahter, M. & Broberg, K. The Epigenetic Effects of Prenatal Cadmium Exposure. *Curr Environ Health Rep* **2**, 195–203 (2015).

28. Barrett, E. S. *et al.* Protective role of the placental efflux transporter BCRP/ABCG2 in the relationship between prenatal cadmium exposure, placenta weight, and size at birth. *Environ Res* **225**, 115597 (2023).
29. Coyle, P., Philcox, J. C., Carey, L. C. & Rofe, A. M. Metallothionein: the multipurpose protein. *Cell Mol Life Sci* **59**, 627–647 (2002).
30. Kantola, M. *et al.* Accumulation of cadmium, zinc, and copper in maternal blood and developmental placental tissue: differences between Finland, Estonia, and St. Petersburg. *Environ Res* **83**, 54–66 (2000).
31. Plöckinger, B., Dadak, C. & Meisinger, V. [Lead, mercury and cadmium in newborn infants and their mothers]. *Z Geburtshilfe Perinatol* **197**, 104–107 (1993).
32. Sakamoto, M. *et al.* Relationships between trace element concentrations in chorionic tissue of placenta and umbilical cord tissue: potential use as indicators for prenatal exposure. *Environ Int* **60**, 106–111 (2013).
33. Ahokas, R. A. & Dilts, P. V. Cadmium uptake by the rat embryo as a function of gestational age. *Am J Obstet Gynecol* **135**, 219–222 (1979).
34. Jackson, T. W., Baars, O. & Belcher, S. M. Gestational Cd Exposure in the CD-1 Mouse Sex-Specifically Disrupts Essential Metal Ion Homeostasis. *Toxicological Sciences* **187**, 254–266 (2022).
35. Sonawane, B. R., Nordberg, M., Nordberg, G. F. & Lucier, G. W. Placental transfer of cadmium in rats: influence of dose and gestational age. *Environ Health Perspect* **12**, 97–102 (1975).
36. Szukalska, M. *et al.* Toxic metals in human milk in relation to tobacco smoke exposure. *Environmental Research* **197**, 111090 (2021).

37. Gandhi, C. R. Cellular Anatomy of the Liver (Hepatocyte, Biliary Epithelial Cells, Endothelial Cells, Kupffer Cells and Hepatic Stellate Cells). in *Pathobiology of Human Disease* (eds. McManus, L. M. & Mitchell, R. N.) 1759–1769 (Academic Press, San Diego, 2014). doi:10.1016/B978-0-12-386456-7.04201-5.
38. Mitra, V. & Metcalf, J. Metabolic functions of the liver. *Anaesthesia & Intensive Care Medicine* **10**, 334–335 (2009).
39. Kalra, A., Yetiskul, E., Wehrle, C. J. & Tuma, F. Physiology, Liver. in *StatPearls* (StatPearls Publishing, Treasure Island (FL), 2025).
40. Sharma, A. & Nagalli, S. Chronic Liver Disease. in *StatPearls* (StatPearls Publishing, Treasure Island (FL), 2025).
41. Yap, K. K. & Mitchell, G. M. Recapitulating the liver niche in vitro. in *Advances in Stem Cells and their Niches* (ed. Nilsson, S.) vol. 6 1–55 (Elsevier, 2022).
42. Lu, Q. *et al.* Metabolic Changes of Hepatocytes in NAFLD. *Front Physiol* **12**, 710420 (2021).
43. Kanwal, F., Neuschwander-Tetri, B. A., Loomba, R. & Rinella, M. E. Metabolic dysfunction–associated steatotic liver disease: Update and impact of new nomenclature on the American Association for the Study of Liver Diseases practice guidance on nonalcoholic fatty liver disease. *Hepatology* **79**, 1212 (2024).
44. Li, Y. *et al.* Updated mechanisms of MASLD pathogenesis. *Lipids in Health and Disease* **23**, 117 (2024).
45. Takahashi, Y., Dungubat, E., Kusano, H. & Fukusato, T. Pathology and Pathogenesis of Metabolic Dysfunction-Associated Steatotic Liver Disease-Associated Hepatic Tumors. *Biomedicines* **11**, 2761 (2023).

46. Shimamura, T., Goto, R., Watanabe, M., Kawamura, N. & Takada, Y. Liver Transplantation for Hepatocellular Carcinoma: How Should We Improve the Thresholds? *Cancers (Basel)* **14**, 419 (2022).
47. Santopaolo, F., Lenci, I., Milana, M., Manzia, T. M. & Baiocchi, L. Liver transplantation for hepatocellular carcinoma: Where do we stand? *World J Gastroenterol* **25**, 2591–2602 (2019).
48. Le, P. *et al.* Estimated Burden of Metabolic Dysfunction–Associated Steatotic Liver Disease in US Adults, 2020 to 2050. *JAMA Network Open* **8**, e2454707 (2025).
49. Perumpail, B. J. *et al.* The prevalence and predictors of metabolic dysfunction-associated steatotic liver disease and fibrosis/cirrhosis among adolescents/young adults. *Journal of Pediatric Gastroenterology and Nutrition* **79**, 110–118 (2024).
50. Kim, D., Kim, W. R., Kim, H. J. & Therneau, T. M. Association between noninvasive fibrosis markers and mortality among adults with nonalcoholic fatty liver disease in the United States. *Hepatology* **57**, 1357–1365 (2013).
51. Alves-Bezerra, M. & Cohen, D. E. Triglyceride metabolism in the liver. *Compr Physiol* **8**, 1–8 (2017).
52. Liss, K. H. H. & Finck, B. N. PPARs and Nonalcoholic Fatty Liver Disease. *Biochimie* **136**, 65–74 (2017).
53. Delli Bovi, A. P. *et al.* Oxidative Stress in Non-alcoholic Fatty Liver Disease. An Updated Mini Review. *Front Med (Lausanne)* **8**, 595371 (2021).
54. Gao, B. & Tsukamoto, H. Inflammation in alcoholic and nonalcoholic fatty liver disease: friend or foe? *Gastroenterology* **150**, 1704–1709 (2016).

55. Luedde, T. & Schwabe, R. F. NF- κ B in the liver—linking injury, fibrosis and hepatocellular carcinoma. *Nat Rev Gastroenterol Hepatol* **8**, 108–118 (2011).
56. Ni, Y.-A., Chen, H., Nie, H., Zheng, B. & Gong, Q. HMGB1: An overview of its roles in the pathogenesis of liver disease. *Journal of Leukocyte Biology* **110**, 987–998 (2021).
57. Wang, X., Zhang, L. & Dong, B. Molecular mechanisms in MASLD/MASH-related HCC. *Hepatology* 10.1097/HEP.0000000000000786
doi:10.1097/HEP.0000000000000786.
58. Weiskirchen, R. Exploring Molecular Mechanisms of Liver Fibrosis. *Int J Mol Sci* **26**, 326 (2025).
59. Lacagnina, S. The Developmental Origins of Health and Disease (DOHaD). *Am J Lifestyle Med* **14**, 47–50 (2019).
60. Wadhwa, P. D., Buss, C., Entringer, S. & Swanson, J. M. Developmental Origins of Health and Disease: Brief History of the Approach and Current Focus on Epigenetic Mechanisms. *Semin Reprod Med* **27**, 358–368 (2009).
61. National Academies of Sciences, E. *et al.* Healthy Development from Conception Through Early Childhood. in *Vibrant and Healthy Kids: Aligning Science, Practice, and Policy to Advance Health Equity* (National Academies Press (US), 2019).
62. Daoust, L. *et al.* The postnatal window is critical for the development of sex-specific metabolic and gut microbiota outcomes in offspring. *Gut Microbes* **13**, 2004070 (2021).

63. Hu, C.-Y. *et al.* Windows of susceptibility and joint effects of prenatal and postnatal ambient air pollution and temperature exposure on asthma and wheeze in Mexican children. *Environ Int* **193**, 109122 (2024).
64. Sanders, A. P. *et al.* Prenatal and early childhood critical windows for the association of nephrotoxic metal and metalloid mixtures with kidney function. *Environment International* **166**, 107361 (2022).
65. Helfer, R. E. The perinatal period, a window of opportunity for enhancing parent-infant communication: An approach to prevention. *Child Abuse & Neglect* **11**, 565–579 (1987).
66. Baptissart, M. *et al.* *Zac1* and the Imprinted Gene Network program juvenile NAFLD in response to maternal metabolic syndrome. *Hepatology* **76**, 1090–1104 (2022).
67. Riegl, S. D. *et al.* The imprinted gene *Zac1* regulates steatosis in developmental cadmium-induced nonalcoholic fatty liver disease. *Toxicological Sciences* **191**, 34–46 (2023).
68. Argente, J. *et al.* Molecular basis of normal and pathological puberty: from basic mechanisms to clinical implications. *The Lancet Diabetes & Endocrinology* **11**, 203–216 (2023).
69. Özen, S. & Darcan, Ş. Effects of Environmental Endocrine Disruptors on Pubertal Development. *J Clin Res Pediatr Endocrinol* **3**, 1–6 (2011).
70. Holder, M. K. & Blaustein, J. D. Puberty and adolescence as a time of vulnerability to stressors that alter neurobehavioral processes. *Frontiers in Neuroendocrinology* **35**, 89–110 (2014).

71. Pervanidou, P. & Chrousos, G. P. Metabolic consequences of stress during childhood and adolescence. *Metabolism* **61**, 611–619 (2012).
72. Ishida, M. & Moore, G. E. The role of imprinted genes in humans. *Molecular Aspects of Medicine* **34**, 826–840 (2013).
73. Paro, P. D. R., Grossniklaus, P. D. U., Santoro, D. R. & Wutz, P. D. A. Genomic Imprinting. in *Introduction to Epigenetics [Internet]* (Springer, 2021). doi:10.1007/978-3-030-68670-3_5.
74. Jirtle, R. L. & Skinner, M. K. Environmental epigenomics and disease susceptibility. *Nat Rev Genet* **8**, 253–262 (2007).
75. Kappil, M., Lambertini, L. & Chen, J. Environmental Influences on Genomic Imprinting. *Curr Environ Health Rep* **2**, 155–162 (2015).
76. Cowley, M. *et al.* Effects of Cadmium Exposure on DNA Methylation at Imprinting Control Regions and Genome-Wide in Mothers and Newborn Children. *Environ Health Perspect* **126**, 037003 (2018).
77. Liang, Y. *et al.* Short-term personal PM_{2.5} exposure and change in DNA methylation of imprinted genes: Panel study of healthy young adults in Guangzhou city, China. *Environmental Pollution* **275**, 116601 (2021).
78. Robles-Matos, N., Artis, T., Simmons, R. A. & Bartolomei, M. S. Environmental Exposure to Endocrine Disrupting Chemicals Influences Genomic Imprinting, Growth, and Metabolism. *Genes (Basel)* **12**, 1153 (2021).
79. Al Adhami, H. *et al.* A systems-level approach to parental genomic imprinting: the imprinted gene network includes extracellular matrix genes and regulates cell cycle exit and differentiation. *Genome Res* **25**, 353–367 (2015).

80. Varrault, A. *et al.* Zac1 Regulates an Imprinted Gene Network Critically Involved in the Control of Embryonic Growth. *Developmental Cell* **11**, 711–722 (2006).
81. Varrault, A. *et al.* hZAC encodes a zinc finger protein with antiproliferative properties and maps to a chromosomal region frequently lost in cancer. *Proc Natl Acad Sci U S A* **95**, 8835–8840 (1998).
82. Spengler, D. *et al.* Regulation of apoptosis and cell cycle arrest by Zac1, a novel zinc finger protein expressed in the pituitary gland and the brain. *EMBO J* **16**, 2814–2825 (1997).
83. Huang, S.-M. & Stallcup, M. R. Mouse Zac1, a Transcriptional Coactivator and Repressor for Nuclear Receptors. *Mol Cell Biol* **20**, 1855–1867 (2000).
84. Huang, S.-M., Schönthal, A. H. & Stallcup, M. R. Enhancement of p53-dependent gene activation by the transcriptional coactivator Zac1. *Oncogene* **20**, 2134–2143 (2001).
85. Riegl, S. D. *et al.* The imprinted gene Zac1 regulates steatosis in developmental cadmium-induced nonalcoholic fatty liver disease. *Toxicological Sciences* **191**, 34–46 (2023).
86. Gabory, A., Jammes, H. & Dandolo, L. The H19 locus: Role of an imprinted non-coding RNA in growth and development. *BioEssays* **32**, 473–480 (2010).
87. Matsuzaki, H., Miyajima, Y., Fukamizu, A. & Tanimoto, K. Orientation of mouse H19 ICR affects imprinted H19 gene expression through promoter methylation-dependent and -independent mechanisms. *Commun Biol* **4**, 1–11 (2021).
88. Liu, C. *et al.* lncRNA H19 interacts with polypyrimidine tract-binding protein 1 to reprogram hepatic lipid homeostasis. *Hepatology* **67**, 1768–1783 (2018).

89. Liu, J., Tang, T., Wang, G.-D. & Liu, B. LncRNA-H19 promotes hepatic lipogenesis by directly regulating miR-130a/PPAR γ axis in non-alcoholic fatty liver disease. *Biosci Rep* **39**, BSR20181722 (2019).
90. Liu, Y. *et al.* LncRNA H19/microRNA-675/PPAR α axis regulates liver cell injury and energy metabolism remodelling induced by hepatitis B X protein via Akt/mTOR signalling. *Molecular Immunology* **116**, 18–28 (2019).
91. Zhu, J. *et al.* H19/miR-148a/USP4 axis facilitates liver fibrosis by enhancing TGF- β signaling in both hepatic stellate cells and hepatocytes. *Journal of Cellular Physiology* **234**, 9698–9710 (2019).
92. Wang, H. *et al.* Long non-coding RNA (lncRNA) H19 induces hepatic steatosis through activating MLXIPL and mTORC1 networks in hepatocytes. *J Cell Mol Med* **24**, 1399–1412 (2020).
93. 10 chemicals of public health concern. <https://www.who.int/news-room/photo-story/photo-story-detail/10-chemicals-of-public-health-concern>.
94. Baldantoni, D., Morra, L., Zaccardelli, M. & Alfani, A. Cadmium accumulation in leaves of leafy vegetables. *Ecotoxicology and Environmental Safety* **123**, 89–94 (2016).
95. Li, L. *et al.* Secondhand smoke is associated with heavy metal concentrations in children. *Eur J Pediatr* **177**, 257–264 (2018).
96. Ganguly, K., Levänen, B., Palmberg, L., Åkesson, A. & Lindén, A. Cadmium in tobacco smokers: a neglected link to lung disease? *European Respiratory Review* **27**, (2018).

97. Lee, J., Kim, Y., Kim, Y., Yoo, H. & Kang, H.-T. Cigarette Smoking in Men and Women and Electronic Cigarette Smoking in Men are Associated with Higher Risk of Elevated Cadmium Level in the Blood. *Journal of Korean Medical Science* **35**, (2019).
98. Hyder, O. *et al.* Cadmium Exposure and Liver Disease among US Adults. *J Gastrointest Surg* **17**, 1265–1273 (2013).
99. Park, E., Kim, J., Kim, B. & Park, E. Y. Association between environmental exposure to cadmium and risk of suspected non-alcoholic fatty liver disease. *Chemosphere* **266**, 128947 (2021).
100. Li, Y. *et al.* Cadmium Exposure in Young Adulthood Is Associated with Risk of Nonalcoholic Fatty Liver Disease in Midlife. *Dig Dis Sci* **67**, 689–696 (2022).
101. Go, Y.-M. *et al.* Low-Dose Cadmium Causes Metabolic and Genetic Dysregulation Associated With Fatty Liver Disease in Mice. *Toxicol Sci* **147**, 524–534 (2015).
102. He, X. *et al.* Inhibition of Mitochondrial Fatty Acid Oxidation Contributes to Development of Nonalcoholic Fatty Liver Disease Induced by Environmental Cadmium Exposure. *Environ. Sci. Technol.* **53**, 13992–14000 (2019).
103. Younossi, Z. M. *et al.* The global epidemiology of nonalcoholic fatty liver disease (NAFLD) and nonalcoholic steatohepatitis (NASH): a systematic review. *Hepatology* **77**, 1335–1347 (2023).
104. Lee, B. P., Dodge, J. L. & Terrault, N. A. National prevalence estimates for steatotic liver disease and subclassifications using consensus nomenclature. *Hepatology* **79**, 666–673 (2024).

105. Nouredin, N., Copur-Dahi, N. & Loomba, R. Monitoring disease progression in metabolic dysfunction-associated steatotic liver disease. *Alimentary Pharmacology & Therapeutics* **59**, S41–S51 (2024).
106. Miao, L., Targher, G., Byrne, C. D., Cao, Y.-Y. & Zheng, M.-H. Current status and future trends of the global burden of MASLD. *Trends in Endocrinology & Metabolism* **35**, 697–707 (2024).
107. Tomeno, W. *et al.* Complications of Non-Alcoholic Fatty Liver Disease in Extrahepatic Organs. *Diagnostics* **10**, 912 (2020).
108. Arshad, T. *et al.* Nonalcoholic Fatty Liver Disease Prevalence Trends Among Adolescents and Young Adults in the United States, 2007-2016. *Hepatol Commun* **5**, 1676–1688 (2021).
109. Li, M., Reynolds, C. M., Segovia, S. A., Gray, C. & Vickers, M. H. Developmental Programming of Nonalcoholic Fatty Liver Disease: The Effect of Early Life Nutrition on Susceptibility and Disease Severity in Later Life. *Biomed Res Int* **2015**, 437107 (2015).
110. Midya, V. *et al.* Association of Prenatal Exposure to Endocrine-Disrupting Chemicals With Liver Injury in Children. *JAMA Network Open* **5**, e2220176 (2022).
111. Yu, E. L. *et al.* Prevalence of Nonalcoholic Fatty Liver Disease in Children with Obesity. *J Pediatr* **207**, 64–70 (2019).
112. Güil-Oumrait, N. *et al.* Prenatal Exposure to Chemical Mixtures and Metabolic Syndrome Risk in Children. *JAMA Network Open* **7**, e2412040 (2024).

113. Santos, B. G. dos *et al.* Puberty as a DOHaD programming window: high-fat diet induces long-term hepatic dysfunction in male rats. *Journal of Developmental Origins of Health and Disease* **14**, 614–622 (2023).
114. Biro, F. M. & Deardorff, J. Identifying Opportunities for Cancer Prevention During Pre-Adolescence and Adolescence: Puberty as a Window of Susceptibility. *J Adolesc Health* **52**, S15–S20 (2013).
115. Jackson, T. W. *et al.* Gestational Cd Exposure in the CD-1 Mouse Induces Sex-Specific Hepatic Insulin Insensitivity, Obesity, and Metabolic Syndrome in Adult Female Offspring. *Toxicol Sci* **178**, 264–280 (2020).
116. Yi, S.-J. *et al.* Environmental cadmium exposure during pregnancy causes diabetes-like phenotypes in mouse offspring: Association with oxidative stress in the fetal liver. *Science of The Total Environment* **777**, 146006 (2021).
117. Reilly, M. P. *et al.* Prepubertal Exposure to Arsenic(III) Suppresses Circulating Insulin-like Growth Factor-1 (IGF-1) Delaying Sexual Maturation in Female Rats. *Reprod Toxicol* **44**, 41–49 (2014).
118. Betanzos-Robledo, L. *et al.* ASSOCIATION BETWEEN CUMULATIVE CHILDHOOD BLOOD LEAD EXPOSURE AND HEPATIC STEATOSIS IN YOUNG MEXICAN ADULTS. *Environ Res* **196**, 110980 (2021).
119. Couto-Santos, F. *et al.* Impact of Early Arsenic Exposure on the Mineral Content and Oxidative Status of the Liver and Kidney of Pubescent and Adult Rats. *Biol Trace Elem Res* **202**, 1644–1655 (2024).

120. Jin, Y. *et al.* Oral exposure of pubertal male mice to endocrine-disrupting chemicals alters fat metabolism in adult livers. *Environmental Toxicology* **30**, 1434–1444 (2015).
121. Li, X. *et al.* Chronic oral exposure to cadmium causes liver inflammation by NLRP3 inflammasome activation in pubertal mice. *Food and Chemical Toxicology* **148**, 111944 (2021).
122. Livak, K. J. & Schmittgen, T. D. Analysis of Relative Gene Expression Data Using Real-Time Quantitative PCR and the $2^{-\Delta\Delta CT}$ Method. *Methods* **25**, 402–408 (2001).
123. Scheidemantle, G. *et al.* Data-dependent and -independent acquisition lipidomics analysis reveals the tissue-dependent effect of metformin on lipid metabolism. *Metabolomics* **20**, 53 (2024).
124. Chappel, J. R., Kirkwood-Donelson, K. I., Reif, D. M. & Baker, E. S. From big data to big insights: statistical and bioinformatic approaches for exploring the lipidome. *Anal Bioanal Chem* **416**, 2189–2202 (2024).
125. Ritchie, M. E. *et al.* limma powers differential expression analyses for RNA-sequencing and microarray studies. *Nucleic Acids Res* **43**, e47 (2015).
126. Larsson, J. *et al.* eulerr: Area-Proportional Euler and Venn Diagrams with Ellipses. (2024).
127. Wickham, H. Data Analysis. in *ggplot2: Elegant Graphics for Data Analysis* 189–201 (Springer International Publishing, Cham, 2016). doi:10.1007/978-3-319-24277-4_9.
128. Hoang, S. A. *et al.* Gene Expression Predicts Histological Severity and Reveals Distinct Molecular Profiles of Nonalcoholic Fatty Liver Disease. *Sci Rep* **9**, 12541 (2019).

129. Coassolo, L. *et al.* Mapping transcriptional heterogeneity and metabolic networks in fatty livers at single-cell resolution. *iScience* **26**, 105802 (2022).
130. Aljabban, J. *et al.* Transcriptome changes in stages of non-alcoholic fatty liver disease. *World Journal of Hepatology* **14**, 1382 (2022).
131. Alkhouri, N., Dixon, L. J. & Feldstein, A. E. Lipotoxicity in Nonalcoholic Fatty Liver Disease: Not All Lipids Are Created Equal. *Expert Rev Gastroenterol Hepatol* **3**, 445–451 (2009).
132. Roumans, K. H. M. *et al.* Hepatic saturated fatty acid fraction is associated with de novo lipogenesis and hepatic insulin resistance. *Nat Commun* **11**, 1891 (2020).
133. Parks, E., Yki-Järvinen, H. & Hawkins, M. Out of the frying pan: dietary saturated fat influences nonalcoholic fatty liver disease. *J Clin Invest* **127**, 454–456.
134. Hernández, E. Á. *et al.* Acute dietary fat intake initiates alterations in energy metabolism and insulin resistance. *J Clin Invest* **127**, 695–708.
135. Ma, Y., Lee, G., Heo, S.-Y. & Roh, Y.-S. Oxidative Stress Is a Key Modulator in the Development of Nonalcoholic Fatty Liver Disease. *Antioxidants* **11**, 91 (2022).
136. Smirne, C. *et al.* Oxidative Stress in Non-Alcoholic Fatty Liver Disease. *Livers* **2**, 30–76 (2022).
137. Moroni-González, D., Sarmiento-Ortega, V. E., Diaz, A., Brambila, E. & Treviño, S. Pancreas–Liver–Adipose Axis: Target of Environmental Cadmium Exposure Linked to Metabolic Diseases. *Toxics* **11**, 223 (2023).
138. Ipsen, D. H., Lykkesfeldt, J. & Tveden-Nyborg, P. Molecular mechanisms of hepatic lipid accumulation in non-alcoholic fatty liver disease. *Cell Mol Life Sci* **75**, 3313–3327 (2018).

139. Prentice, K. J., Saksi, J. & Hotamisligil, G. S. Adipokine FABP4 integrates energy stores and counterregulatory metabolic responses. *Journal of Lipid Research* **60**, 734–740 (2019).
140. Zhou, C. *et al.* FABP4 in LSECs promotes CXCL10-mediated macrophage recruitment and M1 polarization during NAFLD progression. *Biochimica et Biophysica Acta (BBA) - Molecular Basis of Disease* **1869**, 166810 (2023).
141. Sarmiento-Ortega, V. E., Moroni-González, D., Díaz, A., Eduardo, B. & Samuel, T. Oral Subacute Exposure to Cadmium LOAEL Dose Induces Insulin Resistance and Impairment of the Hormonal and Metabolic Liver-Adipose Axis in Wistar Rats. *Biol Trace Elem Res* **200**, 4370–4384 (2022).
142. Chen, R. *et al.* Emerging Role of High-Mobility Group Box 1 (HMGB1) in Liver Diseases. *Mol Med* **19**, 357–366 (2013).
143. Li, L. *et al.* Nuclear factor high-mobility group box1 mediating the activation of toll-like receptor 4 signaling in hepatocytes in the early stage of nonalcoholic fatty liver disease in mice. *Hepatology* **54**, 1620 (2011).
144. Dewidar, B., Meyer, C., Dooley, S. & Meindl-Beinker, N. TGF- β in Hepatic Stellate Cell Activation and Liver Fibrogenesis—Updated 2019. *Cells* **8**, 1419 (2019).
145. Rabionet, M., Engel, R. & Sandhoff, R. Chapter 1 - Structure and function of mammalian sphingolipids in health and disease. in *Cellular Lipid in Health and Disease* (ed. Ntambi, J. M.) 1–65 (Academic Press, 2023). doi:10.1016/B978-0-323-95582-9.00016-4.

146. Green, C. D., Maceyka, M., Cowart, L. A. & Spiegel, S. Sphingolipids in metabolic disease: The good, the bad, and the unknown. *Cell Metabolism* **33**, 1293–1306 (2021).
147. Hannun, Y. A. & Obeid, L. M. Sphingolipids and their metabolism in physiology and disease. *Nat Rev Mol Cell Biol* **19**, 175–191 (2018).
148. Montefusco, D., Lambert, J., Anderson, A., Allegood, J. & Cowart, L. A. Analysis of the Sphingolipidome in NAFLD. *Methods Mol Biol* **2455**, 279–303 (2022).
149. Hajduch, E., Lachkar, F., Ferré, P. & Foufelle, F. Roles of Ceramides in Non-Alcoholic Fatty Liver Disease. *J Clin Med* **10**, 792 (2021).
150. Mashek, D. G. Hepatic lipid droplets: A balancing act between energy storage and metabolic dysfunction in NAFLD. *Molecular Metabolism* **50**, 101115 (2021).
151. Xie, D. *et al.* Cadmium exacerbates liver injury by remodeling ceramide metabolism: Multiomics and laboratory evidence. *Science of The Total Environment* **923**, 171405 (2024).
152. Leamy, A. K., Egnatchik, R. A. & Young, J. D. Molecular Mechanisms and the Role of Saturated Fatty Acids in the Progression of Non-Alcoholic Fatty Liver Disease. *Prog Lipid Res* **52**, 10.1016/j.plipres.2012.10.004 (2013).
153. Mei, S. *et al.* Differential Roles of Unsaturated and Saturated Fatty Acids on Autophagy and Apoptosis in Hepatocytes. *J Pharmacol Exp Ther* **339**, 487–498 (2011).
154. Nolan, C. J. & Larter, C. Z. Lipotoxicity: Why do saturated fatty acids cause and monounsaturates protect against it? *Journal of Gastroenterology and Hepatology* **24**, 703–706 (2009).

155. Zhu, Y. *et al.* Chronic exposure to low-dose cadmium facilitated nonalcoholic steatohepatitis in mice by suppressing fatty acid desaturation. *Ecotoxicology and Environmental Safety* **233**, 113306 (2022).
156. Zhu, Y. *et al.* Saturated fatty acids synergizes cadmium to induce macrophages M1 polarization and hepatic inflammation. *Ecotoxicology and Environmental Safety* **259**, 115040 (2023).
157. Li, S. *et al.* The Role of Oxidative Stress and Antioxidants in Liver Diseases. *Int J Mol Sci* **16**, 26087–26124 (2015).
158. Klaassen, C. D., Liu, J. & Diwan, B. A. Metallothionein Protection of Cadmium Toxicity. *Toxicol Appl Pharmacol* **238**, 215–220 (2009).
159. Luo, L. *et al.* De-silencing Grb10 contributes to acute ER stress-induced steatosis in mouse liver. (2018) doi:10.1530/JME-18-0018.
160. Moorwood, K., Smith, F. M., Garfield, A. S. & Ward, A. Imprinted Grb10, encoding growth factor receptor bound protein 10, regulates fetal growth independently of the insulin-like growth factor type 1 receptor (Igf1r) and insulin receptor (Insr) genes. *BMC Biol* **22**, 127 (2024).
161. Kadota, Y., Kawakami, T., Sato, M. & Suzuki, S. Mouse mesoderm-specific transcript inhibits adipogenic differentiation and induces trans-differentiation into hepatocyte-like cells in 3T3-L1 preadipocytes. *BMC Research Notes* **15**, 164 (2022).
162. Li, W., Zhu, C., Li, Y., Wu, Q. & Gao, R. Mest Attenuates CCl₄-Induced Liver Fibrosis in Rats by Inhibiting the Wnt/ β -Catenin Signaling Pathway. *Gut Liver* **8**, 282–291 (2014).

163. Darci-Maher, N. *et al.* Cross-tissue omics analysis discovers ten adipose genes encoding secreted proteins in obesity-related non-alcoholic fatty liver disease. *eBioMedicine* **92**, 104620 (2023).
164. Li, W., Kuang, Z., Zheng, M., He, G. & Liu, Y. Multi-omics integrative analysis to access role of coiled-coil domain-containing 80 in lipid metabolism. *Biochemical and Biophysical Research Communications* **526**, 813–819 (2020).
165. Krzistetzko, J., Géraud, C., Dormann, C., Riedel, A. & Leibing, T. Association of Differentially Altered Liver Fibrosis with Deposition of TGFBI in Stabilin-Deficient Mice. *Int J Mol Sci* **24**, 10969 (2023).
166. Lee, S. G. *et al.* TGFBI remodels adipose metabolism by regulating the Notch-1 signaling pathway. *Exp Mol Med* **55**, 520–531 (2023).
167. Sansilvestri Morel, P. *et al.* Procollagen C-Proteinase Enhancer-1 (PCPE-1) deficiency in mice reduces liver fibrosis but not NASH progression. *PLoS One* **17**, e0263828 (2022).
168. Yang, W. *et al.* METTL3 alters AK3 RNA expression in an m6A-dependent manner to affect the proliferation and metastasis of hepatocellular carcinoma. *International Journal of Biological Macromolecules* **282**, 137213 (2024).
169. National Research Council (US) Subcommittee on Zinc Cadmium Sulfide. Appendix I: Cadmium Exposure Assessment, Transport, and Environment Fate. in *Toxicologic Assessment of the Army's Zinc Cadmium Sulfide Dispersion Tests* (National Academies Press (US), Washington (DC), 1997).
170. Genchi, G., Sinicropi, M. S., Lauria, G., Carocci, A. & Catalano, A. The Effects of Cadmium Toxicity. *Int J Environ Res Public Health* **17**, 3782 (2020).

171. Charkiewicz, A. E., Omeljaniuk, W. J., Nowak, K., Garley, M. & Nikliński, J. Cadmium Toxicity and Health Effects—A Brief Summary. *Molecules* **28**, 6620 (2023).
172. Kuhnert, P. M., Kuhnert, B. R., Bottoms, S. F. & Erhard, P. Cadmium levels in maternal blood, fetal cord blood, and placental tissues of pregnant women who smoke. *American Journal of Obstetrics & Gynecology* **142**, 1021–1025 (1982).
173. Khanjani, N., Jafari, M. & Ahmadi Mousavi, E. Breast milk contamination with lead and cadmium and its related factors in Kerman, Iran. *J Environ Health Sci Eng* **16**, 323–335 (2018).
174. Cong, L. *et al.* Multiplex Genome Engineering Using CRISPR/Cas Systems. *Science* **339**, 819–823 (2013).
175. Townsend, D., Witkop Jr., C. J. & Mattson, J. Tyrosinase subcellular distribution and kinetic parameters in wild type and c-locus mutant C57BL/6J mice. *Journal of Experimental Zoology* **216**, 113–119 (1981).
176. Hughes, E. D. *et al.* Genetic variation in C57BL/6 ES cell lines and genetic instability in the Bruce4 C57BL/6 ES cell line. *Mamm Genome* **18**, 549–558 (2007).
177. Truett, G. E. *et al.* Preparation of PCR-Quality Mouse Genomic DNA with Hot Sodium Hydroxide and Tris (HotSHOT). *BioTechniques* **29**, 52–54 (2000).
178. Berky, A. J. *et al.* Risk of lead exposure from wild game consumption from cross-sectional studies in Madre de Dios, Peru. *Lancet Reg Health Am* **12**, 100266 (2022).
179. Leighton, P. A., Ingram, R. S., Eggenschwiler, J., Efstratiadis, A. & Tilghman, S. M. Disruption of imprinting caused by deletion of the H19 gene region in mice. *Nature* **375**, 34–39 (1995).

180. Ripoche, M. A., Kress, C., Poirier, F. & Dandolo, L. Deletion of the H19 transcription unit reveals the existence of a putative imprinting control element. *Genes Dev.* **11**, 1596–1604 (1997).
181. Himoto, T. & Masaki, T. Current Trends of Essential Trace Elements in Patients with Chronic Liver Diseases. *Nutrients* **12**, 2084 (2020).
182. Tinkov, A. A. *et al.* Association between serum trace element, mineral, and amino acid levels with non-alcoholic fatty liver disease (NAFLD) in adult women. *Journal of Trace Elements in Medicine and Biology* **83**, 127397 (2024).
183. Huang, S. *et al.* The association between prenatal cadmium exposure and birth weight: A systematic review and meta-analysis of available evidence. *Environmental Pollution* **251**, 699–707 (2019).
184. Zhu, H.-L. *et al.* Environmental cadmium exposure induces fetal growth restriction via triggering PERK-regulated mitophagy in placental trophoblasts. *Environment International* **147**, 106319 (2021).
185. Zinia, S. S. *et al.* Effects of heavy metal exposure during pregnancy on birth outcomes. *Sci Rep* **13**, 18990 (2023).
186. Pokharel, A. & Wu, F. Dietary exposure to cadmium from six common foods in the United States. *Food and Chemical Toxicology* **178**, 113873 (2023).
187. Wu, L. *et al.* Magnesium intake and mortality due to liver diseases: Results from the Third National Health and Nutrition Examination Survey Cohort. *Sci Rep* **7**, 17913 (2017).

188. Shidfar, F., Faghihi, A., Amiri, H. L. & Mousavi, S. N. Regression of Nonalcoholic Fatty Liver Disease with Zinc and Selenium Co-supplementation after Disease Progression in Rats. *Iran J Med Sci* **43**, 26–31 (2018).
189. Chen, H. Iron metabolism in non-alcoholic fatty liver disease: A promising therapeutic target. *Liver Research* **6**, 203–213 (2022).
190. Lonardo, A. & Weiskirchen, R. Copper and liver fibrosis in MASLD: the two-edged sword of copper deficiency and toxicity. *mtod* **4**, N/A-N/A (2024).
191. Zhang, R. *et al.* Curcumenol triggered ferroptosis in lung cancer cells via lncRNA H19/miR-19b-3p/FTH1 axis. *Bioact Mater* **13**, 23–36 (2021).
192. Jimenez, F. R., Ruggiero, C. H. & Cousins, R. J. Intestinal lncRNA H19 and miRNA-675 expression Influenced by Metal Transporter ZIP14. *The FASEB Journal* **34**, 1–1 (2020).
193. Cianfarani, S. *et al.* Insulin-Like Growth Factor-I and -II Levels Are Associated with the Progression of Nonalcoholic Fatty Liver Disease in Obese Children. *The Journal of Pediatrics* **165**, 92–98 (2014).
194. Kessler, S. M. *et al.* Transient Hepatic Overexpression of Insulin-Like Growth Factor 2 Induces Free Cholesterol and Lipid Droplet Formation. *Front Physiol* **7**, 147 (2016).
195. Lopez, M. F. *et al.* Disruption of the Igf2 gene alters hepatic lipid homeostasis and gene expression in the newborn mouse. *American Journal of Physiology-Endocrinology and Metabolism* **315**, E735–E744 (2018).
196. Gui, W. *et al.* Knockdown of insulin-like growth factor 2 gene disrupts mitochondrial functions in the liver. *J Mol Cell Biol* **13**, 543–555 (2021).

197. Monnier, P. *et al.* H19 lncRNA controls gene expression of the Imprinted Gene Network by recruiting MBD1. *Proceedings of the National Academy of Sciences* **110**, 20693–20698 (2013).
198. Susiarjo, M., Sasson, I., Mesaros, C. & Bartolomei, M. S. Bisphenol A Exposure Disrupts Genomic Imprinting in the Mouse. *PLoS Genet* **9**, e1003401 (2013).
199. Babraham Bioinformatics - FastQC A Quality Control tool for High Throughput Sequence Data. <https://www.bioinformatics.babraham.ac.uk/projects/fastqc/>.
200. Langmead, B. & Salzberg, S. L. Fast gapped-read alignment with Bowtie 2. *Nat Methods* **9**, 357–359 (2012).
201. Tarasov, A., Vilella, A. J., Cuppen, E., Nijman, I. J. & Prins, P. Sambamba: fast processing of NGS alignment formats. *Bioinformatics* **31**, 2032–2034 (2015).
202. Zhang, Y. *et al.* Model-based Analysis of ChIP-Seq (MACS). *Genome Biol* **9**, R137 (2008).
203. The Galaxy Community. The Galaxy platform for accessible, reproducible, and collaborative data analyses: 2024 update. *Nucleic Acids Research* **52**, W83–W94 (2024).
204. Pruitt, K. D., Tatusova, T. & Maglott, D. R. NCBI Reference Sequence (RefSeq): a curated non-redundant sequence database of genomes, transcripts and proteins. *Nucleic Acids Research* **33**, D501–D504 (2005).
205. Karolchik, D. *et al.* The UCSC Table Browser data retrieval tool. *Nucleic Acids Res* **32**, D493–D496 (2004).
206. Robinson, J. T. *et al.* Integrative Genomics Viewer. *Nat Biotechnol* **29**, 24–26 (2011).

207. Bailey, T. L. STREME: accurate and versatile sequence motif discovery. *Bioinformatics* **37**, 2834–2840 (2021).
208. Sherman, B. T. *et al.* DAVID: a web server for functional enrichment analysis and functional annotation of gene lists (2021 update). *Nucleic Acids Res* **50**, W216–W221 (2022).
209. Huang, D. W., Sherman, B. T. & Lempicki, R. A. Systematic and integrative analysis of large gene lists using DAVID bioinformatics resources. *Nat Protoc* **4**, 44–57 (2009).
210. Ingenuity Pathway Analysis | QIAGEN Digital Insights. *Bioinformatics Software | QIAGEN Digital Insights* <https://digitalinsights.qiagen.com/products-overview/discovery-insights-portfolio/analysis-and-visualization/qiagen-ipa/>.
211. Varrault, A. *et al.* Identification of Plagl1/Zac1 binding sites and target genes establishes its role in the regulation of extracellular matrix genes and the imprinted gene network. *Nucleic Acids Res* **45**, 10466–10480 (2017).
212. Dror, I., Rohs, R. & Mandel-Gutfreund, Y. How motif environment influences transcription factor search dynamics: Finding a needle in a haystack. *Bioessays* **38**, 605–612 (2016).
213. Xu, X. *et al.* Targeted therapeutics and novel signaling pathways in non-alcohol-associated fatty liver/steatohepatitis (NAFL/NASH). *Sig Transduct Target Ther* **7**, 1–39 (2022).
214. Bessone, F., Razori, M. V. & Roma, M. G. Molecular pathways of nonalcoholic fatty liver disease development and progression. *Cell Mol Life Sci* **76**, 99–128 (2018).

215. Nguyen-Lefebvre, A. T., Selzner, N., Wrana, J. L. & Bhat, M. The hippo pathway: A master regulator of liver metabolism, regeneration, and disease. *The FASEB Journal* **35**, e21570 (2021).
216. Driskill, J. H. & Pan, D. The Hippo Pathway in Liver Homeostasis and Pathophysiology. *Annu Rev Pathol* **16**, 299–322 (2021).
217. Goh, Y. P. S. *et al.* Eosinophils secrete IL-4 to facilitate liver regeneration. *Proceedings of the National Academy of Sciences* **110**, 9914–9919 (2013).
218. Weng, S.-Y. *et al.* IL-4 Receptor Alpha Signaling through Macrophages Differentially Regulates Liver Fibrosis Progression and Reversal. *eBioMedicine* **29**, 92–103 (2018).
219. Peng, K. *et al.* Effects of UBE3A on Cell and Liver Metabolism through the Ubiquitination of PDHA1 and ACAT1. *Biochemistry* **62**, 1274–1286 (2023).
220. Norris, A. C. *et al.* Deficiency of the lipid flippase ATP10A causes diet-induced dyslipidemia in female mice. *Sci Rep* **14**, 343 (2024).
221. Constitution of the World Health Organization. <https://www.who.int/about/governance/constitution>.
222. Clark, S. N., Anenberg, S. C. & Brauer, M. Global Burden of Disease from Environmental Factors. *Annu Rev Public Health* **46**, 233–251 (2025).
223. 10 chemicals of public health concern. <https://www.who.int/news-room/photo-story/detail/10-chemicals-of-public-health-concern>.

APPENDICES

Appendix A

Supplementary Table 2.1: Sample Numbers and Statistics

Supplementary Table 2.2: qRT-PCR Primer Sequences

Supplementary Table 2.3: Lipidomics Data and Statistics

Supplementary Table 2.4: Lipid Class Key

*These tables are available as a downloadable document on the repository page for this
ETD.*

APPENDIX B

Supplementary Table 3.1: Dam Water Consumption, Dam Food Consumption, Dam Weight Change, Litter Sizes, and PND 21 Survival Data

Supplementary Table 3.2: Sample Numbers and Statistics

These tables are available as a downloadable document on the repository page for this ETD.